Gold in the Central Lapland Greenstone Belt, Finland
V. Juhani Ojala (ed.)
Geological Survey of Finland, Special Paper 44, 7–56, 2007.

PALEOPROTEROZOIC METAMORPHISM AND DEFORMATION IN CENTRAL LAPLAND, FINLAND

by
Pentti Hölttä[1], Markku Väisänen[1,2], Jukka Väänänen[3], Tuomo Manninen[4]

Hölttä, P., **Väisänen, M., Väänänen, J. & Manninen, T. 2007**. Paleoproterozoic metamorphism and deformation in Central Lapland, Finland. *Geological Survey of Finland, Special Paper 44,* 7–56, 23 figures 2 tables and 2 appendices.

Three main ductile deformations, D1-D3, and contemporaneous and later shear zones account for most structures in Central Lapland. The oldest tectono-metamorphic feature is the bedding-parallel, mostly microscopic S1, overprinted by the main foliation S2, which is the most prominent structural feature seen in almost all rock types throughout the study area. Subhorizontal S2 is an axial plane foliation to tight or isoclinal, inclined to recumbent F2 folds. Kinematic indicators in the central and southern parts of the study area indicate a northward transport direction, but close to the S and SW border the Lapland Granulite Belt it may be of opposite direction. F3 folds deform the D2 structures. F3 folding show an extreme variety regarding the fold vergence with N-vergent folds in south, SW-W-vergent folds in north and E-vergent folds in west close to the Kolari shear system. Apparently, the F3 folding seems to be associated with complex tectonic movement directions, from S to N direction in the south, from NE to SW in the north and northeast part, and from W to E in the western part of the study area.

Several metamorphic zones have been mapped in the area. These are I) granulite facies migmatitic amphibolites south of the granulite complex (including the so called Tanaelv belt next to the granulites); II) high pressure mid-amphibolite facies rocks south of Zone I, characterised by garnet-kyanite-biotite-muscovite assemblages with local migmatisation in metapelites, garnet-hornblende-plagioclase assemblages in mafic rocks, local cordierite-orthoamphibole rocks intercalated with mafic volcanics; III) low-pressure mid-amphibolite facies rocks south of Zone II, garnet-andalusite-staurolite-chlorite-muscovite assemblages with retrograde chloritoid and kyanite in metapelites, hornblende-plagioclase-quartz±garnet in metabasites; IV) greenschist facies rocks of the Central Lapland Greenstone Belt, fine-grained white mica-chlorite-biotite-albite-quartz in metapelites, actinolite-albite-chlorite-epidote-carbonate in metabasites; V) prograde metamorphism south of Zone IV from lower amphibolite facies (andalusite-kyanite-staurolite-muscovite-chlorite±chloritoid schists, V.1–2) to mid-amphibolite facies (kyanite-andalusite-staurolite-biotite-muscovite gneisses,V.3) and upper amphibolite facies garnet-sillimanite-biotite gneisses (V.5); VI) amphibolite facies pluton-derived metamorphism related with heat flow from central and western Lapland granitoids, where Zone VI.2 represents both andalusite and sillimanite-present, and Zone VI.3 only sillimanite-present, andalusite absent gneisses. Pelitic rocks exhibit decompressional PT paths where andalusite grade metamorphism was preceded by higher pressure. Metamorphism was partly related with tectonic thickening during overthrusting of the Lapland Granulite Belt to the south, but the present metamorphic structure may record later, postmetamorphic faulting and folding events.

Key words (GeoRef Thesaurus AGI): metamorphic rocks, metapelite, metabasite, mineral assemblages, P-T conditions, Central Lapland Greenstone Belt, Paleoproterozoic, Finland.

[1] *Geological Survey of Finland, P.O. BOX 96, FI-02151 Espoo, Finland*

[2] *present address: Department of Geology, FI-20014 University of Turku, Finland*

[3,4] *Geological Survey of Finland, P.O. Box 77, FI-96101 Rovaniemi, Finland*

email: [1] pentti.holtta@gtk.fi [2] markku.vaisanen@utu.fi [3] jukka.vaananen@gtk.fi [4] tuomo.manninen@gtk.fi

INTRODUCTION

The Central Lapland Greenstone Belt and adjacent areas bordering the classical Lapland Granulite Belt in the south and south-west, have recorded six hundred million years of Paleoproterozoic depositional evolution from c. 2.5 Ga to 1.88 Ga (Lehtonen et al. 1998, Hanski et al. 2001). The structural and metamorphic history of the Lapland Granulite Belt has been constrained in many papers (e.g. Eskola 1952, Hörmann et al. 1980, Raith et al. 1982, Marker 1988, Barbey & Raith 1990, Korja et al. 1996, Perchuk et al., 2000), but systematic large-scale regional metamorphic and structural mapping has not been accomplished in the adjacent lower grade Proterozoic areas, although many special studies have dealt with the tectonometamorphic evolution of these regions (Gaál et al. 1978, Kärkkäinen 1982, Gaál et al. 1989, Ward et al. 1989, Rastas and Kilpeläinen 1991, Sorjonen-Ward et al. 1997, Lehtonen et al. 1998, Tuisku & Makkonen 1999, Hölttä & Väisänen 2000, Perchuk et al., 2000, Evins & Laajoki, 2002). However, the structural and metamorphic history of these areas is in a key position in tectonic modelling of the Proterozoic orogeny in the northern Fennoscandian Shield.

The purpose of this work is (i) to map the regional metamorphic zones in Central Lapland (Fig. 1) by describing the distribution of metamorphic mineral assemblages in metapelites and metabasites and by using geothermometry and geobarometry, (ii) describe the petrography and mineral chemistry of metapelites and metabasites, (iii) outline the main deformation phases and their relationship to metamorphism. This paper is mainly descriptive, trying to give a general framework for further development of both tectonic models and detailed structural and metamorphic analysis of metamorphogenic ore genesis.

GEOLOGICAL SETTING

The Proterozoic evolution of the Central Lapland area started with rifting of the Archean crust, producing andesitic lava flows and dacitic to rhyolitic ash-flow tuffs and ignimbrites of *the Salla Group* at the Archaean-Proterozoic boundary. These subaereally erupted volcanics are followed by crustally contaminated komatiites, siliceous high-Mg basalts and mafic volcanic rocks of *the Onkamo Group.* The 2.4 Ga old Koitelainen layered intrusion cuts the volcanic rocks of the Salla Group but not those of the Onkamo Group. This initial rifting-related volcanism was followed by the sedimentation of arkosic quartzites, carbonate rocks and mica schists of *the Sodankylä Group,* probably before 2.2 Ga that is the age of the mafic/ultramafic sills of the gabbro-wehrlite association (Hanski 1996) that have intruded these metasediments. Investigations of sedimentary facies of these metasediments suggest a continental margin setting. Deepening of the sedimentary basin caused accumulation of fine-grained sediments like phyllites and black schists of the *Matarakoski Formation, the Savukoski Group*. These pelitic metasediments are conformably overlain by basaltic and peridotitic komatiites and picrites of *the Sattasvaara Formation.* Emplacement of the 2.05 Ga old Keivitsa layered intrusion gives a minimum age for the Savukoski Group. The sedimentary-volcanic associations described above are in tectonic contact with *the Kittilä Group,* interpreted as an allochtonous oceanic unit comprising various MORB- (mid-ocean ridge basalts), OIB- (ocean-island basalt) and IAT-type (island arc tholeiitic) volcanic rocks, ophiolitic mantle rocks of Nuttio, and chemical sediments (Hanski 1997). The allochtonous nature of this group is, however, questioned by Sorjonen-Ward et al. (1997), who regard it as an ensialic, autochtonous unit. Younger quartzites and conglomerates of *the Lainio* and *the Kumpu Groups* cap all the previous rocks with unconformity. These molasse-type sediments contain pebbles of ca 1.88 Ga magmatic rocks, providing the maximum age of sedimentation (Hanski et al. 2000). Detailed descriptions of the above mentioned stratigraphic successions are provided by

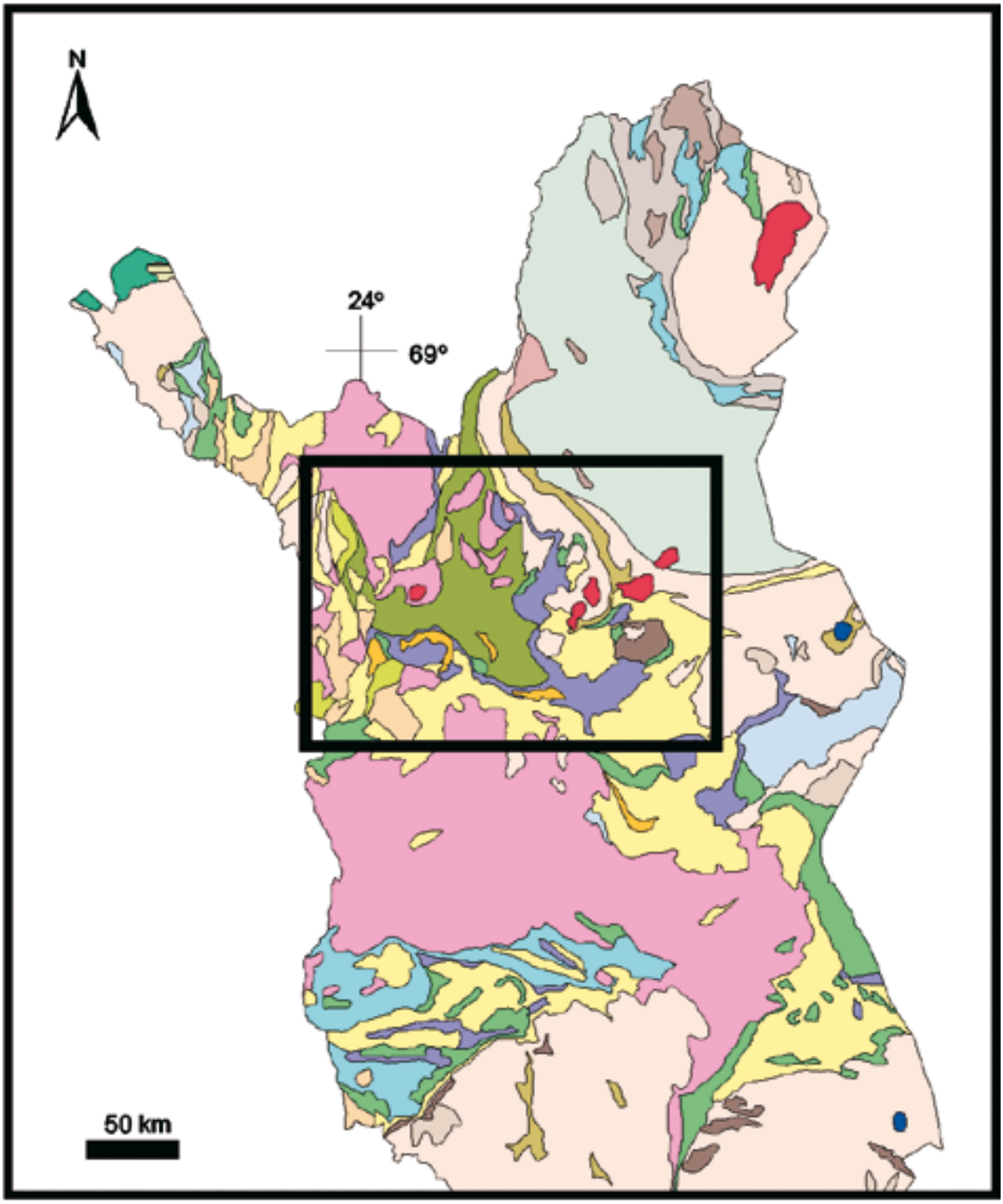

Fig. 1. The location of the study area as indicated by the box on the geological map of Finland after Korsman et al., 1997.

Lehtonen et al. (1998) and Hanski (2001) and Hanski et al. (2001).

The oldest dated Proterozoic intrusion is the Nilipää granite in the northern side of the Central Lapland Granitoid Complex. Th U-Pb age on zircon in this granite is 2.1 Ga, but also younger granitoids, dated at c. 1.84 Ga, occur in the complex (Huhma, 1986). Rocks of the so called Haaparanta Suite occur in the western part of Central Lapland and comprise c. 1.88–1.89 Ga deformed (foliated) tonalites, granodiorites and monzonites (Lehtonen et al. 1998), but granitoids of this age have been found also in the Sodankylä area in eastern Lapland (Räsänen & Huhma 2001). They probably represent the magmatism associated with the main

Svecofennian accretional tectonics. So called Hetta granites in the northern part of the Kittilä greenstone area are fine- to medium-grained, variously foliated, granodioritic to tonalitic intrusive rocks. Some of them are dated at c. 1.80 Ga, while some contain an older inherited component (Huhma 1986), suggesting the origin of deeper source by crustal anatexis. Youngest granitoids in the area are post-orogenic, 1.77 Ga old Nattanen-type granites (Huhma 1986; Haapala et al. 1987; Wennerstöm and Airo 1998).

Rastas and Kilpeläinen (1991) and Lehtonen et al. (1998) made structural analyses on selected key areas in Central Lapland. They reported a polyphase folding from various directions with at least two late folding phases, of which E-W folding is younger than N-S folding. Gaál et al. (1978), however, had an opposite opinion. Ward et al. (1989) and Sorjonen-Ward et al. (1997) on the other hand, provided a kinematic approach. They suggested a plate motion from two directions: the Svecofennian movement from south to north and a more or less simultaneous transport of the Lapland Granulite Belt from north to south or southwest. This created folds of opposing vergences in north and south, respectively. Dextral rotation caused some of the interference patterns seen on geophysical maps. The overall structural style of the area resembles that of a fold and thrust belt (Ward et al. 1989).

Deformation

We describe here those ductile deformation events which are closely related with the evolution of the regional metamorphism (D1–D3). Apart from these there is later postmetamorphic deformation that e.g. accounts for the evolution of late shear zones (Lehtonen et al. 1998; Väisänen, 2002).

Structural correlation across such a large area is problematic without detailed geochronological data of different tectonic episodes, recalling the possibility that even a single deformation can locally produce superimposed structures (e.g. Burg 1999). Since the now exposed orogen probably was formed by plate motions from different directions, at different times, and at varying intensities, the resulting tectonic mosaic is extremely heterogeneous. Therefore, the grouping of structures under labels D1–D3 below is only descriptive and is based on the overprinting criteria within smaller subareas. There are many different kinds of tectonic and metamorphic blocks exposed in the area and therefore, we do not believe that different structures (e.g. D3 structures) in different places were formed simultaneously. Therefore in a strict sense, the structures can not be correlated. The geometrical structure analysis has its limitations in Central Lapland.

Volcanic and sedimentary depositional structures (bedding) are quite common in Central Lapland, helping to identify rock types and the paleoenvironment. Unambiguous younging criteria were, however, observed very rarely during mapping, the observations were mostly made on quartzites. This hampered the identification of possible overturning of the strata. According to Ward et al. (1989) and Evins & Laajoki (2002), however, in spite of recumbent folding, there are sufficient younging data to preclude the existence of large-scale fold nappes in Central Lapland.

D1 deformation

The oldest tectono-metamorphic feature in Central Lapland is the bedding-parallel foliation, S1. It can be seen in mica rich sedimentary rocks within F2 fold hinges, perpendicular to S2 axial plane foliation, but rarely observed macroscopically. S1 is also preserved as inclusion trails within andalusite, garnet and staurolite porphyroblasts. Hölttä and Väisänen (2000) called it as S1a foliation (predating D1), because the origin of the foliation was ambiguous and it was not a mappable unit. However, the S1 foliation appears to be locally even stronger than S2. Therefore, we believe that it is of tectonic origin, older than S2 and deserves a separate D1 term, in accordance with terminology in Lehtonen et al. (1998). However, we did not detect any folds associated with S1 that would have been clearly overprinted by D2 deformation.

D2 deformation

The most prominent structural feature seen in most rock types throughout the study area is the main foliation, S2. In most cases it is subparallel to bedding, but in some competent rock types such as quartzites and sandstones, the foliation can be in larger angle to bedding. Minerals defining the foliation are protolith and metamorphic grade dependent: in lowest grade rocks foliation in pelitic rocks comprises chlorite and muscovite, whereas in higher grade rocks chlorite is replaced by biotite. When associated with F2 folds, S2 is an axial plane foliation to commonly tight or isoclinal folds deforming bedding, S0, and the bedding-parallel, microscopic S1. The orientation of the main foliation and the early folds vary, but in most places S2 is gently dipping to flat-lying, and the folds

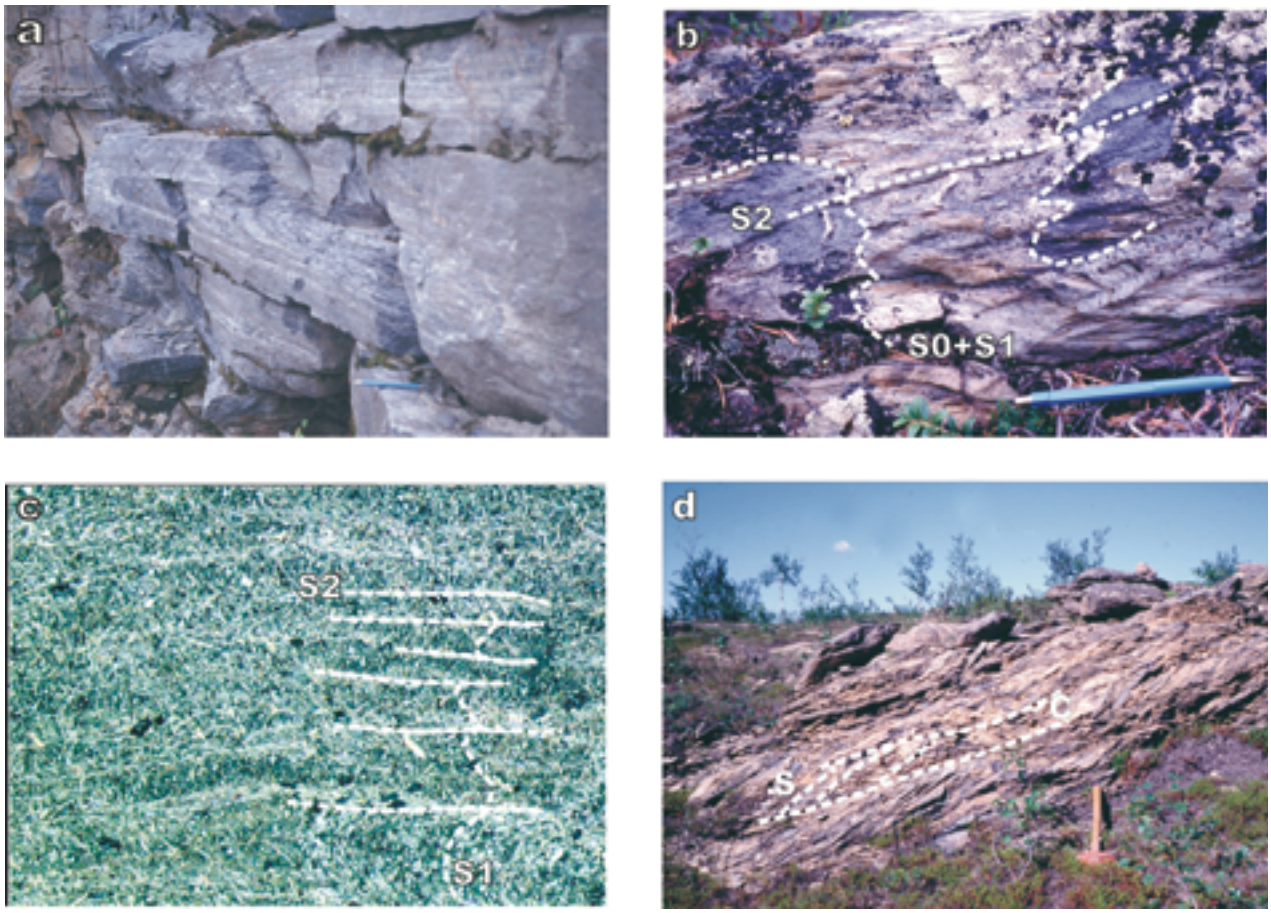

Fig. 2. (a) Recumbent folds on a vertical wall of an abandoned marble quarry in Äkäsjokisuu. Pen in the lower right corner points north. N 7490585, E 3355993. (b) Recumbent N-vergent folds in chlorite-muscovite schist in Rajala. Pen points north. N 7502895, E 3460515. (c) Photomicrograph of the rock in Fig. 2b displaying a vertical S1 and horizontal S2. Field of view is 5 mm. (d) Sheared ultramafic rock in Tarpomapää displaying a metre scale NNE-vergent S-C structure. The hammer shaft points north. N 7527806, E 3453228. Locations of the photograph sites are presented in Fig. 7.

are either recumbent or reclined (Figs 2a and 2b). Vertical axial planes with steep fold axes also exist. The field observations suggest that this early deformation was caused by horizontal movements related to thrust tectonics. However, it is not sure if S2 was originally horizontal throughout Central Lapland (see also Ward et al. 1989 and Evins & Laajoki 2002).

In the study area, the gently dipping to horizontal foliations are still preserved in many places, with an approximately NNE-SSW elongation lineation on the foliation plane. In Figs 2b, 2d, 3a and 3b, four independent observations from different parts of the study area are presented to argue that the movement direction was from SSW to NNE. The measurements of the main lineations are plotted on Fig. 4 and F2 folds on Fig. 5. Some of the S2 form lines, main thrusts, shear zones and tectonic transport directions are presented in Fig. 7.

In Fig. 2b, the fold vergence in recumbent F2 folds indicate a northward transport direction in an outcrop situated close to the Sirkka shear zone (Fig. 7). Fig. 2d displays a vertical section of an ultramafic rock, partly altered to serpentinite. This belongs to the same rock series as the Nuttio serpentinite that, according to Hanski (1997), is a piece of mantle part of an ophiolite. The outcrop displays a well-developed S-C structures that occurs both in millimetre and metre scales, indicating top-to-the NNE movement direction. Fig. 3a shows a spectacular example of a sigmoidal garnet, where shear sense is top-to-the N. The example in Fig. 3b shows a thin section photomicrograph of a strongly deformed quartzite with a well-developed quartz rod lineation on a subhorizontal foliation plane. Small-scale shear bands show top-to-the NNE movement direction.

The examples above indicate northward transport during D2. It is possible, however, that the structures described above were reactivated during D3 and some of them display a composite D2+D3 structure (see below). Kinematic information from this tectonic stage is lacking in this work from the S and SW border the Lapland Granulite Belt. Korja et al. (1996),

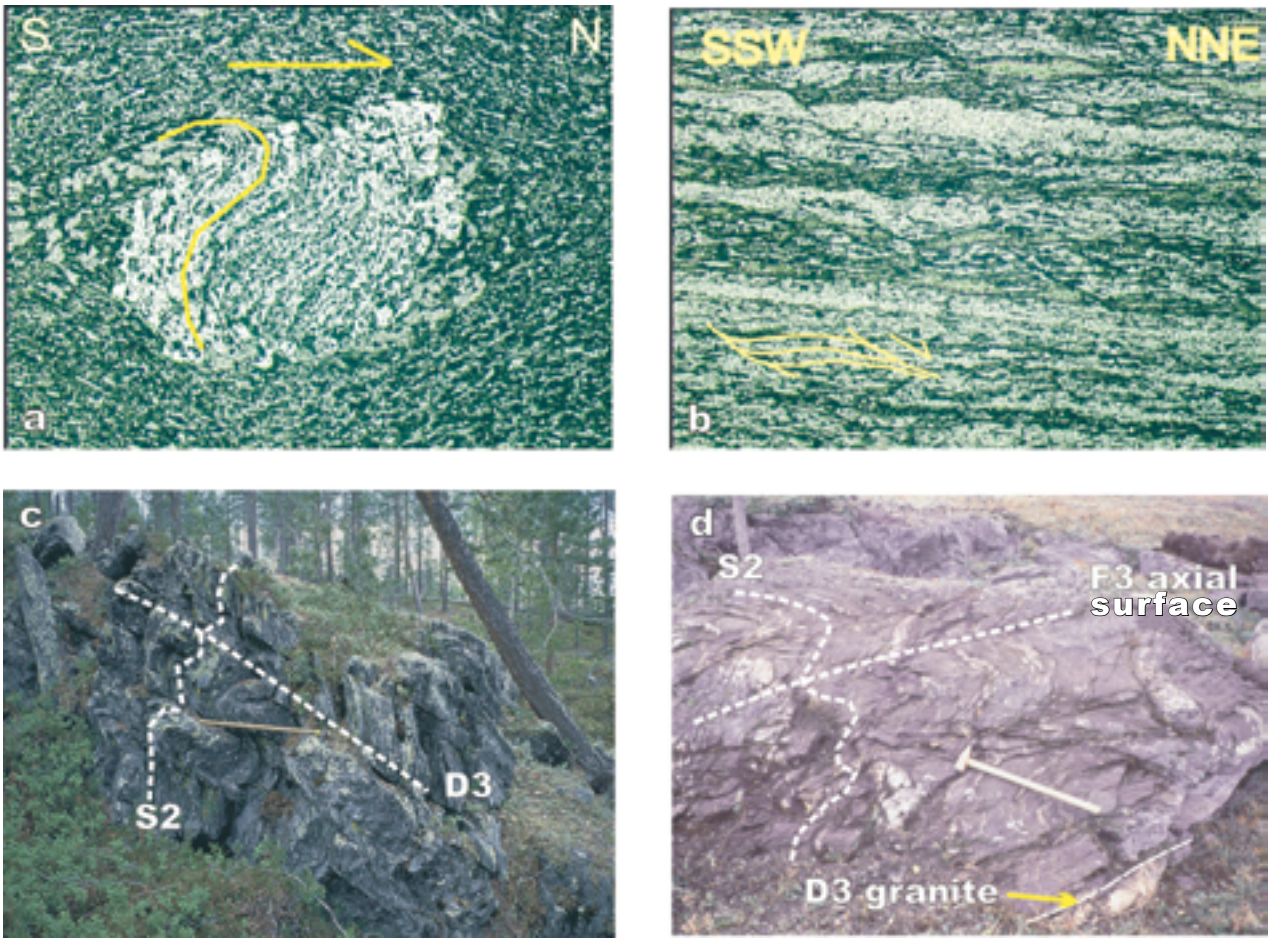

Fig. 3. (a) Sigmoidal garnet in mica schist, north is to the right. Field of view is 10 mm. Nuttion Tuorelaki. N 7515889, E 3457831. **(b) Dextral shear** bands in quartzite. Field of view is 10 mm. Petkula. N 7510986, E 3490942. **(c) Subvertical S2 is folded by E-W late folds with gently S-dipping** axial surfaces. Hammer shaft points north. Petäjävaara. N 7476509, E 3495903. **(d) Mica schist folded by inclined N-vergent late folds. Pink granite** is folded and intrudes along axial surfaces (lower right corner). The hammer shaft points north. Pikku-Venevaara. N 7482989, E 3516295. Location of the photograph sites are presented in Fig. 7

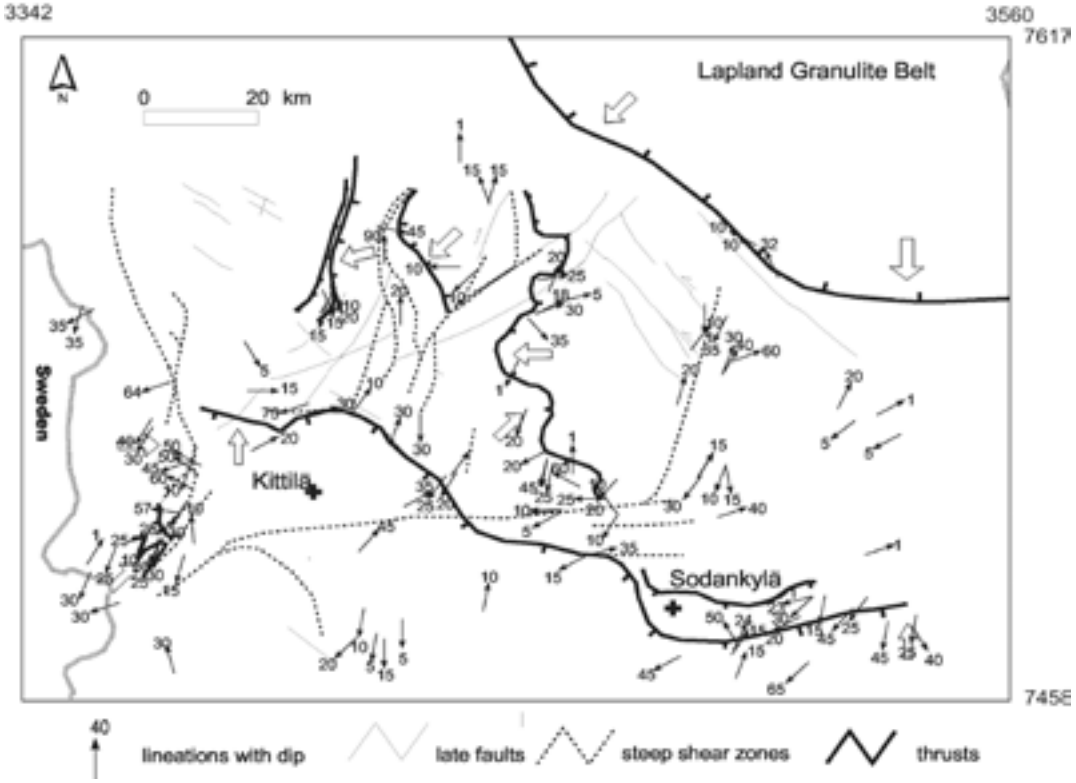

Fig. 4. Measurements of lineations. Broad arrows show the interpreted tectonic transport directions.

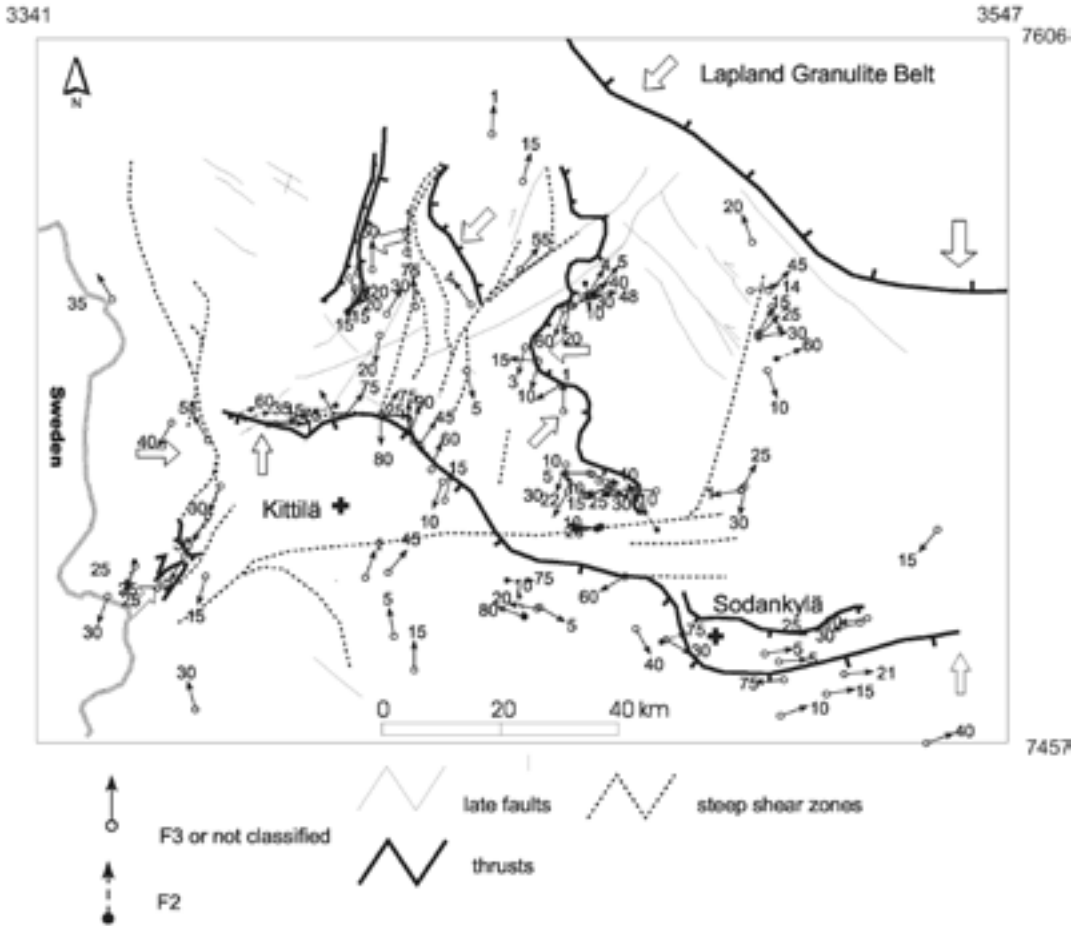

Fig. 5. Measurements of the F2 and F3 folds. Boad arrows show the interpreted tectonic transport directions.

however, describe SE verging recumbent folding, but the correlation to structures described above and below is unclear.

D3 deformation

The geological structures described above are overprinted by a set or sets of late folds (here collectively called F3 folds) and late shear zones of various orientation and attitudes (Väisänen 2002). Folds with E-W, N-S, NE-SW and NNW-SSE axial traces are all observed and measured, but the E-W and N-S orientations dominate. The dips of the axial surfaces of F3 folds also vary from horizontal through moderately dipping to vertical. These observations closely resemble that of a polyphase folding previously described as F3 and F4 by Rastas and Kilpeläinen (1991) and Lehtonen et al. (1998).

We did not find any unambiguous systematic and repetitive overprinting relationships of late folds of different orientations in this work. On the contrary, some observations suggest that they could have been formed approximately simultaneously or in the course of the same progressive deformation, possibly accompanied by rotation. These include e.g. (i) the similar fold geometry, (ii) the similar metamorphic grade using mineral growth as criteria, (iii) same relationship to vein material (carbonate veins, quartz veins, iron carbonate veins), (iv) fold axes of different orientation and attitude were found occasionally within same outcrops without any obvious overprinting relationships.

In general, in the southern and south-eastern part of the study area (Sodankylä area), late folds, plotted as F3 in Fig. 5, are E-W trending, their axial surfaces range from vertical to moderately dipping, locally even

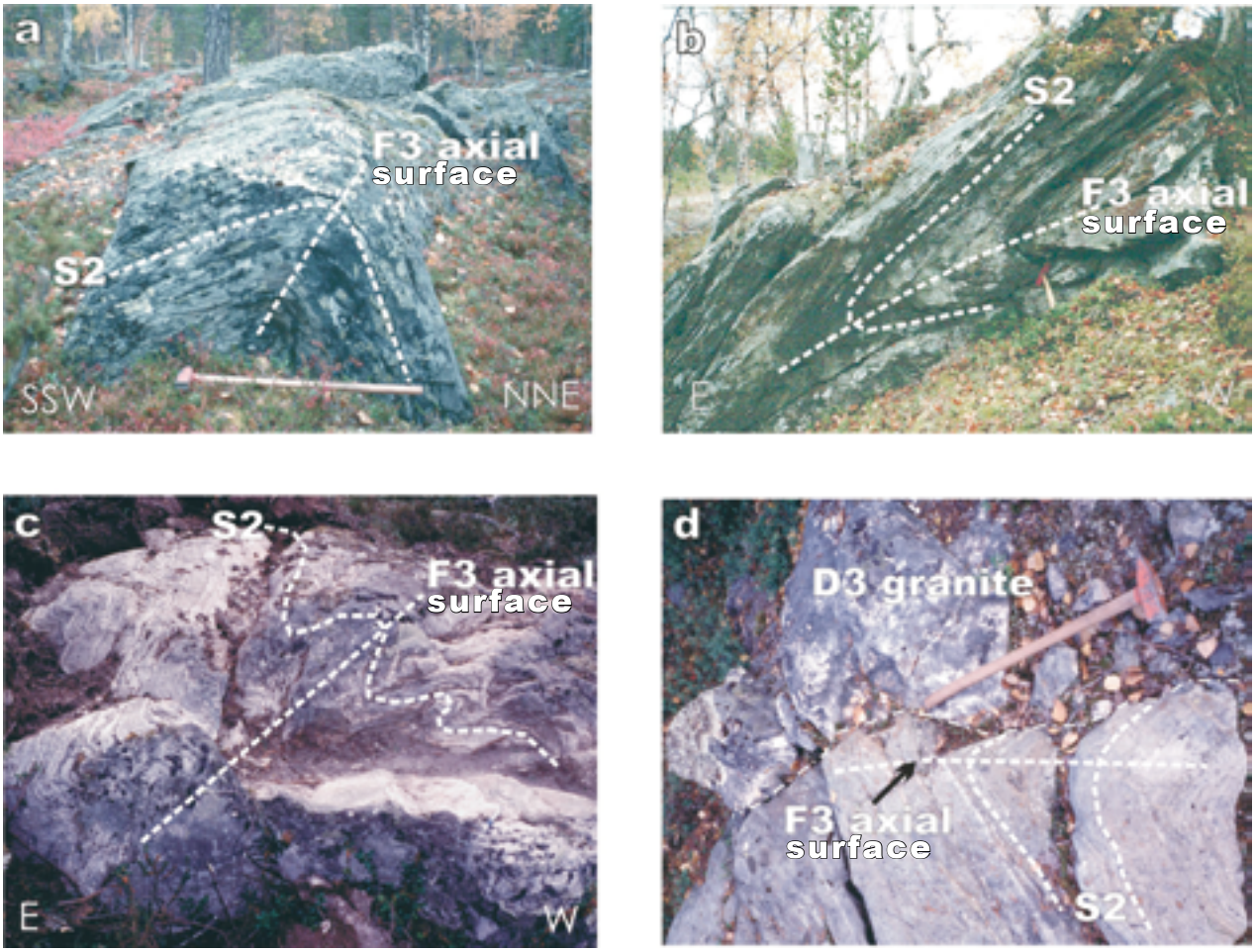

Fig. 6. (a) Asymmetric NNE-vergent late fold with a steep northern fold limb and a gently dipping southern limb. Rovalaki. N 7511749, E 3463811. (b) Inclined W-vergent late fold, view looking south. Haapanalehto. N 7555046, E 3458000. (c) W-vergent inclined fold, view looking south. Lompolo, N 7557161, E 3409693. (d) Granite dike intrudes along the N-S axial surface of a late fold, the hammer shaft pointing north. Vuomilehto. N 7553309, E 3496939. The thin dot-dash line shows the contact of granite with the folded felsic gneiss. Locations of the photograph sites are presented in Fig. 7.

subhorizontal with N-vergent fold asymmetry (Fig. 3c). Occasionally, pink granite dikes, folded and injected along axial surfaces, suggest at least some syn- to late tectonic granitoid magmatism (Figs 3d and 6d). Late folds are upright to steeply inclined, displaying a northward vergence in the central part of the area (Fig. 6a), but eastward vergent in SW and W part of the area close to the Kolari Shear system (Sorjonen-Ward et. al. 1997). W-vergent folds have been observed in N and NE part of the area, close to shear zones (Figs 6b and 6c), and late folds appear to be upright in the north-central part of the area. Kinematically, the late folding seems to be associated with a complex tectonic movement directions with S to N direction in the south, from NE to SW or ENE to WSW in the northern and northeastern parts, and from W to E in the western part of the study area (see Fig. 7).

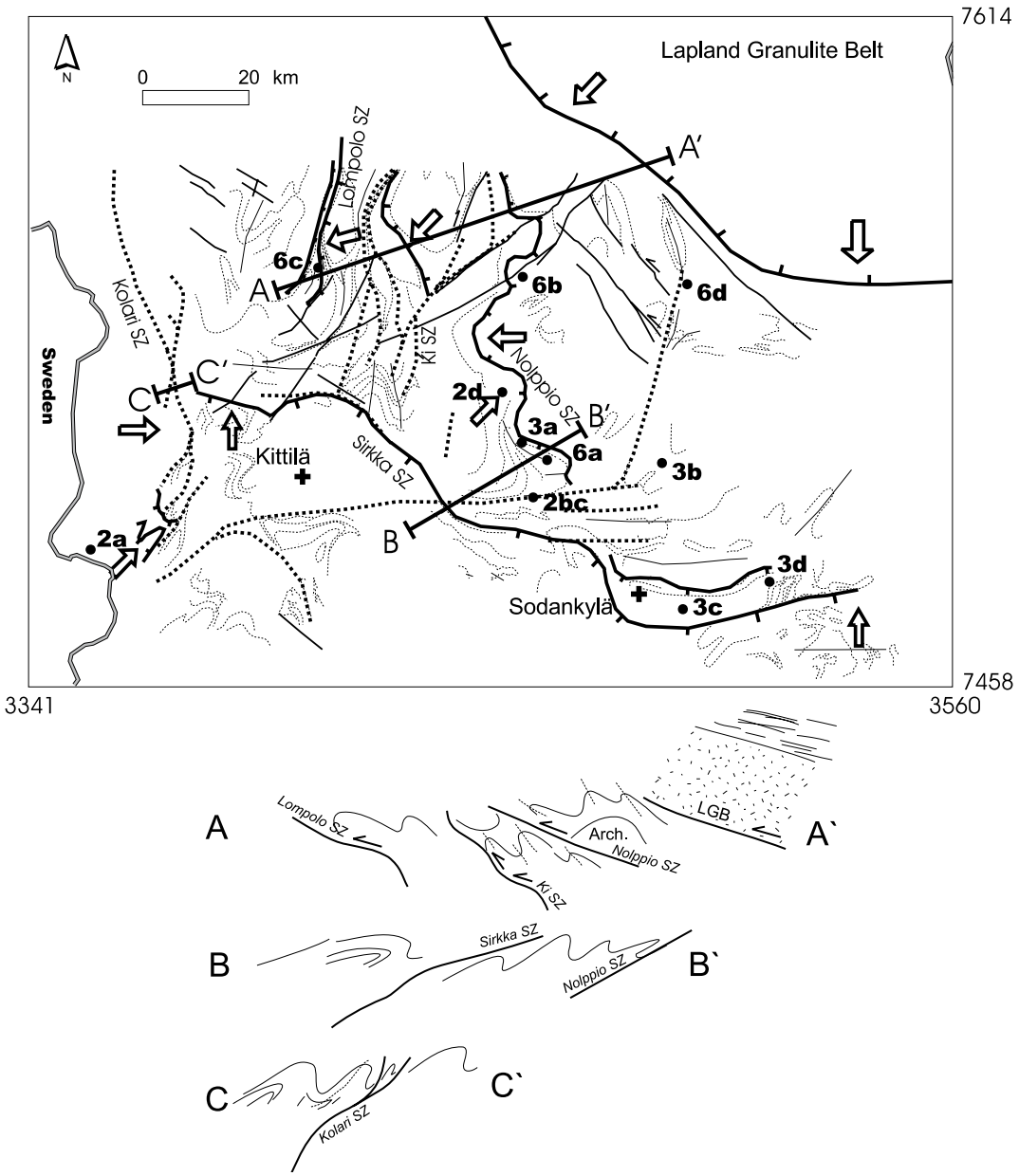

Fig. 7. Tectonic map of the Central Lapland Granitoid Complex. Arrows show the interpreted tectonic transport directions. Thick solid lines with ticks are thrusts, dashed thick lines are steep shear zones, solid medium lines are late faults, dashed medium lines are S2 form lines, thin solid lines are S3 axial surfaces. Ki SZ = Kiistala Shear Zone, SZ = Shear Zone, LGB = Lapland Granulite Belt. Below the map, schematic vertical sections along lines A-A', B-B' and C-C'. Numbers with letters show the locations of the photographs presented in Figs 2, 3 and 6.

Metamorphism

Based on the observed mineral assemblages in mafic and pelitic rocks, the following metamorphic zones have been observed in the study area (Fig. 8). Mineral assemblages in each zone are listed in Table 1. Mineral abbreviations are after Kretz (1983).

I Granulite facies migmatitic mafic rocks with grt-hbl-pl-qtz±cpx±opx assemblages, rare peraluminous migmatites with grt-bt-sil-pl-qtz. Assemblage grt-hbl-cpx-pl-qtz was observed only in this zone in the study area.

II Mid-amphibolite facies high pressure rocks, grt-ky-st-bt-ms-pl-qtz assemblages in pelites, local minor migmatisation, grt-hbl-pl-qtz in mafic rocks, locally cordierite-orthoamphibole.

III Mid-amphibolite facies low-pressure rocks, grt-and-st-chl-ms-pl-qtz±bt assemblages with retrograde chloritoid and kyanite, hbl-pl-qtz±grt in metabasites, typically a strong retrograde metamorphism with extensive chloritisation.

IV Greenschist facies rocks, fine-grained ms-chl-bt-ab-qtz in metapelites, act-chl-ep-ab-crb-qtz in mafic rocks.

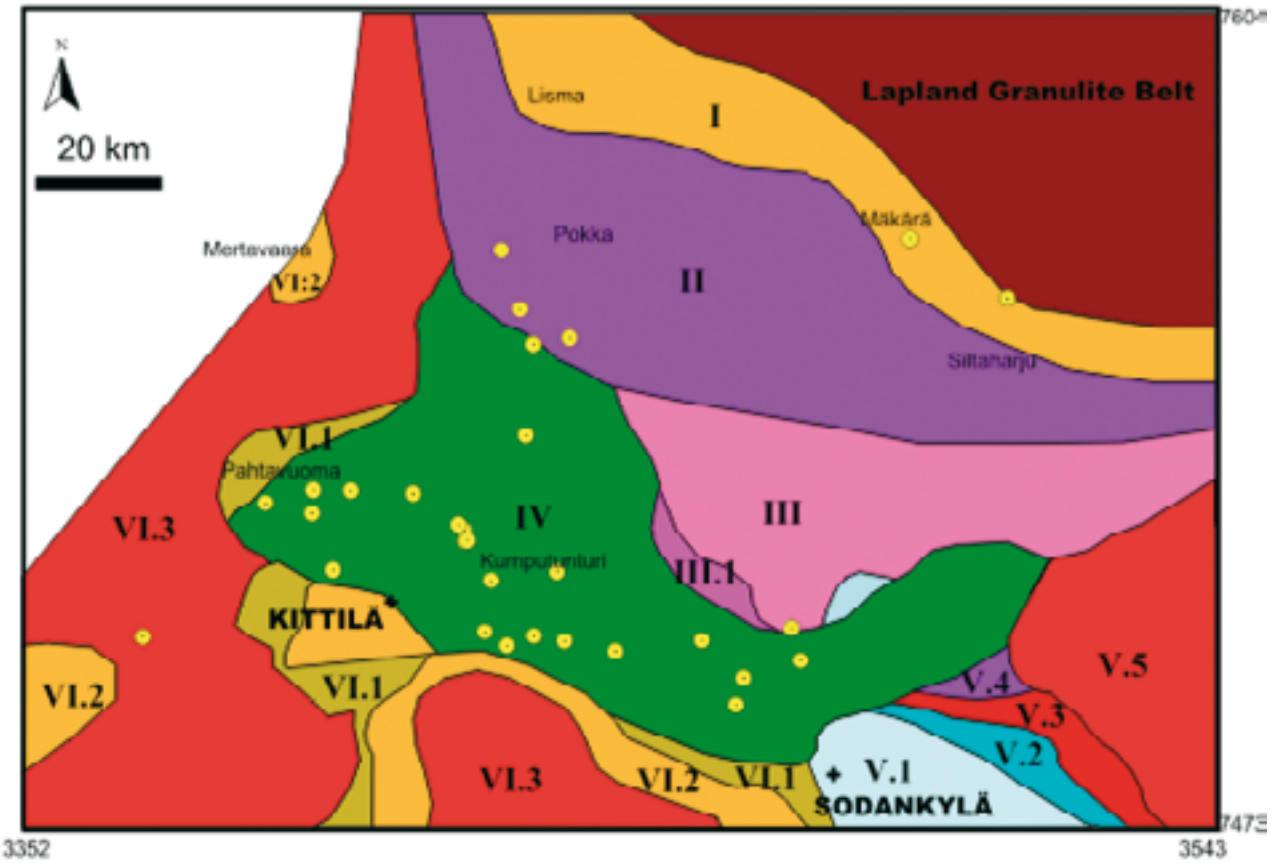

Fig. 8. Metamorphic map of the study area. See Tabel 1 and text for explanation of the zones, indicated by the Roman numerals. Yellow spots indicate the known gold desosits after Eilu (1999).

Table 1. Observed silicate mineral assemblages in metapelites and metabasites.

Zone	Assemblages	Retrograde minerals
I	– grt-bt-sil-ms-chl-pl-qtz±kfs – *grt-hbl-pl-qtz±cpx±bt±cum±ep±chl±ttn* – *hbl-pl-qtz±bt±ep±chl* – *grt-hbl-opx-cpx-cum-pl-qtz*	ms, ep, chl, cum, grt, partly hbl
II	– grt-bt-ms-qtz±ky±st±pl – ky-bt-pl-qtz – grt-bt-qtz±pl±cc – *hbl-pl-qtz±grt±ep±chl* – *tre-chl±ol±crb* – *tre-spl-pl-chl* – *tre-cor-pl-ch* – *oam-crd-pl-qtz±bt* – *oam-pl-qtz-chl±bt* – *grt-bt-chl-pl-qtz±oam±crd* – *grt-oam-chl-pl-qtz*	chl, ep
III	– grt-st-ms-chl-qtz ±ctd±and±ky±pl – ms-chl-qtz±tur – *hbl-pl-qtz±grt±ep±chl* – *grt-cum-qtz*	ctd, ky, partly ms, chl, st
III.1	– grt-ms-bt-chl-st-pl-qtz±ctd – bt-ms-qtz±tur±chl±pl	ctd, chl, partly ms, chl

Continue next page.

Zone	Assemblages	Retrograde minerals
IV	– chl-ms-qtz±pl±bt±tur±mnz – bt-chl-qtz±crb – *chl-act-pl-qtz±ep±crb ±ttn* – *chl-pl-qtz±crb±rt±ep* – *act-pl-ep-qtz-±rt* – *act-chl±cum* – *chl-crb-ep-pl±qtz* – *bt-chl-qtz-±ms* – *bt-ms-pl-qtz-mnz* – *bt-cum-qtz±pl* – *ol-crb-srp-op* – *srp-op* – *ol-tre-op±opx*	
V.1	– and-chl-ms-qtz±cld±ky±pl – st-cld-chl-pl-qtz±ky – ky-chl-ms-qtz±pl±and – and-bt-ms-pl-qtz±chl – ms-bt-ky-qtz±grt±chl	partly cld, chl
V.2	– st-ms-chl-pl-qtz±ky±tur – and-ms-chl-pl-qtz±st±ky – ky-st-ms-chl-pl-qtz	chl (?)
V.3	– st-ky-ms-chl-bt-pl-qtz±sil – st-ky-and-sil-ms-chl-bt-pl-qtz – st-bt-ms-pl-qtz±chl – ky-st-bt-ms-pl-qtz±grt – ky-bt-ms-pl-qtz±and	chl, partly ms
V.4	– ky-st-bt-ms-pl-qtz±grt±st – bt-ms-pl-qtz	
V.5	– st-sil-bt-ms-pl-qtz±grt±ky – sil-bt-ms-pl-qtz±chl±grt	chl, partly ms
VI.1	– bt-ms-qtz-tur±chl±pl±crd ±and±grt – bt-scp-crb-qtz – bt-cum-chl-qtz – chl-ms-qtz±bt±pl – bt-ms-kfs-pl-qtz – bt-ms-ep-pl-qtz – *grt-bt-crb-tlc±cum* – *grt-bt-crb-cum* – *grt-bt-Fets-crb±cum±qtz* – *grt-Fets-bt-chl-qtz* – *hbl-chl-ep-qtz-crb* – *hbl-pl-qtz-ep-ttn* – *hbl-pl-bt* – *hbl-ep-pl* – *bt-chl-ep-qtz* – *cpx-tr-scp-bt-qtz* – *cpx-tr-bt-kfs-qtz±scp* – *cpx-hbl-kfs-pl-qtz-ttn± bt*	
VI.2	– bt-ms-pl-qtz±and±chl±tur – ms-chl-pl-qtz±grt – grt-st-bt-ms-pl-qtz – and-crd-bt-ms-qtz±grt±chl±st – and-st-bt-ms-pl-qtz±sil ±grt±chl – grt-st-bt-pl-qtz±sil±and ±chl – bt-ms-ky-crd-qtz±and±sil ±chl – ky-and-sil-ms-crd-qtz – and-bt-ms-qtz-pl±crd±sil – *hbl-pl-qtz±grt*	chl, partly ms, partly st
VI.3	– bt-ms-pl-kfs-qtz±sil±pl±chl – st-sil-bt-ms-pl-qtz±grt – bt-ms-sil-pl-qtz±chl – bt-ms-crd-qtz±sil±pl – grt-bt-ms-pl-qtz±st±chl – grt-bt-sil-pl-qtz – grt-bt-ms-ep-pl-qtz – grt-bt-ms-sil-kfs-qtz – grt-bt-cum-chl-crd-pl-qtz – *hbl-pl-qtz±ep±chl±cpx*	chl, ep, partly ms, partly crd, partly st

V Prograde metamorphism from lower amphibolite facies (and-ky-st-ms-chl-cld-pl-qtz schists = V.1) to mid-amphibolite facies (ky-and-st-ms-pl-qtz gneisses =V.2, st-als-bt-ms-pl-qtz gneisses = V.3, ky-st-bt-ms-pl-qtz-grt gneisses = V.4 and upper amphibolite facies grt-sil-bt bearing gneisses = V.5), hbl-pl-qtz in metabasites.

VI Amphibolite facies, pluton-derived metamorphism-related with Central and Western Lapland granitoids, grt-and-ky-sil-crd-bt-ms assemblages, grade increasing from ms-bt-chl schists (VI.1) to and-sil-st-bt-ms gneisses (VI.2), and to grt-bt-ms-sil (VI.3) gneisses towards the granitoid contacts, locally migmatites, hbl-pl-qtz±grt and hbl-pl-qtz±cpx in metabasites.

Petrography

Zone I

In Zone I, mafic rocks are mostly migmatitic, the proportion of tonalitic leucosome varying from few per cents to >50 % of the rock volume. Garnet-bearing migmatites have the assemblage grt-hbl-pl-qtz±cpx, indicating that migmatites were at least partly produced in a melting reaction

(1) hbl + pl + qtz = grt + cpx + liq.

This reaction is considered as a transition reaction from amphibolite to granulite facies in high pressures, although in some compositions it may take place also in amphibolite facies (Pattison, 2003). High degree of melting and thermobarometric results indicate in this case granulite facies conditions. Metatexites and schlieren-type migmatites are common, epidote, chlorite and cummingtonite being retrograde phases after amphibole and pyroxene. Primary brownish green hornblende has commonly been altered into bluish amphibole. Orthopyroxene is rare but it occurs locally in the grt-hbl-opx-cpx-cum-pl-qtz assemblage, where cummingtonite is a retrograde phase. The texture of the mafic rocks is granoblastic, and main minerals are mostly in textural equilibrium forming dihedral angles. Leucosomes have a typical magmatic texture, where interstitial quartz is surrounding idiomorphic and subidiomorphic plagioclase crystals. In the Mäkärä area, close to the Lapland Granulite Belt contact zone, garnet occurs both as big grains and narrow coronas between hornblende and plagioclase (Fig. 9a) in clinopyroxene-absent rocks, indicating, instead of reaction (1), a continuous reaction

(2) hbl + pl = grt + qtz + H_2O.

In the Mäkärä area, there are metavolcanic rocks with primary volcanic textures like amygdules, and randomly oriented, euhedral plagioclase phenocrysts in a fine-grained matrix. These rocks have the high-grade assemblage with grt-amph-pl-qtz±cpx but annealing has not destroyed the primary magmatic texture, although these rocks have metatexite interlayers. Garnet forms coronas around plagioclase in these rocks, too. In the Lisma area, there are metadolerites in which clinopyroxene is altered from crystal rims into brownish green hornblende, indicating a reaction that took place during cooling,

(3) cpx + pl + H_2O = hbl

and garnet coronas are formed between clinopyroxene and plagioclase (Fig. 9b) in a reaction

(4) cpx + pl = grt + qtz.

Melting reaction (1) has a steep dP/dT slope so that melting is favoured by increasing temperature (Pattison, 2003). Reactions (2) and (4) have shallow positive dP/dT slopes that indicate either near-isobaric cooling or pressure increase during cooling or heating.

Zone II

The rocks in the zone II represent lower grade metamorphic conditions than in the zone I. Mafic rocks are not migmatized but metapelites have leucosomes in small abundances in the northern part of the zone II. Migmatization of the metapelitic gneisses is schlieren-type. Leucosomes form 5–20 mm wide veins and they are compositionally tonalitic, indicating melting in water-saturated conditions (Whitney & Irving 1994, Mouri & Korsman 1999). Bt-st-grt-ms-ky-pl-qtz assemblages are common (Figs 9e, 14a, 14c.). Rims of staurolite and kyanite crystals have often altered respectively, into sericite, and garnet into chlorite and biotite, some kyanites are intergrown with muscovite, biotite and staurolite inclusions occur in muscovite, garnets are crystallized on staurolite rims, and garnet has sometimes staurolite inclusions, indicating that peak metamorphic conditions were probably close to the univariant KFMASH reaction boundary (Fig. 23a)

(5) bt + st + qtz = grt + ms + als + H_2O.

The PT conditions of the reaction (5) are close to the univariant melting reaction

(6) bt + ms + st + pl + qtz = grt + ky + liq

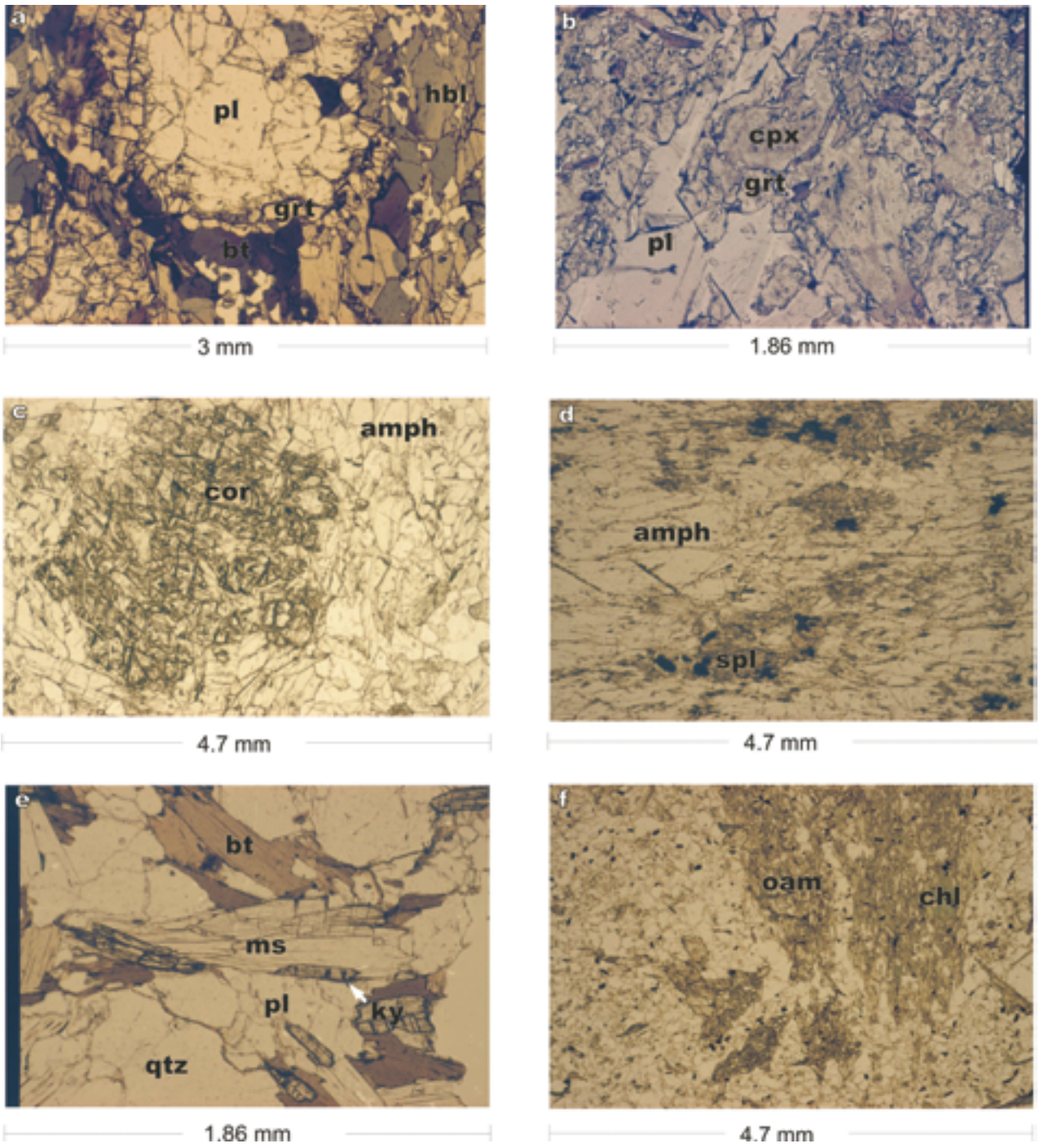

Fig. 9. Metamorphic textures and reactions in Zones I–III. a) garnet corona between hornblende and plagioclase. Zone I, sample PSH-97-20.2, N 7572940, E 3494520, b) garnet corona between clinopyroxene and plagioclase in metadolerite. Zone I, sample PSH-00-42.1 N7590218, E 3440182, c) corundum in a mafic rock. Zone II, sample PSH-99-100.3, N 7579148, E 3437489, d) spinel inclusions in tremolitic amphibole. Zone II, sample PSH-99-101.2, N 7578910, E 2561370, e) kyanite replacing muscovite. Zone II, sample JTV-98-49.1, N 7576663, E 3445005, f) chlorite, quartz and biotite replacing orthoamphibole, sample PSH-97-2.1, N 7544660, E 3494130.

in the system CNKFMASH (Fig. 23b). Because metapelites are migmatitic in the zone II, it is evident that the reaction (6) or the divariant melting reactions emanating from this univariant caused most migmatisation in staurolite and kyanite bearing rocks.

In the Pokka area, there are boninitic mafic rocks whose mineral assemblage is colourless-pale green tremolite and anorthitic plagioclase. These rocks locally contain corundum, which is texturally in equilibrium with amphibole and plagioclase (Fig. 9c). Also spinel inclusions occur in amphibole (Fig. 9d). In the same area, migmatitic pelitic gneisses have the assemblage grt-ky-bt-ms-pl-qtz.

In a few localities, there are schists that have the assemblage grt-bt-qtz±pl±cc. In places, garnets in carbonate-bearing schist (sample PSH-00–62.1) have

inclusion-free domains that have preserved the crystal shape of the reactant garnet-producing mineral, probably epidote (Fig. 11a). Epidote and chlorite are common retrograde phases after amphibole in mafic rocks of Zone II. Amphibole is often green to bluish green hornblende. In the Siltaharju area, there are hyrdo thermally altered cordierite-orthoamphibole rocks, which are intercalated with mafic metavolcanic rocks. Typically, in these rocks coarse-grained, orthoamphibole-bearing layers alternate with quartz and plagioclase-bearing layers, giving the rock a spectacular centimetre-scale banded structure. Orthoamphiboles garnets of the area may be up to centimetre in size, the latter containing many quartz inclusions. There are some exposures where the peak metamorphic mineral assemblage is not retrograded, but in most cases amphiboles and biotites are strongly altered into chlorite which occurs only as a retrograde phase. Orthoamphiboles typically occur as pseudomorphs that are totally replaced by chlorite, quartz and biotite (Fig. 9f). Unaltered orthoamphiboles are mostly brownish gedrites having, crystals sometimes almost colourless anthophyllite rims.

Zone III

Metapelites in Zone III are strongly schistose, although the primary bedding structures are still observable in many places. Grt-st-ms-chl-qtz±cld±and±ky±pl and ms-chl-qtz±tur are typical mineral assemblages. Chloritoid was observed only in the southern parts of Zone III. Biotite is rare in rocks that have grt-st-Al_2SiO_5-ms assemblages, and when present it is only an accessory or a retrograde phase. Instead, biotite is common in mica gneisses which have less aluminium or more calcium than the Al-rich pelitic gneisses of the zone, having bt-ms-qtz±tur±chl±pl or grt-bt-qtz±pl±ep±crb assemblages. Biotite-bearing gneisses occur sporadically throughout the area so that any biotite-in isograd cannot be defined. Garnet-staurolite-andalusite-chlorite assemblages are common, and staurolite tends to form pseudomorphs after garnet, together with chlorite (Fig. 10a). This indicates the divariant FMASH cooling reaction

(7) grt+H_2O=st+chl+qtz.

Garnet has sometimes chloritoid inclusions, which may indicate that some garnet was formed in the univariant FMASH reaction

(8) cld + qtz = chl + grt + st + H_2O.

Kyanite occurs as small crystals that overgrow andalusite and muscovite and in coronitic aggregates on staurolite and muscovite, often together with chlorite (Figs 10b–10c). The latter texture indicates that much of the kyanite was formed in a divariant FMASH cooling reaction

(9) st + qtz + H_2O = chl + als.

Kyanite occurs also as inclusions in andalusite and may therefore also be an earlier phase than andalusite. However, inclusions in andalusite are similarly randomly oriented as kyanites in the matrix (Fig. 10b), reflecting more likely that kyanite overgrows andalusite that occurs as big helisitic grains which may be centimetre-sized. The reaction relationship of andalusite with staurolite is not clear, but sometimes andalusite has staurolite inclusions, indicating that andalusite was at least partly produced in the reaction (9).

In garnet-absent rocks chloritoid occurs in chlorite and muscovite-filled pseudomorphs after staurolite, often together with kyanite (Fig. 10d) indicating that chloritoid was formed in a cooling reaction

(10) chl + st + qtz + H_2O = cld + als.

Chloritoid also occurs in pseudomorphs after garnet that are filled with chlorite, chloritoid, muscovite, quartz and sometimes andalusite (Fig. 10f), but biotite not being present in the thin section. These pseudomorphs have many relic garnet inclusions. It is possible that garnet first decomposed into chlorite and staurolite in the reaction (7) and then staurolite was consumed and chloritoid was formed in the cooling reaction (10).

Zone III.1

In the southwestern side of Zone III, there is a narrow zone belt honzon where, unlike in Zone III, biotite occurs in peraluminous rocks. Sedimentary rocks in this zone are more coarse-grained and gneissose compared with the schists in Zone III. Therefore this zone is considered a separate metamorphic Zone III.1. Some peraluminous rocks contain garnet, staurolite and retrograde chloritoid, but Al_2SiO_5 polymorphs where not observed in this zone. Biotite is mostly randomly oriented and occurs in muscovite and chlorite-filled pseudomorphs, where biotite overgrows muscovite and chlorite and replaces also garnet from the rim. Pseudomorphs are sometimes elongated, having the crystal form of staurolite. Small randomly oriented staurolite crystals are sometimes present in these pseudomorphs. These textures indicate that the reaction

(11) chl + ms (± grt) = bt + st + qtz + H_2O

proceeded into both directions during cooling and reheating (Fig. 23c), staurolite having been decomposed

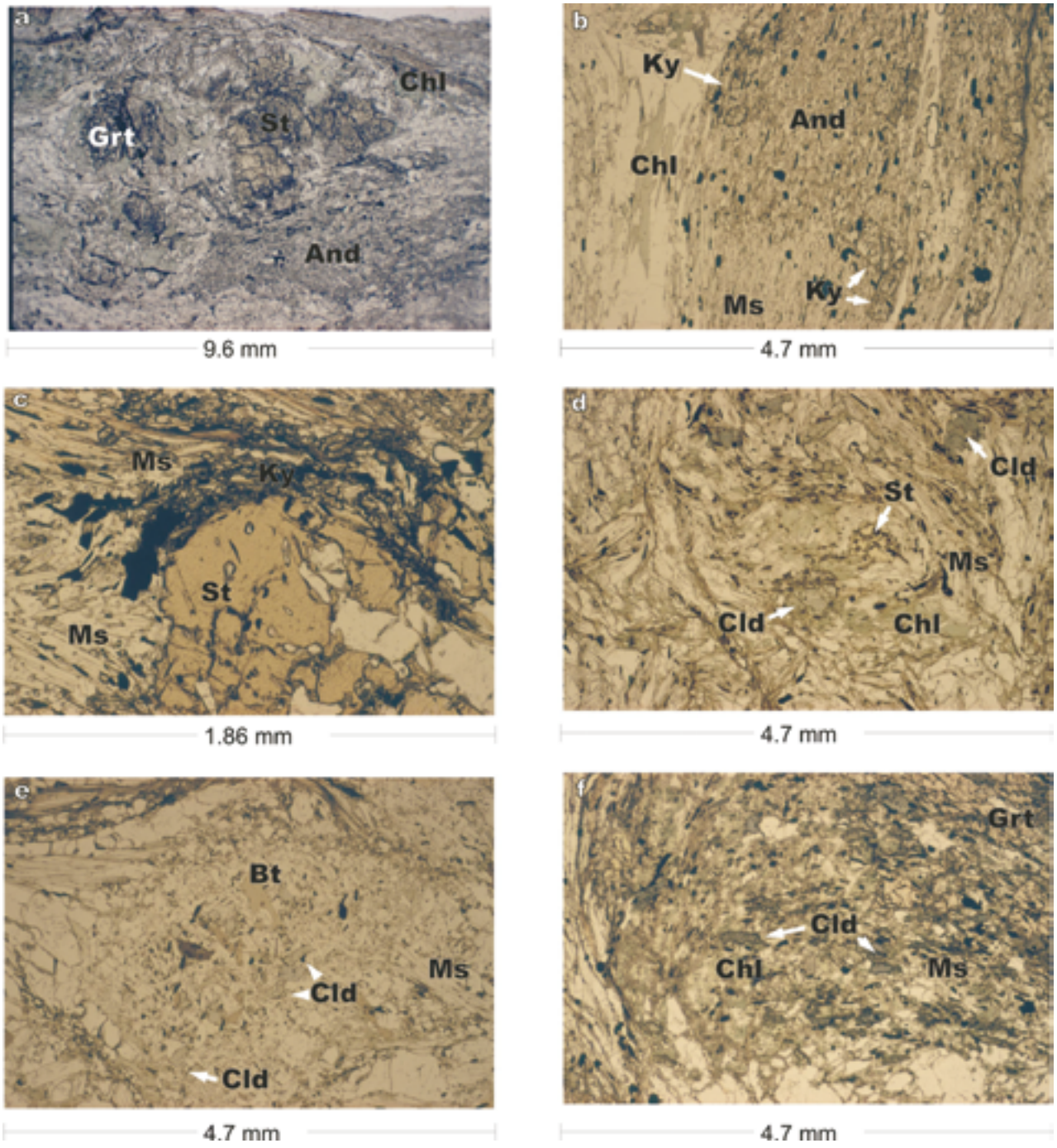

Fig. 10. Metamorphic textures and reactions in the zone III. a) Staurolite and chlorite replacing garnet, a big andalusite in the lower right corner of the figure. Sample PSH-98-60, N 7518130, E 3481410, b) Small kyanite crystals overgrowing andalusite and muscovite. Sample PSH-97-11.1, N 7517280, E 3478240, c) Small kyanite grains intergrown with muscovite on staurolite rims. Sample PSH-01-14.2, N 7521952, E 3519947, d) Chloritoid, chlorite and muscovite filled pseudomorph after staurolite, sample PSH-97-7.3, N 7528450, E 3485900, e) Biotite, chloritoid and muscovite filled pseudomorph. Sample PSH-98-41.2, N 7517980, E 3457930, f) Chlorite, chloritoid, muscovite and quartz filled pseudomorph after garnet. Sample PSH-97-7.4, N 7528450, E 3485900.

into chlorite and muscovite and then recrystallized with biotite again. Chloritoid occurs only in these pseudomorphs (Fig. 10e, PSH-98–41), having obviously been crystallized in the reaction

(12) st + chl + H_2O = cld + qtz

during cooling (Fig. 23c).

Zone IV

Zone IV represents the lowest grade metamorphic zone in the study area. The rocks sampled for this study are ultramafic, mafic and intermediate metavolcanic rocks and pelitic schists, although the latter are rare in Zone IV. Mafic and ultramafic metavolcanic rocks,

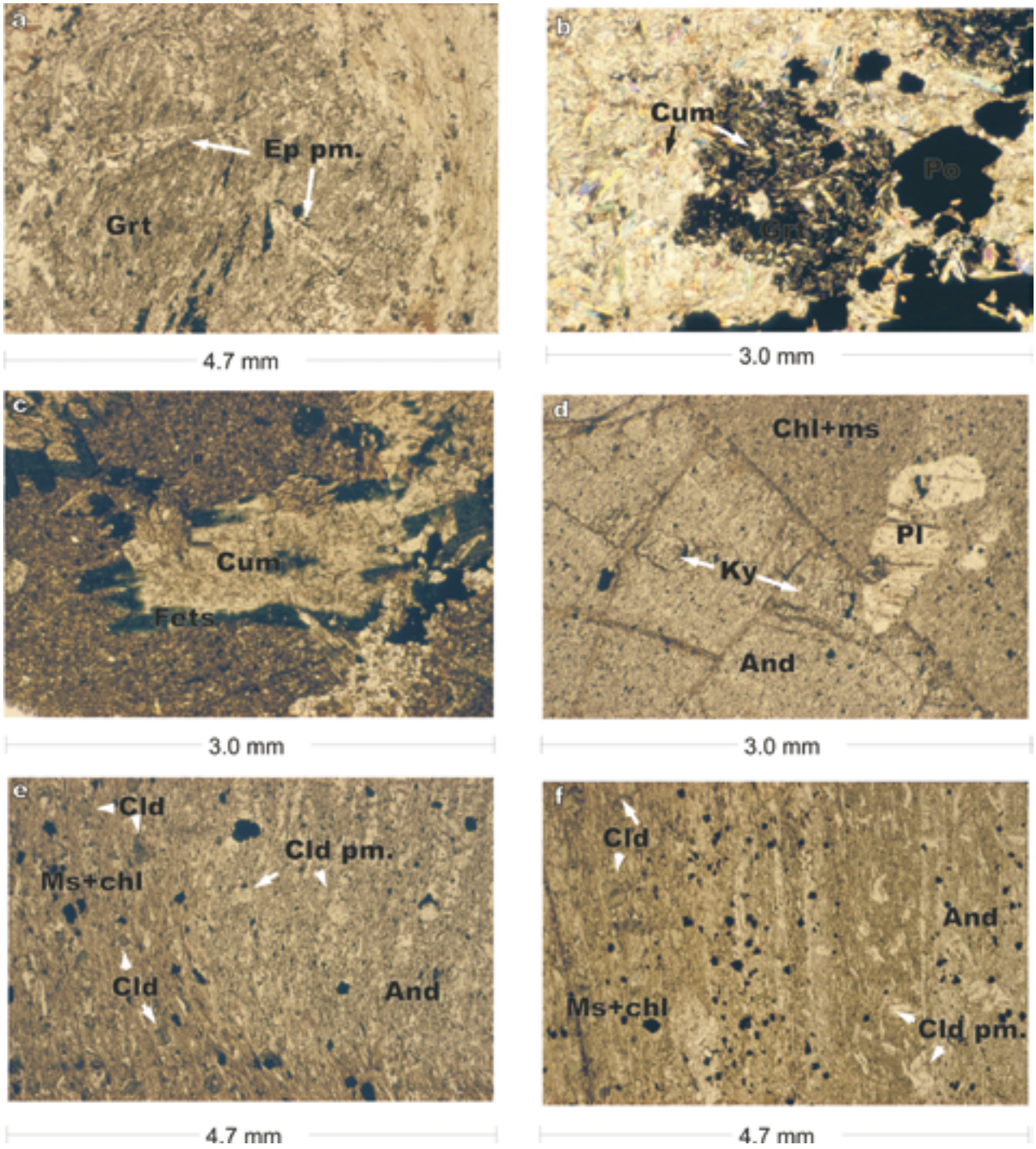

Fig. 11. Metamorphic textures and reactions in Zones III and V.1. a) A pseudomorph after epidote where the original crystal shape is preserved in garnet. Zone III, sample PSH-00-62.1, N 7548844, E 3460628, b) Cummingtonite inclusions in garnet. Sample PSH-00-1.4, N 7523465, E 2512075, c) Cummingtonite altering from rims to ferrotschermakite. Sample PSH-00-1.8, N 7525947, E 3385536, d) Kyanite inclusion in andalusite. Sample PSH-98-8.2, N 7480252, E 3486120, e) Chloritoids in the rock matrix and possible chloritoid pseudomorphs in andalusite. Sample PSH-98-4, N 7471821, E 3495325, f) Chloritoid inclusions in andalusite north of Zone IV. Sample PSH-98-59.3, N 7512570, E 3486600.

belonging to the Savukoski and Kittilä Groups, are the most abundant rock types in Zone IV. These rocks have generally preserved their primary volcanic textures with randomly oriented plagioclase phenocrysts, although in many cases these are carbonatized and epidotized. Carbonate seems to be more common in the NW part of the greenschist zone than in its eastern parts. Ultramafic rocks have usually preserved their magmatic mineral compositions, which are ol-tre-op±opx.

Pelitic schists are fine-grained, and if not pervasively sheared, they have preserved the primary structures, commonly seen as millimetre to centimetre scale sedimentary layers. Typical mineral assemblages are

chl-white mica-qtz-opaque minerals±pl±bt±tur±mnz and bt-chl-qtz-op±crb. The coarsest average grain size in the studied samples was ca. 0.05–0.1 mm, but finer-grained schists are common. Schists with the coarsest grain size are texturally granoblastic. Biotite and chlorite sometimes occur as porphyroblasts whose grain size is up to 0.5–1 mm in diameter.

Zone V

Zone V consist mostly of metapelites, and it shows a progressively increasing metamorphic grade from fine-grained andalusite schists to coarse-grained sillimanite gneisses east of the Sodankylä village (Fig. 8). Zone V.1 consists of pelitic schists which have centimetre-sized andalusites and ca 3–10 mm staurolite porphyroblasts in a fine-grained (ca 0.02–0.1 mm) matrix. The matrix of the rock is formed of chlorite, muscovite, chloritoid and quartz, and also magnetite grain aggregates are common. The matrix grain size is finest in rocks close to Sodankylä. The average grain size of the matrix generally coarsens southwards and eastwards in this Zone. Kyanite occurs as randomly oriented prisms (normally 0.2–0.5 mm in length but some prisms may be several millimetres) in the rock matrix and on andalusite grain boundaries and as inclusions in andalusite (Fig. 11d). Chloritoid inclusions in andalusite are rare, but andalusite often has inclusion free domains which have the shape of the chloritoid crystals in the matrix (Fig. 11e) which indicates that in cld-bearing rocks andalusite was formed in the reaction

(13) cld + qtz = and + chl + H_2O.

Some andalusite porphyroblasts have retrograde coronas formed of inner muscovite layer and outer chlorite layer. Plagioclase, when present, occurs like kyanite as randomly oriented idiomorphic 0.5–1 mm grains having many quartz and sometimes chloritoid inclusions. Biotite-bearing assemblages are rare, and tiny garnet was observed only in one thin section. Millimetre-sized pseudomorphs filled with chlorite, albite and muscovite are common, evidently these are hydrated plagioclases, staurolites and andalusites. Chloritoid is sometimes present in these pseudomorphs, indicating back-reaction (13). Monazite is a common accessory mineral in Zone V.1.

Prograde chloritoid occurs also north of the greenschist facies zone IV in a small area in the southern part of the zone III, where its textural relationships (inclusions in plagioclase and in andalusite, Fig. 11f) are exactly the same as in the zone V.1. It is possible that the greenschists are lying on the rocks of Zone III and Zone V, the metamorphic zonation of the pelite formation continuing under the allochthonous greenschists.

In Zone V.2, chloritoid disappears, evidently in the reactions (9), (10), (13) or in

(14) cld + qtz = chl + st + H_2O

(Fig. 23d). Metapelites in Zone V.2 are medium grained gneisses, not schists as in Zones V.1–2. Melting has not started and primary bedding is visible in many places. Staurolite and andalusite may be up to 1–2 cm in size, and kyanite prisms up to 1 cm are common. There are andalusite-bearing layers without kyanite and also kyanite-bearing layers without andalusite. Kyanite and andalusite occur also together, in these rocks kyanite is found in the matrix, as inclusions in andalusite, and as needles on andalusite rims (Fig. 12a). Kyanite inclusions found in andalusite may be an effect of two-dimensional thin sections, because on outcrops kyanite needles growing into andalusite are common.

In Zone V.3, biotite becomes stable occurring often as large flakes, and grain size the matrix of the coarsens in pelitic rocks. Sillimanite also rarely occurs as fibrolitic grains. Chlorite is less abundant in biotite-rich than in biotite-poor rocks, therefore it is possible that Zone V.3 represents the divariant KFMASH chlorite breakdown reaction (11) chl + mu = bt + st + qtz + H_2O, (Fig. 23d) that has consumed chlorite in some layers but not completely everywhere. In some outcrops andalusite, kyanite and sillimanite are found in the same thin section; in these rocks fibrolitic sillimanite is crystallized on plagioclase and mica rims rather than replaces kyanite or andalusite (Fig. 12b). This texture indicates that temperature increased into the field where the divariant KFMASH reaction

(15) st + ms = bt + als + H_2O

took place (Fig. 23d). Chlorite is often a retrograde phase, and in some exposures staurolites have almost completely altered into chlorite and muscovite, indicating back-reaction (11).

In Zone V.4, garnet was observed in one exposure where it occurs in textural equilibrium with relatively coarse-grained kyanite in the assemblage ky-st-bt-ms-pl-qtz-grt (Fig. 12c). This texture indicates that garnet was formed in reaction (5) bt + st + q = grt + ms + ky + H_2O. The assemblage and absence of other Al_2SiO_5 minerals indicates similar metamorphic conditions as in Zone II, differing clearly in pressure from the progressive zoning in V.1–3 and V.4.

In Zone V.5 andalusite was not detected any more and kyanite occurs only as small relics. Staurolites up to 1 cm and garnets and plagioclases up to 5–6 mm are common. Sillimanite is fibrolitic and replaces

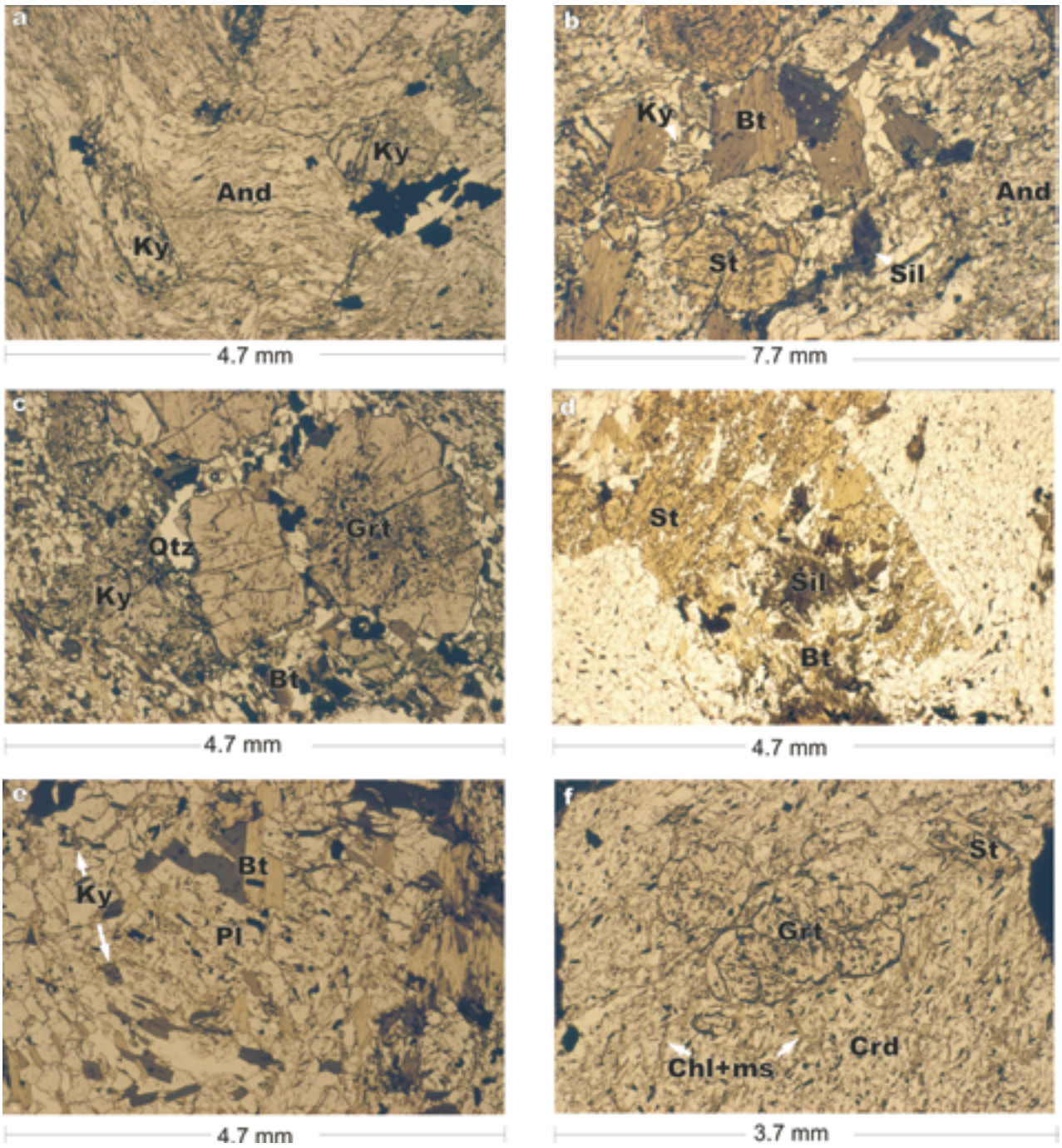

Fig. 12. Metamorphic textures and reactions in the zones V and VI. a) kyanite-andalusite assemblage, zone V.3, sample PSH-99-72.1, N 7485560, E 3511380; b) kyanite-andalusite-sillimanite-staurolite-biotite assemblage, zone V.4, sample PSH-00-113.2, N 7491153, E 3503060; c) garnet-kyanite-biotite-muscovite assemblage, zone V.4, sample PSH-98-53.2, N 7494530, E 3505680; d) fibrolitic sillimanite and biotite replacing staurolite, zone V.5, sample PSH-01-17.1, N 7521105, E 3535306; e) kyanite inclusions in plagioclase, zone V.5, sample PSH-01-17.2, N 7521105, E 3535306; f) garnet inclusions in cordierite, zone VI.2, sample PSH-98-69.1, N 7469020, E 3472710.

sometimes staurolite porphyroblasts together with biotite (Fig. 12d). These assemblages indicate that the reactions (5) and (15) locally consumed all staurolite in the sillimanite field. The matrix micas have strong preferred orientation (S3) but matrix quartz and feldspar have a granoblastic texture. Some garnet porphyroblasts are helisitic, containing plenty of quartz inclusions, but others are almost inclusion-free. When present, kyanite occurs locally as randomly oriented, small grains, and it commonly exists as inclusions in plagioclase, probably representing prograde relics (Fig. 12e).

Zone VI

Zone VI covers the area around granitoids of the central and western Lapland. At the western margin of Central Lapland Granitoid Complex, the grade

of metamorphism increases progressively towards the complex without abrupt change. In the eastern and northern side of the Central Lapland Granitoid Complex the change in grade from Zone IV and from Zone V is connected with shear zones.

In Zone VI.1, metapelites are fine-grained schists (average matrix grain size < 0.1 mm). Locally, biotite forms flakes up to 5 mm in a fine-grained matrix, and in one exposure there was one ca 10 mm cordierite; tiny andalusites and garnets are very rare in this Zone. In the country rock of the Pahtavuoma Cu-ore, garnet is locally present in the alteration zone as 1–3 mm idiomorphic grains, in skarns that are formed between amphibole-rich and carbonate-rich layers. The garnet-bearing assemblage is grt-bt-crb±cum±Fets. Garnet has often cummingtonite inclusions and cummingtonite is altered from rims to bluish green ferrotschermakite, which occurs also as idiomorphic grains, several millimetres in size (Figs 11b–c). These textures indicate that garnet and ferrotschermakite were formed in the reaction

(16) cum + cal = grs + Fets.

Another garnet-bearing locality is in the southern side of Zone IV, where garnet occurs in an iron-rich rock in the assemblage grt-amph-qtz. In the Pahtavuoma area schists with the matrix assemblage bt-qtz-cc locally have scapolite porphyroblasts 3–7 mm in diameter. Scapolite is not restricted only in this zone and in these assemblages but occurs also elsewhere in the Central Lapland area. Descriptions of the scapolite-bearing rocks are given by Tuisku (1985) and Frietsch et al. (1997).

In Zone VI.2, metapelites are medium grained gneisses with granoblastic matrix. Andalusite is a common Al-silicate but it often co-exist with fibrolitic sillimanite. Cordierite was observed only in a few localities. In the cordierite-bearing rocks garnet, when rarely present, occurs as inclusions in cordierite and on andalusite rims (Fig. 12f). Cordierite has also many muscovite inclusions, whose optical orientation does not differ from muscovite in the matrix, and it seems to replace andalusite from rims. It has also some chlorite inclusions, so the univariant KFMASH reaction

(17) chl + ms + and + qtz = bt + crd + H_2O

may have produced cordierites. In the cordierite-bearing rocks garnet, when rarely present, occurs as inclusions in cordierite and on andalusite rims (Fig. 12f). Because cordierite has some staurolite inclusions, the garnet may also have been a reactant and earlier mineral than cordierite in a reaction such as

(18) grt + and + H_2O = crd + st + qtz.

Fibrolitic sillimanite often replaces andalusite from rims, indicating reaction

(19) and = sil

Kyanite was observed only in one outcrop (PSH-98–11). There andalusite, kyanite and sillimanite occur in the same Mg-rich, coarse-grained metapelite. Assemblages in this rock are bt-ms-ky-crd-qtz±and±sil±chl, bt-ms-crd-qtz±sil and ky-and-sil-ms-crd-qtz. Sillimanite occurs as fibrolitic grain aggregates, kyanite forms coarse-grained prisms up to 5–10 millimetres and andalusite occurs as centimetre-sized helisitic grains with abundant quartz inclusions. Sillimanite often replaces andalusite in grain boundaries (Fig. 13a) but rarely kyanite, which forms intergrowths with muscovite and cordierite. Kyanite and andalusite occur as inclusions in cordierite, and cordierite coronas are formed between kyanite and biotite, cordierite forming embayments into biotite (Figs 13b–c). Sillimanite replaces this muscovite and sometimes occurs as inclusions in cordierite together with muscovite. Although often close to each other, andalusite and kyanite were not found in contact, therefore their cystallization order is unclear. However, if they underwent similar metamorphism than Zones V.1–4, kyanite crystallization may have been roughly simultaneous with andalusite. With increasing temperature they were partly altered into sillimanite and cordierite was formed in a continuous reaction between Al-silicate (ky, and, sil) and biotite

(20) bt + als + qtz = crd + ms.

In garnet and staurolite-bearing rocks of Zone VI.2, andalusite contains inclusions of quartz, biotite, muscovite, chlorite, skeletal staurolite and euhedral garnet (Fig. 13e), indicating that andalusite was formed in reactions such as (5), (15) and

(21) chl + st + qtz = grt + and + H_2O.

In the Mertavaara area there are garnet and andalusite-bearing muscovite-free rocks, where both garnet and andalusite have staurolite inclusions, indicating reactions (5) and (21).

Strong retrogression is a typical feature in Zone VI.2. Hydration has often destroyed previous garnet, andalusite and staurolite that are now pseudomorphs, filled with fine grained muscovite, biotite and chlorite. Garnets have also been altered into plagioclase and chlorite (Fig. 13f), and sometimes staurolite, plagioclase and biotite replace garnet from rims indicating back-reaction (5). Some back-reaction (16) obviously took place in andalusite-bearing rocks, because andalusite is often rimmed by staurolite.

Zone VI.3 represents sillimanite grade, where the

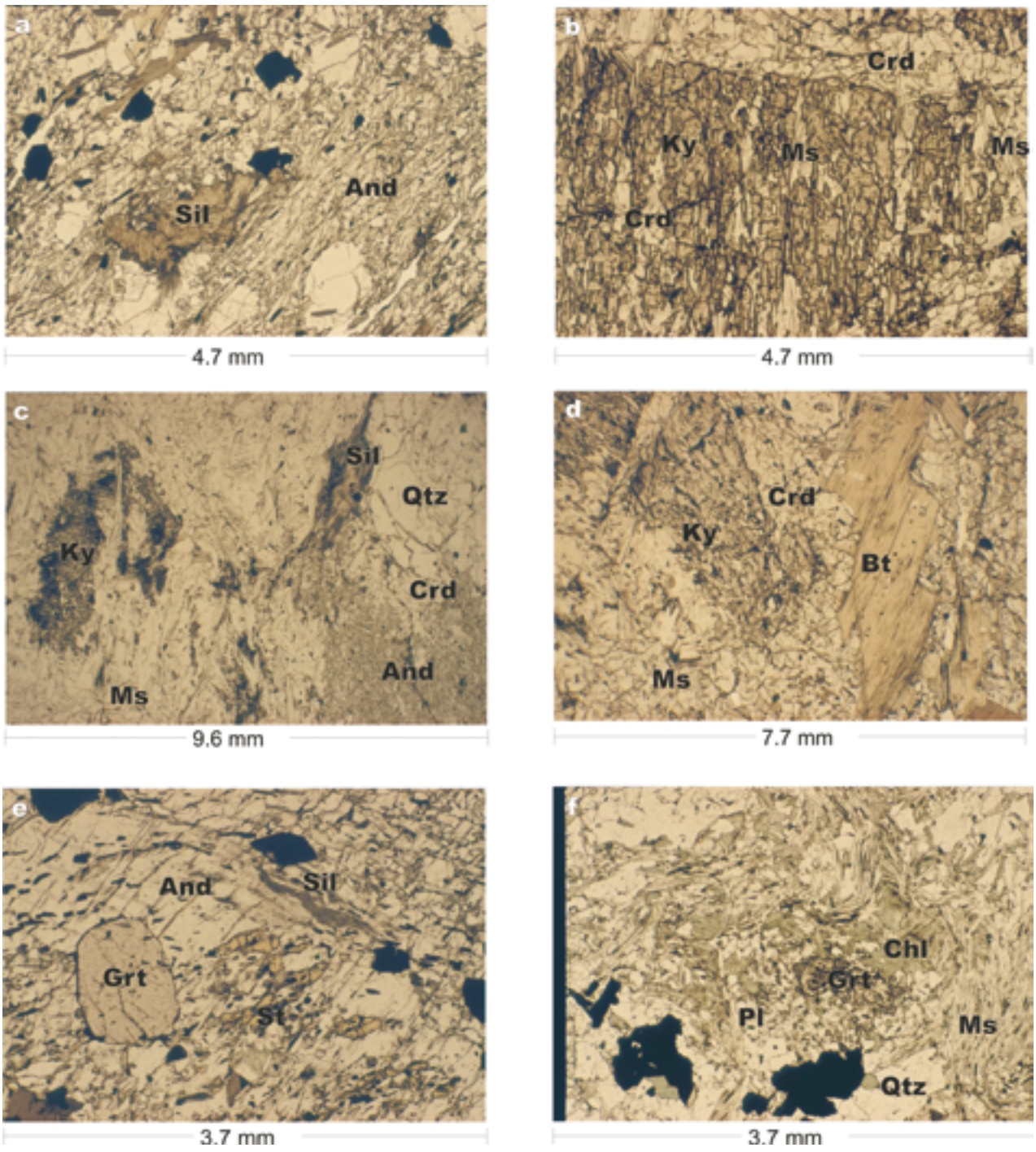

Fig. 13. Metamorphic textures and reactions in Zone VI.2 a) Fibrolite needles on andalusite rim, sample PSH-98-97.3, N 7495066, E 3416256, b) Kyanite intergrowths with cordierite and muscovite. Sample PSH-98-11B, N 7466644, E 3466995, c) Coexisting andalusite, fibrolitic sillimanite and kyanite, andalusite is replaced by cordierite corona. Sample PSH-98-11.2, N 7466644, E 3466995, d) Cordierite corona between kyanite and biotite. Sample PSH-98-11B, e) Staurolite, sillimanite and garnet inclusions in andalusite. Sample PSH-98-97.5, N 7495066, E 3416256, f) Garnet altering into plagioclase and chlorite. Sample PSH-98-18.2C, N 7485693, E 3447609.

high grade seems to be caused mainly by granitoid intrusions. Sillimanite is the only Al_2SiO_5 polymorph in this zone. There may be some changes in grade inside the zone, depending e.g. on the distance from granitoid contacts, but those variations could not be mapped during the course of this study. Locally metapelites are migmatitic, for example on the western side of the Central Lapland Granitoid Complex, where pelitic rocks become migmatitic close to the contact of granitoids, having granitic leucosomes as narrow stromatic veins. In Zone VI.3, sillimanite is the only Al_2SiO_5 mineral, although these rocks still contain grt-als-st-bt-ms-chl-pl-qtz assemblages, typical for Zone VI.2. This indicates, that the Al_2SiO_5-forming

reactions observed in Zone VI.2 started in the andalusite and continued in the sillimanite field in Zone VI.3. The western part of the zone VI.3 is characterized by potassium-feldspar-rich, reddish gneisses, which often are plagioclase-free. Idiomorphic and subidiomorphic potassium-feldspars are surrounded by interstitial quartz in these rocks, a texture suggesting that feldspars were crystallized from melt.

In mafic rocks, clinopyroxene is a rare mineral. With normally a granoblastic texture. In these rocks, epidote and chlorite are retrograde minerals, typically occurring in fractures and shear planes.

Metamorphic zones and gold mineralization

The Central Lapland area has tens of known gold occurrences; some of those are economic (Eilu, 1999). These occurrences belong to the orogenic gold deposit group following the classification of Groves et al. (1998). They argued, that orogenic gold deposits were formed during compressional to transpressional deformation processes at convergent plate margins in accretionary or collisional orogens. According to McCuaig & Kerrich (1998), the accretionary environment is indicated by the distribution of orogenic gold deposits in belts of great geological complexity, with gradients of lithology, strain, and metamorphic grade. Most – although not all – and the largest of these deposits occur in terranes that were metamorphosed in greenschist facies. In Fig. 8, there are plotted most of the known gold occurrences in the study area. This figure shows, that the majority of them are located in the greenschist facies Zone IV. The country rocks of orogenic gold deposits are mostly strongly altered, mafic and ultramafic volcanic rocks, having white mica, biotite and carbonate assemblages in the alteration zones (Korkiakoski 1992, Eilu 1994, Patison 2007).

Deformation and the growth of metamorphic minerals

In Central Lapland, the early structural evolution (D1+D2) is characterized by subhorizontal folds and foliations observed throughout the study area, although in some subareas this might have caused more steeply dipping structures. The late structural evolution (D3 and later) is characterized by highly variable strike, dip and intensity of different structural elements. Because the area is generally poorly exposed, the relationship of the metamorphic mineral growth with these deformations can be reliably demonstrated only in a few localities.

In Zone I, the rock texture is normally granoblastic, indicating annealing close to the metamorphic peak. In Zone II, the main foliation of the rock (S2) wraps around garnets and staurolites which have curved inclusion trails, suggesting syntectonic growth with D2 (Fig. 14a). Some big garnets have plenty of quartz inclusions in the core but very few in the edge (Fig. 14b), indicating rapid growth during the early stage of the garnet crystallization. Many kyanites are elongated along the S2 (Fig. 14a), but generally randomly oriented kyanites overgrow S2. Some muscovites in these rocks are similarly randomly oriented (Fig. 14c). These features suggest that kyanite growth partly took place during a static period of deformation in reactions such as (7) or (11).

In Zone III, garnet and staurolite have curved inclusion trails, indicating syntectonic growth during D2. S2 wraps around these porphyroblasts (Fig. 3a). S2 is not curved around andalusite, but andalusite growth evidently took place during D2 because the early S2 crenulation cleavage is preserved as inclusion trails in andalusite. The S2 crenulation cleavage is absent or weak in the matrix close to andalusite (Fig. 14d). Kyanite and chloritoid are fine-grained and overgrow S2 as randomly oriented crystals (Figs 10d–f and 14e) although chloritoid occurs also elongated along S2. In Zones II–III, observations could only rarely be made from fold, hinges, so e.g. Fig. 14d can record a situation on the limb of F3 fold where S2 and S3 are parallel, consequently the crenulation cleavage in andalusite in Fig. 14b could represent either S2 or S3. In the cordierite-orthoamphibole rocks of the Siltaharju area, orthoamphibole is generally elongated along S2, but may also randomly overgrow the F3 fold hinges (Fig. 15a).

Zone V is relatively well-exposed, so that observations on the porphyroblast growth could be made on the fold hinges. In this area, D3 deformation formed upright, slightly reclined and even recumbent folds, whose axial surfaces are in E-W direction and vergences to the north. F3 folds have a well developed axial plane crenulation cleavage, S3. In Zone V.1, andalusite and staurolite occur as helisitic porphyroblasts having many quartz and magnetite inclusions trails which are sometimes sligthly curved near the grain boundaries when the bedding parallel S1/S2 foliation is well developed in the matrix. Generally andalusite overgrows S1/S2, but occasionally S1/S2 foliation wraps around andalusite porphyroblasts. S1/S2 wraps clearly around chloritoid grains (Fig. 11e). In Zones V.2 and V.3, andalusite, kyanite, staurolite and plagi-

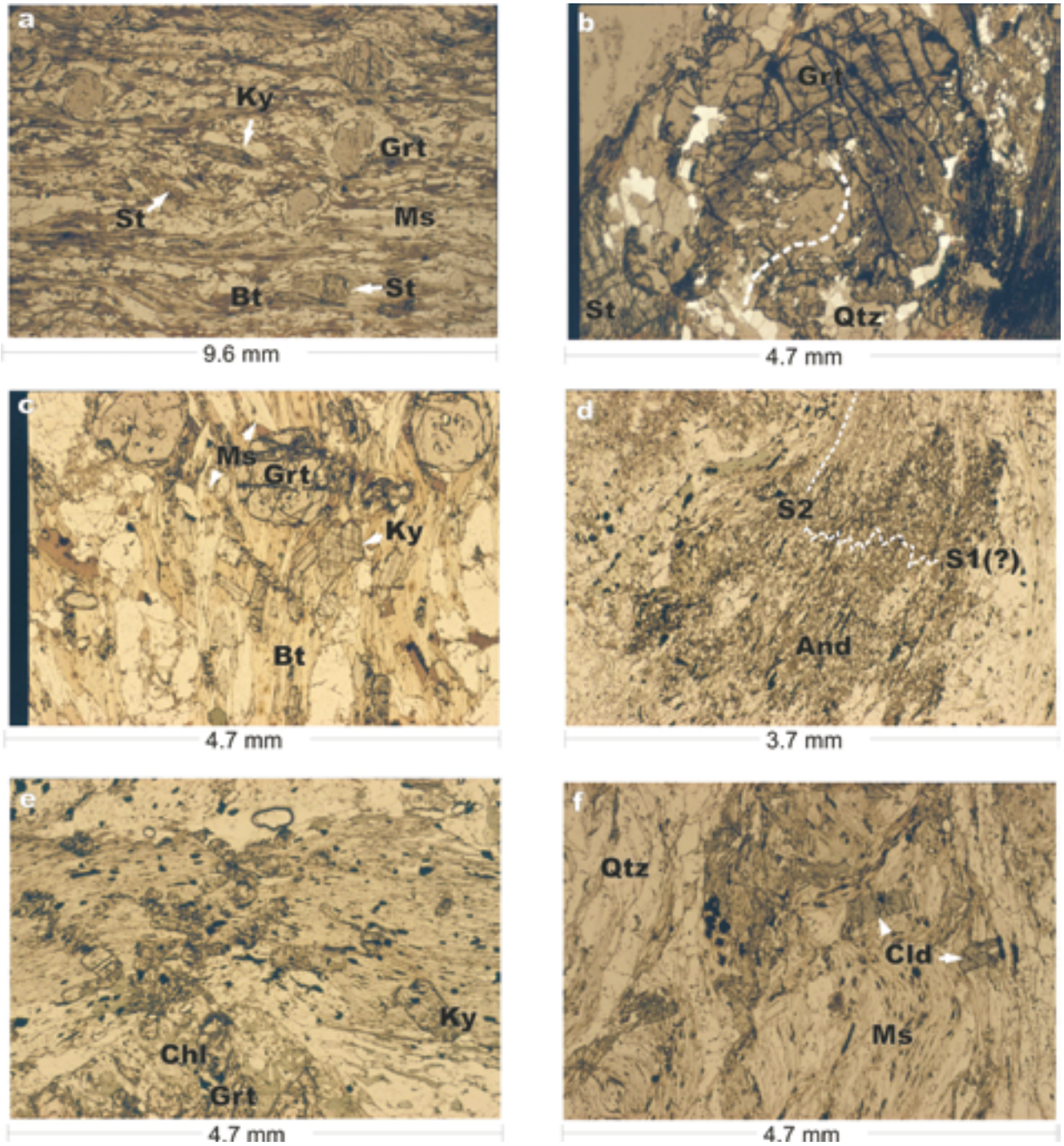

Fig. 14. Textures indicating the relationship of mineral growth with deformation phases in Zones II–III. a) Curved inclusion trails in staurolite and garnet and S2 parallel kyanite. Zone II, sample PSH-99-102.2, N 7563820, E 3450900, b) Curved quartz inclusion trails in a garnet with an inclusion-poor rim. Zone II, sample JTV-98-32.1, N 7552059, E 3457464, c) Randomly oriented kyanites and muscovites overgrowing the S2 schistosity. Zone II, sample PSH-99-99, N 7576623, E 3445579, d) S2 Crenulation in andalusite. Zone III, sample PSH-98-60, N 7518130, E 3481410, e) Randomly oriented kyanite grains overgrowing the main foliation. Zone III, sample PSH-97-11.1, N 7517280, E 3478240, f) Randomly oriented chloritoids overgrowing the main foliation. zone III, sample PSH-97-7.2, N 7528450 E 3485900.

oclase overgrow the S3 crenulation cleavage which can be seen as inclusion trails in these minerals (Figures 15b–c). This observation was also made by Evins & Laajoki (2002), their D2 corresponding with D3 of this study. The S3 crenulation cleavage sometimes wraps around andalusite and staurolite, indicating that their growth took place during D3. Kyanite mostly occurs as randomly oriented grains (Fig. 15c). The relationship of kyanite to D3 deformation is similar to that of orthoamphibole in the Siltaharju area, although this does not mean that D3 was coeval everywhere in Central Lapland. In Zones V.3–V.5, rock textures show signatures on annealing, matrix minerals forming dihedral angles. In annealed rocks, biotite sometimes occur as randomly oriented flakes.

Also in the zone VI.2, the F3 crenulation cleavage is

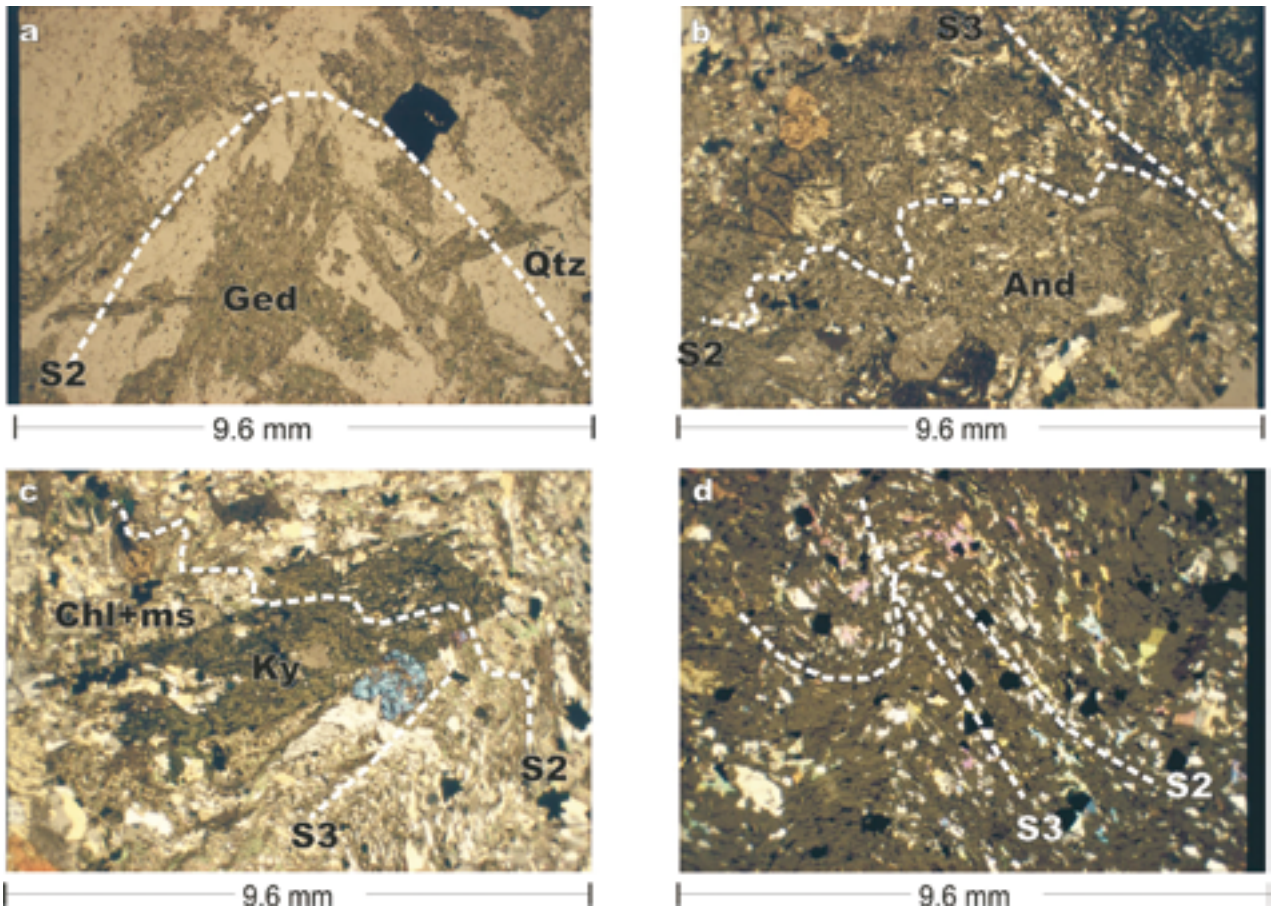

Fig. 15. Textures indicating the relationship of mineral growth with deformation phases in the zones II–VI. a) chloritized orthoamphiboles overgrowing F3 fold hinges, sample PSH-97-32.4, zone II, N 7544700, E 3494300; b) S3 crenulation as inclusion trails in andalusite, sample PSH-99-72.2, zone V.3, N 7485560, E 3511380; c) S3 crenulation as inclusion trails in kyanite prism, same exposure than in Fig. 16b, sample PSH-99-72.5; d) open S3 crenulation in andalusite, zone VI.2, sample PSH-98-97.5, N 7495066 E 3416256.

seen as inclusion trails in big andalusite porphyroblasts. In the western part of the study area, the S3 crenulation cleavage wraps around andalusites grains, which have sigmoidal quartz inclusion trails (Fig. 15d).

Above mentioned textural features indicate that regional metamorphism started during D2 and in the northern zones it may have reached its peak during the D2. In Zone V.1, the PT conditions were in the chloritoid field during D2. Some andalusite and staurolite may have crystallized already then, but as in Zone VI.2, their growth took place mainly during D3, especially in Zones V.2–V.5 where chloritoid is not stable. In Zone V.1 the D3, structures are more brittle forming shear planes where all minerals are deformed.

Mineral compositions

Analytical procedure

Mineral analyses were done in the laborotory of the Geological Survey of Finland, and at the microprobe laboratory of Department of Earth Sciences in the Uppsala University using CAMECA SX-50 microprobes. The beam width was 10 µm for micas and feldspars and 1 µm for other minerals. The sample current was 25 nA for micas, garnets and amphiboles 15 nA for feldspars and cordierites. The acceleration voltage was 15 kV. Natural standards and the ZAF correction program were used. All analyses at the Uppsala University microprobe laboratory were done using sample current of 15 nA and acceleration voltage of 20 kV and. Altogether 1700 microprobe analyses were done from the study area. Selected analyses from various metamorphic zones are presented in Appendix 1.

Garnet

Although the Lapland Granulite Belt was not included in this study, one garnet was analysed for comparison from peraluminous migmatite of this belt, whose zoning profile is presented in Fig. 16a

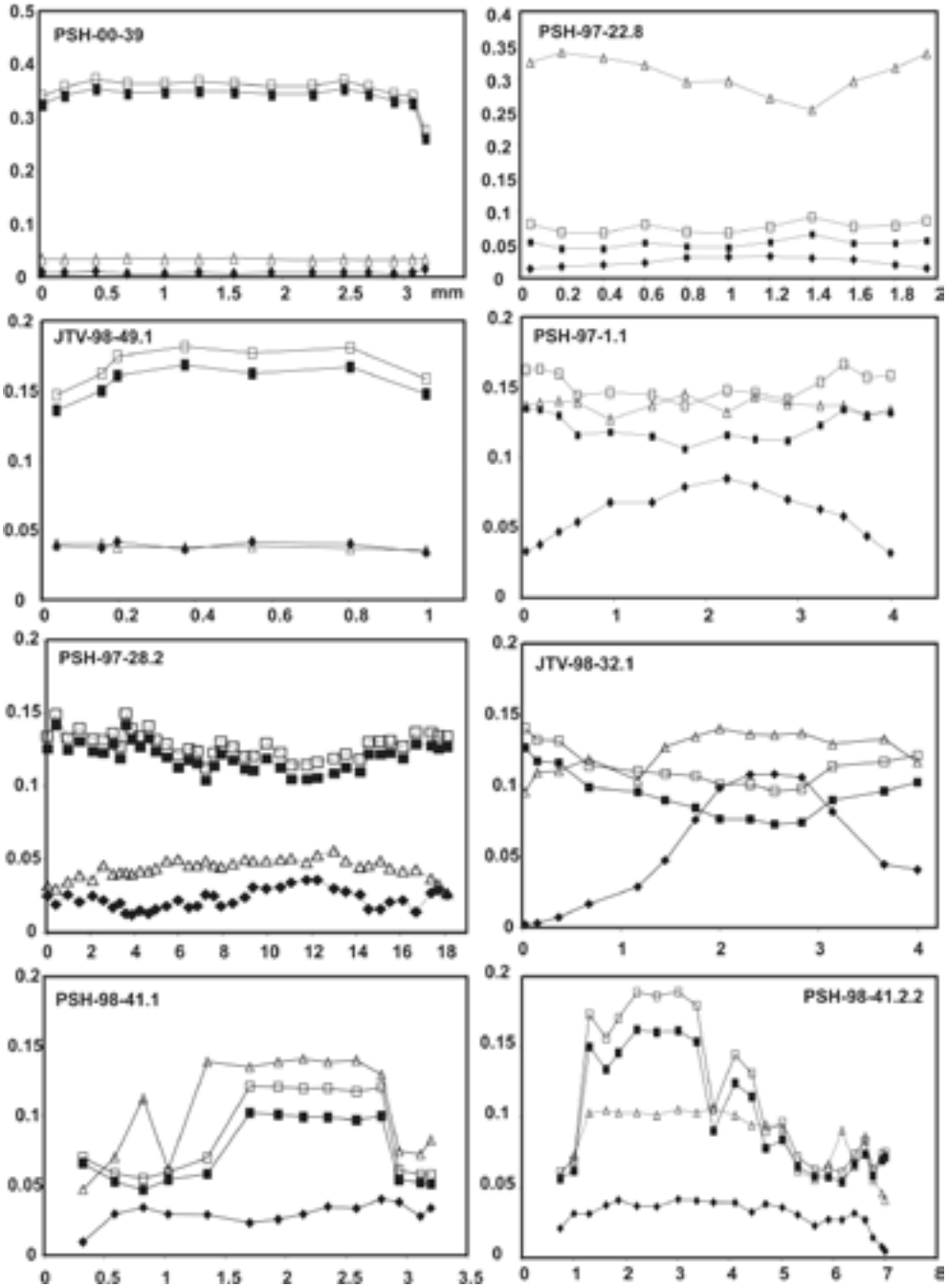

Fig. 16a. Composition profiles of garnets. Y-axis of the figures is the mole fraction. Symbols: open squares = Mg/(Mg+Fe), filled squares = Mg/(Fe+Mn+Mg+Ca), open triangles = Ca/(Fe+Mn+Mg+Ca), filled diamonds = Mn/(Fe+Mn+Mg+Ca). Sample PSH-00-39, Lapland Granulite Belt, N 7599934, E 3460762; sample PSH-97-22.8, zone I, N 756382, E 3493470; sample JTV-98-49.1, zone II, N 7576663, E 3445005; sample JTV-98-32.1 (the same garnet as in Fig. 14b), zone II, N 7552059, E 3457464; sample PSH-97-28.2, zone III, N 7543200, E 3495550; sample PSH-97-1.1, zone III, N 7544752, E 3493952; sample PSH-98-41.1, sample PSH-98-41.2, zone III, N 7517980, E 3457930.

(PSH-00–39). This garnet is Mg-rich with Mg-number (Mg/Mg+Fe) at around 0.35, which is clearly higher than in any analysed garnet in the other metamorphic zones.

In Zone I, garnets were analysed only in mafic rocks. Garnet in the sample PSH-97–22.8 is Ca-rich compared with other garnets, the X_{Ca} is from 0.25 to 0.34, increasing from core to rim (Fig. 16a). X_{Mg} in this garnet is low, from 0.05–0.07. Sample PSH-00–40 has also Ca-rich garnets with X_{Ca} from 0.31–0.32, but the X_{Mg} is higher, from 0.08 in the rim to 0.14 in the core.

In Zone II, garnets were analysed in metapelites. Compositionally, small inclusion-free garnets are only weakly zoned, but the zoning is much stronger in large garnets like JTV-98–32.1 in Fig. 16a. In this garnet, X_{Mg} is increasing and X_{Ca} and X_{Mn} decreasing from the core to the rim. In many of the zone III gar-

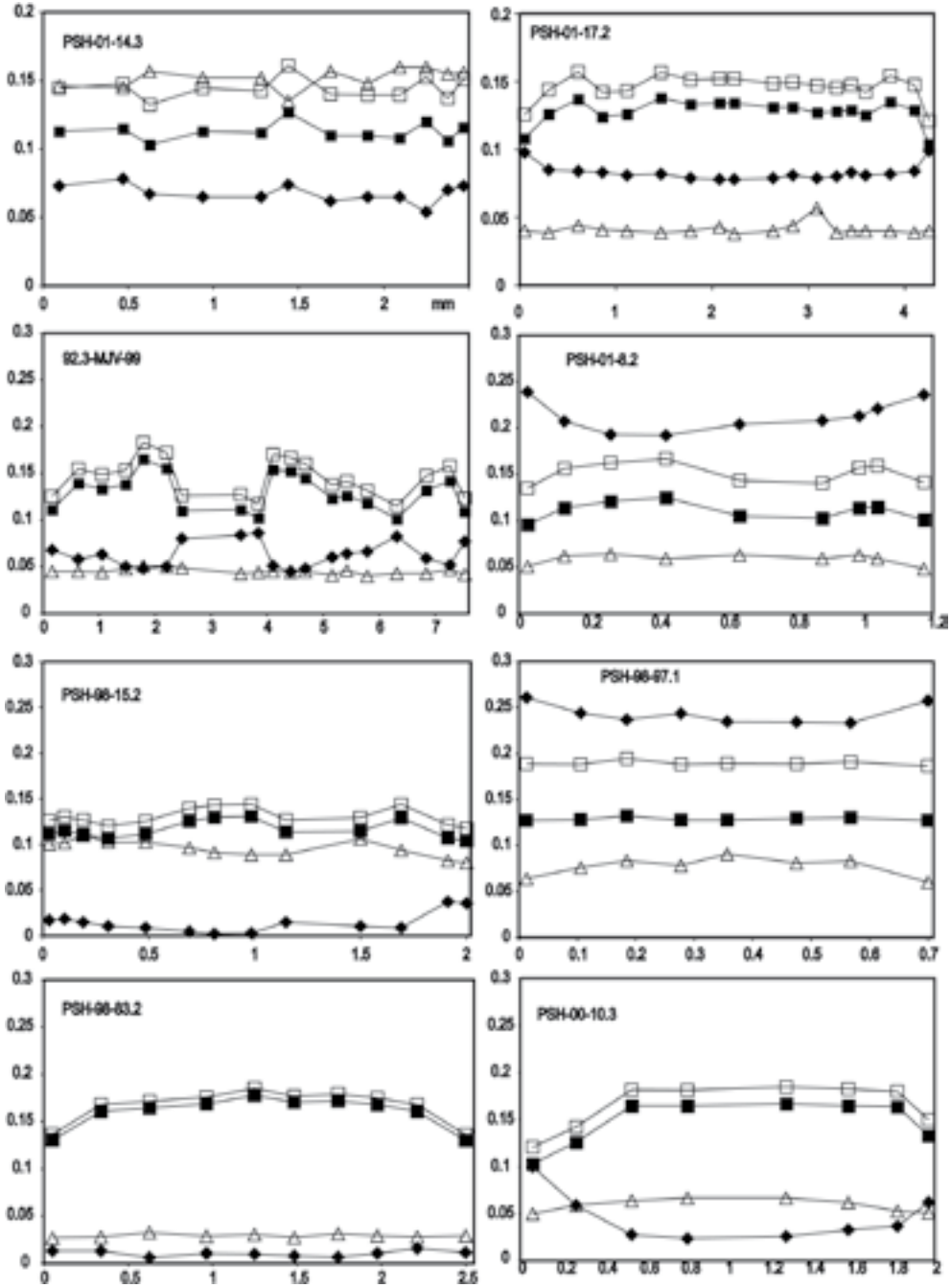

Fig. 16b. Composition profiles of garnets. Sample PSH-01-14.3, zone III, N 7521952, E 3519947; sample PSH-01-17.2, zone V.4, N 7521105, E 3535306; sample 92.3-MJV-99, zone V.4, N 7476970, E 3533028; sample PSH-01-8.2, zone V.4, N 7504537, E 3513451; sample PSH-98-15.2, zone VI.2, N 7481728, E 3449834; sample PSH-98-97.1, zone VI.2, N 7495066, E 3416256; sample PSH-98-83.2, zone VI.3, N 7493544, E 3378613; sample PSH-00-10.3, zone VI.3, N 7557588, E 3409926. Symbols as in Fig. 16a.

nets, both in pelitic and mafic compositions, the X_{Mg} is increasing from the core to the rim and the X_{Mn} is decreasing. Big garnets of the samples PSH-98–41.1 and PSH-98–41.2.2 from Zone III.1 have several decreases and increases in Ca and Mg in composition profiles that are made across large grains (Fig. 16a). This probably does not indicate several PT changes during the garnet crystallization because the decreases in X_{Mg} in the core area of the grain are near fractures which were healed during the late garnet growth. The general zoning pattern in these garnets is that that they have Ca and Mg rich core areas and these components are decreasing to the rim.

Garnet extracted from the sample PSH-97–28.2 (Fig. 16a) is from cordierite-orthoamphibole rock of Zone III. The zoning profile across this garnet is 18 mm, and it shows only a slight increase in X_{Mg} from the core (0.10–0.12) to the rim (0.12–0.14). It has Ca

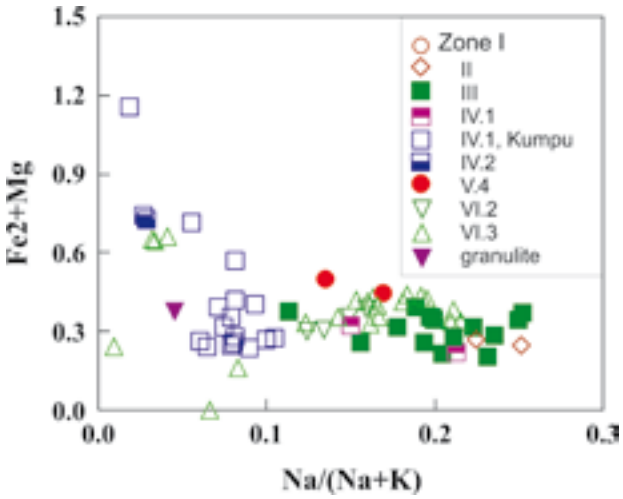

Fig. 17. Fe2++Mg vs. Na/(Na+K) plot of muscovites.

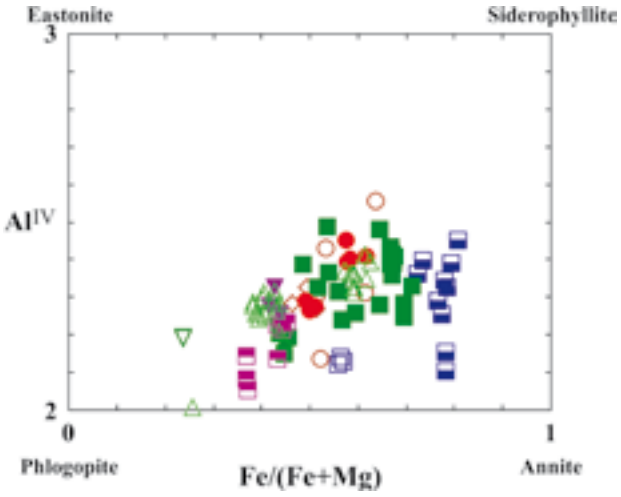

Fig. 18. Plot of biotites in the phl-ann-east-sid field. Symbols as in Fig. 17.

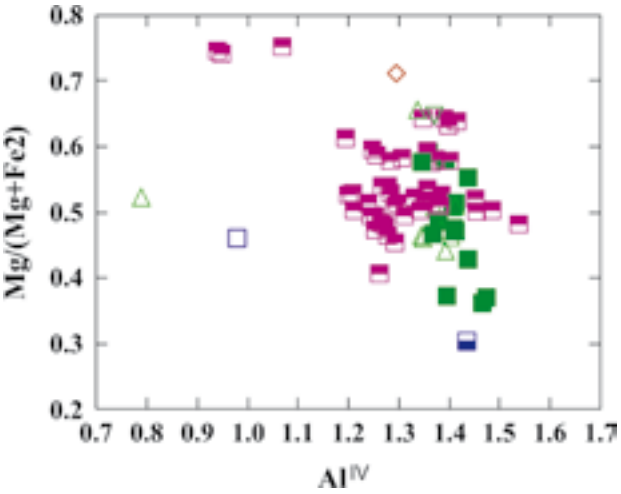

Fig. 19. AlVI vs. Si of chlorites. Symbols as in Fig. 17.

and Mn in small abundances, X_{Ca} slightly decreasing to the rim. Garnets from skarns and iron formations from Zone VI.1 are very Mg-poor and rich in grossular and almandine.

Muscovites in the rocks of the Kumpu group (Zone IV) clearly differ from most other white micas in their Na contents (Fig. 17). The Na/(Na+K) is lower than 0.1 in the white micas of the Kumpu formation in Zone IV, but higher than 0.1 in most muscovites from the other zones. Muscovites from other rocks in the zone IV have higher Na/(Na+K) ratios, indicating that their crystallization does not represent the same PT conditions than muscovites from the Kumpu formation (cf. Guidotti 1984). Some muscovites from Zone VI.3 and in the Lapland Granulite Belt also have low Na/(Na+K), which indicates a retrograde origin for these white micas. Fe and Mg contents are slightly higher in muscovites with low Na/(Na+K) than in other white micas.

Biotites have Mg-numbers roughly between $Mg_{30–60}$, depending generally on the Mg content of garnet, and therefore both the PT conditions and the whole rock Fe/Mg ratio (Table 2 and Fig. 18). Biotites in skarns and iron-formations in Zone VI.1 have the lowest Mg-numbers. Al^{VI} values are lowest in biotites from the greenschist facies zone IV. TiO_2 is from 1–3 wt% in the other zones but 3.2–3.7 wt% in the zone I samples and 4.1–4.3 wt% within biotites in the Lapland Granulite Belt.

Chlorites have highly variable Mg-numbers from Mg_{30}–Mg_{75}, mostly varying between Mg_{40}–Mg_{70}. The Si content is higher in most chlorites from the zone IV (Si 2.9–3.4) than in chlorites from the other zones (Si 2.7–2.9). Si content is high also in chlorites from one sample from Zone VI.3 (Fig. 19), indicating that these chlorites are retrograde. Al^{VI} is lower in many chlorites from zone IV (0.9–1.6) than in the other zones (1.3–1.5) but Al^{VI} also overlaps within various metamorphic zones, indicating that chlorite in amphibolite facies zones is mostly retrograde.

Calcic amphiboles are mostly actinolites in Zone IV, with a few ferroactinolitic compositions, following the amphibole classification by Leake (1978). Actinolitic and ferroactinolitic hornblendes occur close to the boundaries of Zone IV. In the other zones amphiboles are magnesiohornblendes, ferrohornblendes, tschermakitic and ferrotschermakitic hornblendes. In the analysed skarns and Fe-rich rocks from the zone VI.1 amphiboles are ferrotschermakites (Fig. 20). In Zone VI.3 Mg-rich actinolite occurs in scapolite, biotite and clinopyroxene-bearing mafic rock. In the zone III the analysed optically zoned amphiboles have bluish green magnesio-hornblende cores and lighter ferrotschermakitic rims. Orthoamphibole from Zone III (sample PSH-97–28.3) have Mg-numbers at $Mg_{33–36}$. The Na_2O content is 1.6–1.8 wt% and Al_2O_3

Table 2. Summary of the composition of garnets, plagioclases and biotites. Garnet compositions deviating remarkably from the average and their sample codes in each metamorphic zone are in italics.

Zone			**grt**	**grt**	**grt**	**grt**	**pl**	**bt**
	Rock type		$100 \cdot X_{Fe}$	$100 \cdot X_{Mn}$	$100 \cdot X_{Mg}$	$100 \cdot X_{Ca}$	$100 \cdot X_{Ca}$	100·Mg-nr
LGB	pelitic	cores	61–63	01	34–35	03	46	56–58
		rims	69–72	01–02	23–26	03		
I	mafic	cores	55–60	03–04	18–22	19–23	48–68	36–48
		rims	57–60	03–04	09–18	19–22	61–71	
PSH-00–40	mafic	core	52–55	02	13–14	31–32	62	*39*
		rim	*55–56*	*03–05*	*07–12*	*31*	*57*	
PSH-97–22.8	*mafic*	*core*	*61–65*	*02–03*	*05–07*	*25–30*	*41*	
		rim	59–61	*01–02*	*04–06*	*32–34*	*47*	
II	pelitic	cores	73–76	05–06	15–17	04–06	32–38	49–54
		rims	75–78	03–04	13–15	03–04		
III	pelitic	cores	68–75	02–11	07–12	11–16	42–53	51–59
		rims	76–89	01–07	05–14	04–11		
PSH-98-41.2.2	pelitic	core	*68–70*	*02–04*	*15–17*	*10–11*	*41*	*33*
		rim	*82–89*	*005–008*	*06–09*	*03–08*		
PSH-97-1.1	mafic	core	66–69	05–07	11–12	13–14	39	
		rim	68–70	03–04	13–14	13–14		
PSH-97-38.2	*mafic*	*cores*	*73–74*	*09–11*	*03–04*	*11–16*	*36*	*29–30*
		rims	74–75	*09–11*	*03–04*	*9–15*		
	crd-oam rocks	cores	79–82	03–05	11–14	03–06	05–19	41–48
		rims	77–82	02–06	12–14	02–06	03–20	
IV.1	mafic						01–20	
	pelitic						09–31	55–63
Kumpu	pelitic							43–44
Kumpu	quartzite							
IV.2	skarn	cores	59–67	15–25	02–03	13–17	49–57	19–22
		rims	62–67	14–17	02–03	13–16		
83.2-MJV-99	Fe-formation	core	72–73	15	04	09–10	86–87	27–28
		rim	72	14	04	11		
V.4	pelitic	cores	74–78	05–08	11–17	04–06	36–51	38–50
		rims	75–77	07–10	10–11	04–05		
PSH-01-8.2	*pelitic*	*core*	*62–63*	*19–24*	*10–13*	*06*	*49*	*49–50*
		rim	*61–62*	*24*	*10*	*05*		
VI.2	pelitic	cores	50–56	23–31	06–13	05–15	38–39	38–60
		rims	52–56	25–31	06–12	06–12		
PSH-98-15.2	pelitic	cores	76–79	*003–02*	*11–13*	*10–11*	*35–38*	*38–41*
		rims	*76*	*02–03*	*11*	*09*	*35–37*	
PSH-98-11	*pelitic*							*76*
PSH-98-16.1	mafic	cores	61–63	07–09	07–08	22–24	40–43	
		rims	61–62	06–07	08	23		
VI.3	pelitic Mn-rich	cores	51–55	23–31	12–15	05–09	40–44	57–60
		rims	52–56	26–31	12–14	04–06		
	pelitic	cores	74–80	01–06	16–18	03–07	40–43	37–58
		rims	75–83	01–04	10–15	03–05		
PSH-98-80.1	pelitic Mn-rich	cores	24–26	57–60	06–08	09–11	97–99	61–62
		rims	24–26	56–59	06–08	09–10		
PSH-98-85.3	pelitic Mn-rich	cores	25–26	41–45	07–08	22–24	97–99	55–56
		rims	27	45	05	23		
	mafic						61–92	74–75

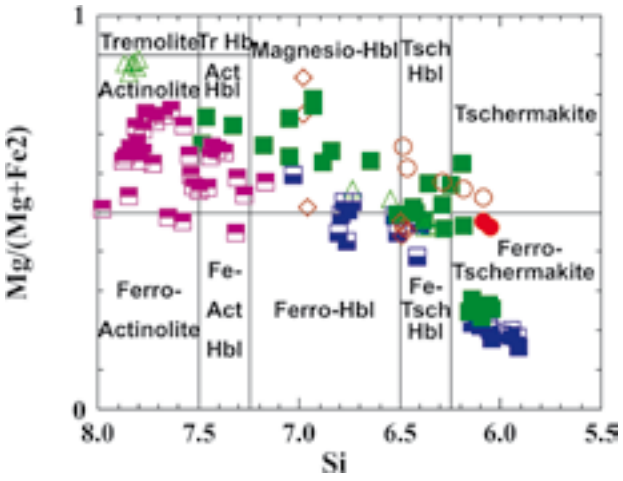

Fig. 20. Classification of the analysed amphiboles. Symbols as in Fig. 17.

14.0–16.1 wt%. Cummingtonite which is an alteration product of ferrohornblende in skarn in the zone VI.1 has Mg-number at around Mg_{30}.

Cordierite was found only in three localities in the study area. In the cordierite-orthoamphibole rock sample PSH-97–28.4 from Zone III, the Mg-number is Mg_{63} and the Na_2O is 0.41–0.42. In a Mg-rich peraluminous rock PSH-98–11B (Appendix 1) In Zone VI.3, the Mg-number is high, Mg_{87}. In Zone VI.2, one cordierite-bearing locality was found, where the cordierite has Mg_{75}. In the two latter samples the Na_2O-content is 0.10–0.14 wt%.

Clinopyroxenes were found from the zones I and VI.3. In Zone I, the Mg-numbers are $Mg_{67–68}$, Al_2O_3 2.7–2.9 wt% and Na_2O 0.58–0.66 wt%. In the zone VI.3, the scapolite-bearing rock PSH-00–69.2 has a high Mg-number, $Mg_{83–86,}$ lower Al_2O_3 (0.59–0.66 wt%) and higher Na_2O content (0.99–1.36 wt%) than other analysed clinopyroxenes, which have 1.2–1.8 wt% Al_2O_3, 0.13–0.36 wt% Na_2O and Mg-numbers of $Mg_{46–66}$. Sample PSH-00–4 which is close to the greenschist facies zone has lower Mg-number and lower Na_2O than sample PSH-00–17 which is farther from the zone IV (Appendix 1).

Plagioclases are albites in the mafic rocks of Zone IV, and also in most pelites. In other Zones, plagioclases are mostly oligoclases and andesines, but also labradorites and depending on the metamorphic grade and Ca-content of the whole rock, even anorthites. (Table 2 and Appendix 1).

Staurolites were analysed from Zones III and VI.3. Mg-numbers are $Mg_{12–19}$ in Zone III and in other Zones $Mg_{23–25}$. The MnO contents are lowest in staurolites of Zone III, 0–0.47 wt%. In Zone VI.3, MnO is from 0.83–1.03. Also the ZnO content varies from 0.04–2.44 wt%, and there is not a correlation with the metamorphic zone.

Chloritoid was analysed only in one locality from Zone III.1, where it is an alteration product of staurolite. There the Mg-number is $Mg_{09–13}$, while the MnO content is low, being 0–0.13 wt%.

Geothermometry and geobarometry

Metamorphic pressures and temperatures were calculated using the Thermocalc v. 3.1 software (Powell & Holland, 1988 1994; Powell & al. 1998). The summary of the results, mineral assemblages used in calculations, and end member activities are presented in Appendix 2. Metamorphic pressures and temperatures were calculated using both the core and rim compositions of garnets with compositions of the matrix and minerals adjacent to garnet, respectively. In Zones II–VI, this method gives a strong pressure decrease and moderate or small temperature decrease from core to rim, as indicated by the arrows in Fig. 21. These differences are mainly caused by the garnet zoning, because normally the compositional differences of other minerals are small when the matrix minerals are compared with those minerals touching garnet. This difference does not necessarily show the real PT path experienced by these rocks, because garnet core may be chemically isolated and does not represent chemical equilibrium with the present rock matrix (Marmo et al. 2002). However, most garnets have only a narrow outer rim, where there is a decvease in X_{Mg} (Fig. 16). This may record diffusion during cooling and reaction only with the adjacent minerals, not with the whole matrix. In these cases the usage of the composition of the garnet core with the matrix minerals probably gives temperatures and pressures that are close to the real maximum T and corresponding P. Some garnets have a strong zoning from the core to rim (e.g. garnets PSH-98–41.1–2 in Fig. 16a), which evidently is growth zoning during changing PT conditions. In these cases the T and P calculated using the compositions of the garnet core and matrix minerals not touching garnet may be meaningless. However, garnets in the sample PSH-98–41 have remarkably higher Mg and Ca contents in the mineral core than in the edges, which indicates higher temperatures and pressures during the early garnet growth.

In Zone I, the peak temperatures and pressures that were achieved using the core compositions of garnets

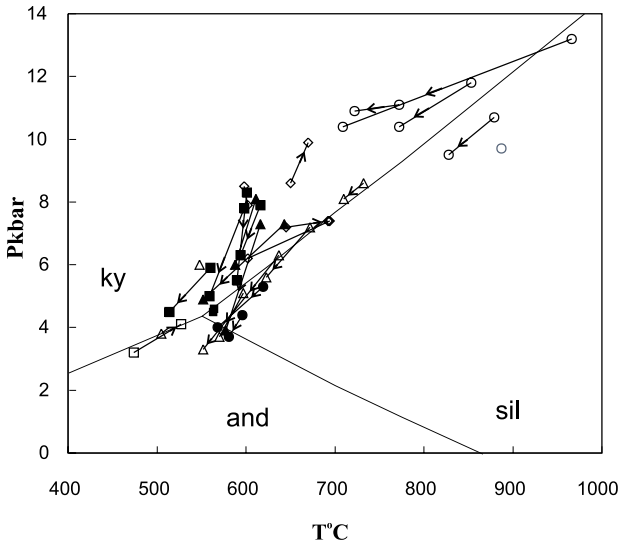

Fig. 21. Thermocalc average PT results plotted on the PT diagram. Symbols: open dots = zone I, diamonds = zone II, filled squares = zone III, filled dots = zone V.5, open triangles = zone VI.2, filled triangles = zone VI.3.

and compositions of matrix amphiboles, plagioclases and pyroxenes (when present) are mostly from 770–890 °C and 9.7–11.8 kbars. Also Tuisku and Makkonen (1999) determined a pressure of around 11 kbars for one sample from Zone I, although their temperature (670 °C), is lower, but it may represent cooling, especially because Tuisku and Makkonen (op. cit.) used double coronas on olivine in an ultramafic rock for their PT determination. One sample (PSH-00–40) gives 966 °C and 13.2 kbars, which is unrealistically high. In this sample the difference between results given by garnet core and rim compositions is greatest (257 °C and 2.8 kbars), so the garnet core may not represent equilibrium with the matrix assemblage. For the Zone I, temperatures and pressures are calculated at a_{H2O} of 0.4, because in this Zone mafic rocks are mostly migmatised, and melting evidently decreased the water activity. Temperatures and pressures calculated using the garnet rim compositions with adjacent plagioclases and amphiboles are 50–80 °C and 0.2–1.4 kbars lower than those given by garnet cores. In most garnets from Zone I, the pressure difference between the garnet core and rim results are not as remarkable as in other zones, which indicates a near-isobaric cooling as suggested also by the reactions in Figures 9a–b. The standard deviations are rather high for both pressures and temperatures because of the uncertainties in the thermodynamic properties of amphibole.

In Zone II, the Thermocalc pressures given by garnet cores are from 7.4–9.9 kbars, to some extent depending on the mineral assemblages and water activities used in calculations. In the three studied samples from Zone II the temperatures given by garnet cores are ca 600–690 °C, the highest temperature (and the lowest pressure) being from the northern part of the zone where melting has already started in metapelites. In the sample JTV-98–28, where the Mg content of garnet is increasing from core to rim the rim compositions give higher pressures and temperatures than cores. In this sample garnet has inclusion-rich core and inclusion free rim. In these kind of samples the garnet zoning represent growth during the prograde stage of metamorphism, and the 'core' pressures and temperatures may be meaningless because they probably do not represent equilibrium with the matrix assemblage.

For Zone III the 'core' temperatures are ca. 560–615 °C when the a_{H2O} is set at 1.0, which may be not far from the real value because these rocks were not melted. Otherwise the assemblage used in the Thermocalc calculations has a strong influence in the pressures. In the zone III, most peraluminous schists have both andalusite and kyanite. If one or both of the Al-silicates are eliminated, the pressures are from 6.1–7.9 kbars, which is too high for the grt-and-st-chl-pl-qtz assemblage, typical for these rocks. However, if both andalusite and kyanite are included in the assemblage used by the Thermocalc, pressures are from 3.9–4.8 kbars, which are reasonable for andalusite-bearing assemblages.

Temperatures for Zone III.1 are similar with the temperatures in Zone III, but the strong zoning in some garnets is reflected in pressures. In the samples PSH-98–41.1–2 which have the strongest garnet zoning in the studied rocks (Fig. 16a), garnet rims give 2.7–2.8 kbar lower pressures (4.5–5.5 kbars) than garnet cores (7.2–8.3 kbars), the 'rim' temperature being ca 10–40 °C lower than the 'core' temperature.

For the greenschist facies zone IV, it was not possible to calculate meaningful Thermocalc temperatures and pressures. In Table 3, there are temperatures calculated using the chlorite thermometer of Cathelineau (1988). Most of these are around 350–400 °C, which are reasonable for the greenschist facies rocks. Temperatures given by the chlorite thermometer for one rock from the Kumpu group are around 260 °C. This is clearly lower than elsewhere in the zone IV, but also chlorite from a metavolcanic rock close to Kumputunturi give a similar low temperature (Fig. 22), indicating that the area close to Kumputunturi represents the lowest metamorphic grade in the greenschist facies zone. On the other hand, most analysed chlorites also from the higher grade zones give temperatures at around 350–400 °C, which indicates the retrograde origin of chlorite and perhaps simultaneous retrogression with the greenschist facies metamorphism in Zone IV. The

Table 3. Examples of chlorite compositions and temperatures given by the chlorite thermometer of Cathelineau (1988)

Sample	**PSH-99-37**	**PSH-99-47**	**PSH-99-52**	**PSH-99-57**	**PSH-99-59**	**MJV-99-83.2**
northing	7480840	7510050	7512820	7500240	7508350	7478895
easting	3478370	3451480	3437620	3491400	3491190	3474068
SiO2	24,23	25,36	26,45	25,88	24,23	22,88
TiO2	0,01	0,07	0,04	0,1	0,12	0,12
Al2O3	23,37	20,8	19,37	21,04	21,53	22,61
FeO	25,75	24,03	25,09	22,38	25,31	32,22
MnO	0,26	0,37	0,44	0,18	0,15	0,26
MgO	14,56	15,19	15,16	17,58	15,12	7,86
Total	88,18	85,82	86,55	87,16	86,46	85,95
Cations/14 oxygens						
Si	2,545	2,716	2,823	2,693	2,596	2,566
AlIV	1,455	1,284	1,177	1,307	1,404	1,434
AlVI	1,435	1,339	1,257	1,271	1,313	1,552
Ti	0,001	0,006	0,003	0,008	0,01	0,01
Fe	2,261	2,152	2,239	1,947	2,268	3,022
Mn	0,023	0,034	0,04	0,016	0,014	0,025
Mg	2,279	2,425	2,412	2,727	2,415	1,314
T°C	407	352	317	359	390	400

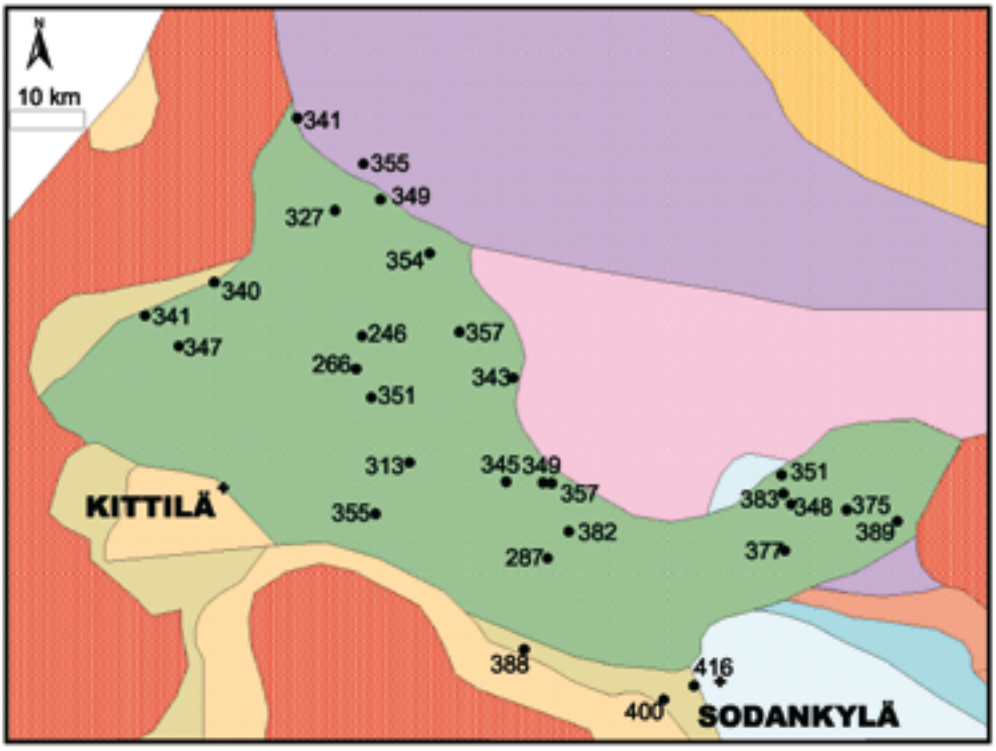

Fig. 22. Regional distribution of the temperatures given by the chlorite thermometer for the greenschist facies Zone IV. Colours for the metamorphic zones are as in Fig. 8.

temperatures are close to 400 °C in Zone VI.1 on the southern side of Zone IV. The sample PSH-00–1.7 (Appendix 2) is from the zone VI.1, located in the western part of the zone IV, where the temperature has been high enough for garnet growth in skarns. The Thermocalc pressure for the core of this garnet is 3.2 kbars, which probably is close to the pressure for the greenschist facies metamorphism before garnet crystallized, probably as a consequence of heat flow from the adjacent granitoids.

Rocks from the sillimanite grade Zone V.5 give Thermocalc pressures which are of the same order (3.7–5.3 kbars when a_{H2O} =1) than those given by grt-st-and-ky assemblages in Zone III. Advective heat flow from granitoids probably caused the sillimanite grade metamorphism in this zone. Thermocalc average PT calculations were not done in this study for Zones V.1-3 because of the absence of garnet, but the coexistence of andalusite and kyanite (Fig. 12a) indicates, however, that metamorphic pressures were close to the andalusite-kyanite boundary also in these rocks.

Both sillimanite-bearing and Al-silicate-absent pelitic rocks as well as garnet amphibolites from Zones VI.2–3 give relatively high 'peak' Thermocalc pressures, (6.1–8.1 kbars at ca 610–730 °C), and similar decreasing pressure trends as other zones in the core-rim thermobarometry (Fig. 21). However, when these rocks have both andalusite and sillimanite (sample PSH-98–97.1, Fig. 13a) or all three Al_2SiO_5 polymorphs (sample PSH-98–11B, Fig. 13c) and all minerals present are used in the Thermocalc calculation, the pressures are low (from 3.3–3.8 kbars), which is in accordance with the presence of andalusite. Cordierite and andalusite-bearing, plagioclase-free sample PSH-98–69.1 gives pressures and temperatures of 4.1–5.1 kbars and 534–627 °C. The high pressures in some samples, as well as the reaction (21) bt + als + qtz = crd + ms which has a relatively flat dP/dT slope indicate decompression also for this zone. The temperatures and pressures in many other samples from Zones V–VI, especially those given by garnet rims, plot in the sillimanite field in Fig. 21.

Phase diagrams

The core-core and rim-rim thermobarometry fits relatively well with the petrogenetic grids for the zones II, III, V and VI in Figures 23a–e, which were constructed using the Thermocalc 3.25 software (Powell & Holland 1988, 1994; Powell et al., 1998; see the web page *http://www.earthsci.unimelb.edu.au/tpg/thermocalc/)*. The whole rock compositions are from samples analysed using the XRF method. These compositions are examples, e.g. a higher Mg/Fe ratio in the whole rock would raise in each case the univariant curves and divariant fields to higher pressures. In Zone II the maximum temperature conditions are interpreted to have been close the reaction boundary bt + ms + st + pl + qtz = grt + ky + liq (Fig. 23b), which fits well with the average pressures and temperatures given by the garnet cores. Neither sillimanite nor andalusite was observed in the zone II, so the post-peak cooling took evidently place in the kyanite field, as illustrated by the arrow in Fig. 23a.

In Zone III, the garnet zoning does not clearly indicate the early high pressure, and kyanite is a late retrograde phase. However, some garnets have chloritoid inclusions, which may indicate that they were reactants in the reaction (8) cld + qtz = grt + st + chl + H_2O, which takes place in pressures ≥ 7 kbars in the compositions represented by the analysed metapelites. Therefore the early pressure in the PT path may have been as high as given by those average PT calculations where the Al-silicate is absent. Same rocks have andalusite, retrograde kyanite and chloritoid which indicates cooling down to conditions, where the univariant cooling reaction chl+st+qtz+H_2O = cld+als took place, straddling at the andalusite-kyanite boundary (Fig. 23c).

In Zone III.1, garnets have altered from rims into biotite, and staurolites are close to these garnets, which indicates that PT conditions were in the field where the divariant KFMASH reaction grt + ms + H_2O = bt + st + qtz takes place (field grt-bt-st in Fig. 23d). This is in accordance with the 7.2–8.3 kbar average pressures given by the garnets that have Mg and Ca rich cores. Because the average Thermocalc pressure for the garnet rims were around 5 kbars, and there seems to be late biotite growth in chlorite-muscovite filled staurolite pseudomorphs, caused by the reaction (15) chl + mu = bt + st + qtz (field chl-bt-st in Fig. 23d), the PT path was probably as indicated by the arrow in Fig. 23d, with some reheating before cooling to the chloritoid field.

In Zone V, the metamorphic field gradient from the chloritoid grade to the sillimanite grade is demonstrated by the dashed arrow in Fig. 23e. Andalusite was produced at least partly by the divariant KFMASH reaction (13) cld + qtz = and + chl + H_2O (field chl-cld-als-ms in Fig. 23e), and chloritoid was consumed by the univariant and divariant reactions (10) als + cld = chl + st + qtz + H_2O and (14) cld + qtz = chl + st + H_2O (field chl-st-cld-ms), the PT conditions being also in these reactions close to the andalusite-kyanite boundary. With rising temperature, sillimanite was formed in the divariant reaction st + ms + qtz = bt + sil + H_2O (field bt-st-als-ms). Crossing the univariant boundary

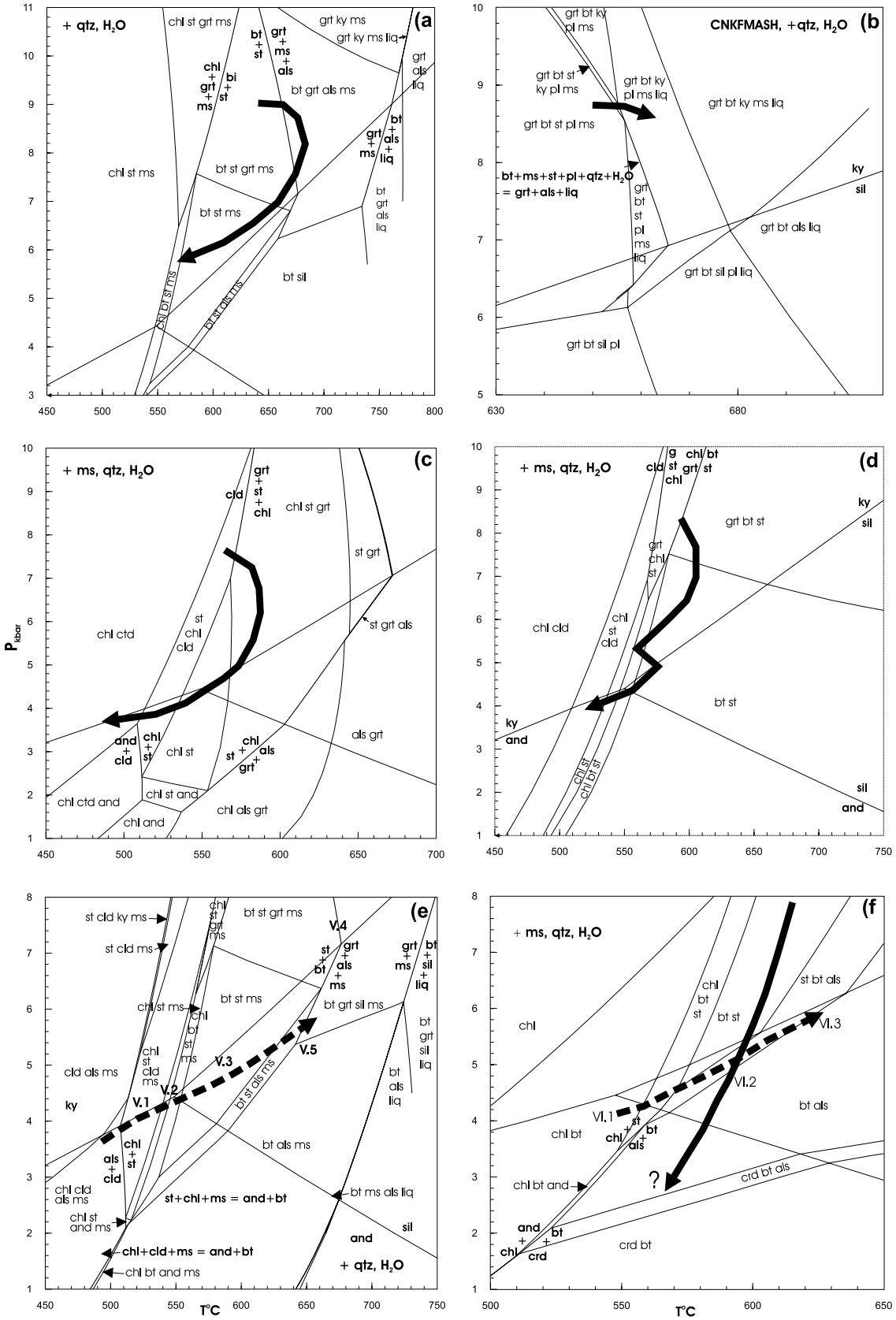

Fig. 23. Pseudosections showing the fields for some of the observed mineral assemblages and reactions in metapelites for various metamorphic zones in the system KFMASH, apart from Fig. 23b which is for the CNKFMASH. Solid arrows are for possible PT paths, dashed arrows are for the metamorphic field gradients. a) = zone II, composition SiO_2 70.16, Al_2O_3 15.57, MgO 3.44, FeO 8.82, K_2O 2.01 mol.%; b) zone II, composition SiO_2 68.15, Al_2O_3 15.12, MgO 3.34, FeO 8.57, CaO 0.63, Na_2O 2.23, K_2O 1.95, mol.%; c) zone III, composition SiO_2 70.16, Al_2O_3 15.57, MgO 3.44, FeO 8.82, K_2O 2.01 mol.%; d) zone III.1 composition SiO_2 71.18, Al_2O_3 15.13, MgO 3.24, FeO 8.72, K_2O 1.73 mol.%; e) zone V.1–5, SiO_2 69.58, Al_2O_3 18.16, MgO 2.12, FeO 7.80, K_2O 2.33 mol.%; f) zone VI.1–3, SiO_2 73.99, Al_2O_3 11.79, MgO 5.44, FeO 5.37, K_2O 3.42 mol.%. Heavy lines are for univariant reactions, narrow lines are borders of the divariant and trivariant fields.

bt + st + q = grt + ms + als + H_2O may have produced garnet-sillimanite assemblages in zone V.5.

The dashed arrow in Fig. 23f illustrates the change in PT conditions from Zones VI.1 to VI.3. Because all three Al_2SiO_5 polymorphs are present in zone VI.2, it is evident that the PT path was not far from their triple point. Because some average pressures are high, from 6.1–8.1 kbars, the PT path was probably as indicated by the solid arrow in Fig. 23f, going down to pressures where the reaction (21) bt + als + qtz = crd + ms (Fig. 13d) starts with decreasing pressure (field crd-bt-als). Reaction (21) is strongly dependent on the Fe/Mg ratio of the rock, in compositions that are Mg richer than the one used in Fig. 23f the reaction takes place in higher pressures. On the other hand, it is also possible that the reaction (21) does not represent decreasing pressure but increasing temperature in near-isobaric conditions, resulting from advective heat flow from the granitoid intrusions.

DISCUSSION

The onset of the tectonic evolution of Central Lapland is characterized by a prolonged extensional rifting of the Archaean basement and the related volcanism, magmatism and sedimentation. This stage lasted at east 500 Ma from ca 2.5 Ga to ca 2.0 Ga (papers in Vaasjoki 2001). The orogenic evolution of Central Lapland that started ca 2.0–1.89 Ga ago, is a combination of two main tectonic events: the northward or northeastward directed Svecofennian tectonic movement that thrusted the earlier formations onto the Archaean basement, and the thrusting of the Lapland Granulite Belt towards the approximately opposite direction (Ward et al. 1997). As a result, the associated structures in different parts of the Central Lapland are not straightforwardly correlated with each other. The correlation of structures is further hampered by the paucity of suitable structurally controlled granitoids that could be dated for time markers for different tectonic events.

The early structural evolution (D1+D2) of Central Lapland is characterized by subhorizontal folds and foliations observed throughout the study area, accepting the possibility that in some subareas this might have caused more steeply dipping structures (Ward et al. 1989), as is common in many younger fold-and-thrust belts. In the southern and central part of the study area, the fold vergences and other kinematic indicators suggest a N or NE directed tectonic movement during this stage. Subhorizontally deformed tonalites suggest that the age of the deformation is around 1.88–1.87 Ga, assuming that the tonalites correlate with the Haaparanta suite intrusions, indicating a typical Svecofennian age of deformation (see e.g. Nironen 1997). Close to the Lapland Granulite Belt, inclined W- to SW-vergent folds were observed, but their correlation with N-NE-vergent structures in the south is not known. It is most plausible that the thrusts were initiated at this period although they were clearly reactivated in later stages.

The late structural evolution (D3 and later) in Central Lapland caused the extreme variety concerning strike, dip and intensity of different structural elements now seen on geological and geophysical maps and observed at outcrop scale. At this stage, the thrusts that were initiated in earlier stage were reactivated and the structural pattern with opposing fold vergences and high strain shear zones developed. Simultaneous or progressive thrusting from different directions towards the oceanic Kittilä group is a peculiar feature in Central Lapland and cannot be explained by a simple head-on thrusting. During thrusting older formations were juxtaposed over younger ones in some places and vice verse in other places. Metamorphic boundaries at thrust planes indicate that thrusting was at least partly late metamorphic or postmetamorphic.

The mineral assemblages and thermobarometry show very large PT differences between metamorphic zones, especially pressure differences are remarkable. When not caused by advective heat from large granitoid massifs, the changes in metamorphic grade are connected with shear zones and D3 thrust planes. The eastward prograde increase in metamorphic grade in the zone V may reflect an oblique cut of the crust, revealed by the D3 thrusting where higher grade eastern zones represent deeper crustal sections. The increase in grade may also be caused by heat flow from granitoids which are abundant in Zone V.5.

The present structural geometry shows an inverted gradient where pressure and temperature increase upwards in the present tectonostratigraphy from greenschist facies in the zone IV through garnet-andalusite-staurolite grade in the zone III and garnet-kyanite grade amphibolite facies in Zone II to granulite facies in Zone I. The inverted gradient could be explained by crustal thickening caused by overthrusting of the hot granulite complex onto the lower grade rocks, as inferred by tectonic transport directions in Fig. 7. Krill (1985) proposed this mechanism for the Karasjok-Levajok area in the western side of the Lapland Granulite Belt in northern Norway, where the metamorphic zonation is similar to that in our study area. Tuisku & Makkonen (1999) explained the high pres-

sure at the margin of the Lapland Granulite Belt as a consequence of subduction of the Karelian foreland under the overriding Kola Plate.

These kind of 'hot-over-cold' models have been proposed also to explain the inverted gradients e.g. in Zanskar Himalaya (Searle & Rex 1989). To preserve the inverted isograds a rapid exhumation and cooling is needed (Thompson & Ridley 1987). Therefore Searle & Rex (1989) favoured a model where subsequent folding and thrusting deformed the normal upward decreasing Barrovian metamorphic sequence, causing the present inverted gradient structure. To some extent similar process may be an explanation also for the southward decreasing grade from Zone I to the zone III south of the Lapland Granulite Belt, where the higher grade gneisses may have been thrusted onto lower grade schists during the late stage of metamorphism, although the granitoids also have had a thermal input into metamorphism in Central Lapland. Thrusting probably thickened the crust in a large area and was followed by decompression as indicated by the inferred PT paths. Peraluminous metasediments were not found in the eastern part of Zone II, so it is unclear whether the eastern side of Zone II underwent similar PT evolution than its western part that exhibit many kyanite-bearing rocks. However, kyanite-bearing metasediments were described by Perchuk et al. (2000) ca 150 km east of our study area, from the southern contact of the Tanaelv belt, as well as by Krill (1985) from the western contact of the Tanaelv belt in Norway, on the western side of the granulite complex. Therefore it is probable that also in our study area, the eastern part of Zone II, represents similar PT-conditions than its western part, as indicated by the Thermocalc pressures of ca 7.5 kbars given by garnet amphibolites and orthoamphibole rocks from the Siltaharju area.

Generally, the Tanaelv belt (Zone I) has been described as a separate unit not belonging to the granulite complex, its metamorphism being caused by hot granulites (Barbey et al. 1980, 1982, 1984; Krill 1985, Perchuk et al. 2000). However, the structures in the Tanaelv belt are similar to those in the Lapland Granulite Belt (Nironen and Mänttäri 2003) and the metamorphic conditions do not differ from those in lower parts of the granulite complex. The lithology of the Tanaelv belt differs from that of the Lapland Granulite Belt but evidently they were metamorphosed together in the same thickening process.

There is a several kbar change in the metamorphic pressure from the kyanite grade Zone II to the andalusite grade Zone III, but the zoning profiles of garnet and the thermobarometry indicate that the zone III also underwent a higher pressure stage, reaching the 'peak' temperatures after thickening and decompression. Zone II may represent the upper plate in thickening which was cooled more rapidly without reaching the andalusite field while still reactive. Lower grade rocks further from the granulites stayed close to their maximum temperature down to the andalusite field or to the andalusite-kyanite boundary, and this period was followed by a near-isobaric cooling to the kyanite field, maybe representing decompression and cooling after extensional collapse. In Zone I, the near-isobaric cooling period took place in much higher pressure, but these cooling events (Figs. 9a–b and 10b) were not necessarily simultaneous in Zones I and II.

During the thickening, the greenschist facies rocks (the Kittilä Group) were probably not in their present position, but they represent a late metamorphic allocthon that was accreted to Zones II and III during late D3. Lithological boundaries around the Kittilä Group are mostly also metamorphic boundaries which supports this idea. However, the rocks Kittilä of the group have been proposed to continue north to the Karasjok area in Norway (Lehtonen et al. 1998) through Zone II, although there is a major change in PT conditions from Zone IV to Zone II. This may mean that the volcanic rocks in Zone II do not belong to the Kittilä Group, but it is also possible that some parts of the oceanic unit were included in the thickening that produced high pressure ampibolite facies rocks in Zone II, and other parts were juxtaposed later with Zones II and III.

ACKNOWLEDGEMENTS

The authors want to express their cordial thanks to Pekka Tuisku, Mikko Nironen and Eero Hanski for critical reviews, which considerably improved the manuscript, to Lassi Pakkanen and Hans Harryson for microprobe analyses, and to Veikko Keinänen, Eelis Pulkkinen, Vesa Kortelainen, Nicole Patison and the GTK technical staff in Kittilä and Sodankylä for help and stimulating discussions in the field. Prof. Pekka Nurmi is thanked for the help in planning and realization of the project, and Director General Elias Ekdahl for the original initiative for studying the metamorphic structure of Central Lapland.

REFERENCES

Barbey, P., Convert, J., Moreau, B., Capdevila, R. & Hameurt, J. 1980. Relationships between granite-gneiss terrains, greenstone belts and granulite belts in the Archaean crust of Lapland (Fennoscandia). Geologische Rundschau 69, 648–658.

Barbey, P., Capdevila, R. & Hameurt, J. 1982. Major and transition trace element abundances in the khondalite suite of the granulite belt of Lapland (Fennoscandia). Evidence for an early Proterozoic flysch-belt. Precambrian Research 16, 273–290.

Barbey, P., Convert, J., Moreau, B., Capdevila, R. & Hameurt, J. 1984. Petrogenesis and evolution of an early Proterozoic collisional orogenic belt : the granulite belt of Lapland and the Belomorides (Fennsocandia). Bulletin of the Geological Society of Finland 56, 161–188.

Barbey, P. & Raith, M. 1990. The granulite belt of Lapland. In: Vielzeuf, D. & Vidal, Ph. (eds.) Granulites and crustal evolution, Kluwer Academic Publishers. NATO ASI Series, Vol. 311, 111–132.

Burg, J-P. 1999. Ductile structures and instabilities; their implications for Variscan tectonics in the Ardennes. Tectonophysics 309, 1–25.

Cathelineau, M. 1988. Cation site occupancy in chlorites and illites as a function of temperature. Clay Minerals 23, 471–485.

Eilu, P. 1994. Hydrothermal alteration in volcano-sedimentary rocks in the Central Lapland Greenstone Belt, Finland. Geological Survey of Finland, Bulletin 374. 145 p.

Eilu, P. 1999. FINGOLD – a public database on gold deposits in Finland. Geological Survey of Finland, Report of Investigation 146. 224 p.

Eskola, P. 1952. On the granulites of Lapland. American Journal of Science, Bowen Volume, Part 1, 133–171.

Evins, P. M. & Laajoki, K. 2002. Early Proterozoic nappe formation: an example from Sodankylä, Finland, northern Baltic Shield. Geological Magazine 139, 73–87.

Frietsch, R., Tuisku, P., Martinsson, O. & Perdahl, J.-A. 1997. Early Proterozoic Cu-(Au) and Fe ore deposits associated with regional Na-Cl metasomatism in northern Fennoscandia. Ore Geology Reviews 12 (1), 1–34.

Gaál, G., Berthelsen, A., Gorbatschev, R., Kesola, R., Lehtonen, M. I., Marker, M. & Raase P. 1989. Structure and composition of the Precambrian crust along the POLAR Profile in the northern Baltic Shield. Tectonophysics 162, 1–25.

Gaál, G., Mikkola, A. & Söderholm, B. 1978. Evolution of the Archean crust in Finland. Precambrian Research 6, 199–215.

Groves, D. I., Goldfarb, R. J., Gebre-Mariam, M., Hagemann, S. G. & Robert, F. 1998. Orogenic gold deposits: A proposed classification in the context of their crustal distribution and relationship to other gold deposit types. Ore Geology Reviews 13, 7–27.

Guidotti, C. V. 1984. Micas in metamorphic rocks. In Ribbe, P.H. (ed.) Micas. Mineralogical Society of America. Reviews in Mineralogy 13, 357–456.

Haapala, I., Front, K., Rantala, E. & Vaarma, M. 1987. Petrology of Nattanen-type granite complexes, northern Finland. Precambrian Research 35, 225–240.

Hanski, E. S. 1997. The Nuttio Serpentinite Belt, Central Lapland: an example of Paleoproterozoic ophiolitic mantle rocks in Finland. Ofioliti 22, 35–46.

Hanski, E. 2001. History of stratigraphical research in northern Finland. In: Vaasjoki, M. (ed.) Radiometric age determinations from Finnish Lapland and their bearing on the timing of Precambrian volcano-sedimentary sequences. Geological Survey of Finland, Special Paper 33, 15–43.

Hanski, E., Huhma, H., & Vaasjoki, M. 2001. Geochronology of northern Finland: a summary and discussion. In: Vaasjoki, M. (ed.) Radiometric age determinations from Finnish Lapland and their bearing on the timing of Precambrian volcano-sedimentary sequences. Geological Survey of Finland, Special Paper 33, 255–279.

Hanski, E., Mänttäri, I., Huhma H. & Rastas, P. 2000. Post-1.88 Ga deposition of the Kumpu and Lainio Group molasse-type sediments in northern Finland: evidence from conventional and NORDSIM zircon dating. 24th Geological Winter Meeting, Trondheim, January 6–9, 2000, Abstracts, p. 75.

Hölttä, P. & Väisänen, M. 2000. Tectonic evolution of the Central Lapland Grenstone Belt – metamorphic and structural observations. In: Lauri J. Pesonen, Annakaisa Korja and Sven-Erik Hjelt (Eds.) Lithosphere 2000: A symposium on the structure, composition and evolution of the lithosphere in Finland. Geological Survey of Finland, Espoo, October 4–5, 2000. Institute of Seismology, University of Helsinki, Report S-41, 161–163.

Hörmann, P.K., Raith, M., Raase, P., Ackermand, D. & Seifert, F. 1980. The granulite complex of Finnish Lapland, Petrology and metamorphic conditions in the Ivalojoki-Inarijärvi area. Geological Survey of Finland, Bulletin 308, 100 p.

Huhma, H. 1986. Sm-Nd, U-Pb and Pb-Pb isotopic evidence for the origin of the early Proterozoic Svecokarelian crust in Finland. Geological Survey of Finland, Bulletin 337. 48 p.

Korja, T., Tuisku, P., Pernu, T. & Karhu, J. 1996. Field, petrophysical and carbon isotope studies on the Lapland Granulite Belt: implications for deep continental crust. Terra Nova 8, 48–58.

Korkiakoski, E. 1992. Geology and geochemistry of the metakomatiite-hosted Pahtavaara gold deposit in Sodankylä, northern Finland, with emphasis on hydrothermal alteration. Geological Survey of Finland. Bulletin 360, 96 p.

Korsman, K. (ed.), Koistinen, T. (ed.), Kohonen, J. (ed.), Wennerström, M. (ed.), Ekdahl, E. (ed.), Honkamo, M. (ed.), Idman, H. (ed.), Pekkala, Y. (ed.) 1997. Suomen kallioperäkartta = Berggrundskarta över Finland = Bedrock map of Finland 1:1 000 000. Espoo. Geological Survey of Finland.

Kretz, R. 1983. Symbols for rock-forming minerals. American Mineralogist 68, 277–279.

Krill, A.G. 1985. Svecokarelian thrusting with thermal inversion in the Karasjok-Levajok area of the Northern Baltic Shield. Norges Geologiske Undersøkelse Bulletin 403, 89–101.

Kärkkäinen, N. 1982. Kittilän vihreäkivien ja niihin liittyvien metapeliittien metamorfoosista. In: Laajoki, K., Paakkola, J. & Tuisku, P. (eds.) Suomen kallioperän ja malmien metamorfoosi ja deformaatio. Res Terrae. Ser. B 5, 98–107 (in Finnish).

Leake, B. E. 1978. Nomenclature of amphiboles. American Mineralogist, 63, 1023–1053.

Lehtonen, M., Airo, M.-L., Eilu, P., Hanski, E., Kortelainen, V., Lanne, E., Manninen, T., Rastas, P., Räsänen, J. & Virransalo, P. 1998. Kittilän vihreäkivialueen geologia: Lapin vulkaniittiprojektin raportti. Summary: The stratigraphy, petrology and geochemistry of the Kittilä greenstone area, northern Finland: a report of the Lapland Volcanite Project. Geological Survey of Finland, Report of Investigation 140. 144 p.

Marker, M. 1988. Early Proterozoic thrusting of the Lapland granulite belt and its geotectonic evolution, northern Baltic Shield . Geologiska Föreningens i Stockholm Förhandlingar 110, 405–410.

Marmo, B. A., Clarke, G. L. & Powell, R. 2002. Fractionation of bulk rock composition due to porphyroblast growth: effect on eclogite facies mineral equilibria, Pam Peninsula, New Caledonia. Journal of Metamorphic Geology 20, 151–165.

McCuaig, T. C. & Kerrich, R. 1998. P-T-t-deformation-fluid characteristics of lode gold deposits: evidence from alteration systematics. Ore Geology Reviews 12 (6), 381–453.

Mouri, H. & Korsman, K. 1999. Partial melting and P-T-t evolution of LP/HT metamorphic terranes: an example from

the Svecofennian K-feldspar-poor leucosome migmatite belt, southern Finland. In: Understanding granites: integrating new and elassic techniques. Geological Society Special Publications, 168. London, 239–253.

Nironen, M. 1997. The Svecofennian Orogen: a tectonic model. Precambrian Research 86, 21–44.

Nironen, M. & Mänttäri, I. 2003. Structural evolution of the Vuotso area, Finnish Lapland. Bulletin of the Geological Society of Finland 75, 93–101.

Patison, N. L. 2007. Structural controls of gold mineralisation in the Central Lapland greenstone belt. Geological Survey of Finland, Special Paper 44, 105–122.

Pattison, D. 2003. Petrogenetic significance of orthopyroxene-free garnet+clinopyroxene+plagioclase±quartz-bearing metabasites with respect to the amphibolite and granulite facies. Journal of Metamorphic Geology 21, 21–34.

Perchuk, L. L., Gerya, T. V., Van Reenen, D. D., Smit, C. A. & Krotov, A.V. 2000. P-T paths and tectonic evolution of shear zones separating high-grade terrains from cratons: examples from Kola Peninsula (Russia) and Limpopo Region (South Africa). Mineralogy and Petrology 69, 109–142.

Powell, R., Holland, T. & Worley, B. 1998. Calculating phase diagrams involving solid solutions via non-linear equations, with examples using THERMOCALC. Journal of Metamorphic Geology 16, 577–588.

Powell, R. & Holland, T. 1994. Optimal geothermometry and geobarometry. American Mineralogist 79, 120–133.

Powell, R. &Holland, T. J. B. 1988. An internally consistent dataset with uncertainties and correlations; 3, Applications to geobarometry, worked examples and a computer program. Journal of Metamorphic Geology 6, 173–204.

Raith, M., Raase, P. & Hörmann, P. K. 1982. The Precambrian of Finnish Lapland: evolution and regime of metamorphism. Geologische Rundschau 71, 230–244.

Rastas, J. & Kilpeläinen, T. 1991. Tektonis-metamorfiset tutkimukset Mertavaarassa, Puljun liuskejaksolla. Institute of Geology and Mineralogy, University of Turku, Publication No 25, 19 p. (in Finnish).

Räsänen, J. & Huhma, H. 2001. U-Pb datings of the Sodankylä schist area, central Finnish Lapland. Geological Survey of Finland, Special Paper 33, 153–188.

Searle, M. P. & Rex, J. 1989. Thermal model for the Zanskar Himalaya. Journal of Metamorphic Geology 7, 127–134.

Sorjonen-Ward, P., Nironen, M. & Luukkonen, E. 1997. Greenstone Associations in Finland. In: Maarten de Wit & Lewis Ashwal (eds.) Greenstone Belts. Clarendon Press, London, 677–698.

Thompson, A. B. & Ridley, J. R. 1987. Pressure-temperature-time histories of orogenic belts. Philosophical Transactions of the Royal Society, London, A321, 27–45.

Tuisku, P. 1985. The origin of scapolite in the Central Lapland schist area, Northern Finland : preliminary results. In: Laajoki, K. & Paakkola, J. (eds.) Proterozoic exogenic processes and related metallogeny : proceedings of the symposium held in Oulu, Finland, August 15–16, 1983. Geological Survey of Finland, Bulletin 331, 159–173.

Tuisku, P. & Makkonen, H. 1999. Spinel-bearing symplectites in Palaeoproterozoic ultramafic rocks from two different geological settings in Finland : thermobarometric and tectonic implications. Geologiska Föreningens i Stockholm Förhandlingar 121 (4), 293–300.

Vaasjoki, M. 2001 (ed.). Radiometric age determinations from Finnish Lapland and their bearing on the timing of Precambrian volcano-sedimentary sequences. Geological Survey of Finland. Special Paper 33, 279 p.

Väisänen, M. 2002. Structural features in the central Lapland greenstone belt, northern Finland. Geological Survey of Finland, Archive report K 21.42/2002/3. 20 p.

Ward, P., Härkönen, I., Nurmi, P., & Pankka, H. S. 1989. Structural studies in the Lapland greenstone belt, northern Finland and their applications to gold mineralizations. Geological Survey of Finland. Special Paper 10, 71–78.

Wennerström, M., & Airo, M-L. 1998. Magnetic fabric and emplacement of the post-collisional Pomovaara Granite Complex in northern Fennoscandia. Lithos 45 (1–4), 131–145.

Whitney, D. L. & Irving, A. J. 1994. Origin of K-poor leucosomes in a metasedimentary migmatite complex by ultrametamorphism, syn-metamorphic magmatism and subsolidus processes. Lithos 32, 173–192.

Appendix 1. Electron microprobe analyses of minerals. n.d. = not determined.

Sample	Rock type	Northing	Easting	Mineral	Zone	Site	SiO2	TiO2	Al2O3	Cr2O3	FeO	MnO	MgO	CaO	Na2O	K2O	BaO	NiO	ZnO	SrO	F	Cl	Total
Biotites																							
JTV-98-47.2	metapelite	7563830	3450920	bt	II	core	36,45	1,68	19,07	0,03	17,27	0,00	11,17	0,00	0,02	9,84	0,16	0,05	n.d.	0,00	0,57	0,03	96,33
JTV-98-49.1	metapelite	7576663	3445005	bt	II	core	36,13	1,79	18,89	0,09	19,18	0,00	10,18	0,03	0,13	9,22	0,07	0,00	0,10	0,00	0,48	0,05	96,35
JTV-98-28.2	metapelite	7552687	3458503	bt	III	core	37,22	1,35	18,58	0,00	16,77	0,10	12,00	0,00	0,26	8,66	0,00	0,01	0,01	0,00	0,69	0,33	95,97
PSH-01-14.3 A	metapelite	7521952	3519947	bt	III	matrix, core	34,68	1,57	18,63	n.d.	18,20	0,09	10,83	0,00	0,10	9,20	0,25	n.d.	n.d.	n.d.	n.d.	n.d.	93,54
PSH-97-28.3	crd-oam rock	7543200	3495550	bt	III	matrix, core	34,45	1,39	16,30	n.d.	22,78	0,03	8,75	0,01	0,08	9,23	0,15	n.d.	n.d.	n.d.	n.d.	n.d.	93,18
PSH-97-28.4 B	crd-oam rock	7543200	3495550	bt	III	matrix, core	35,89	1,33	18,89	n.d.	20,03	0,00	10,46	0,00	0,31	8,77	0,18	n.d.	n.d.	n.d.	n.d.	n.d.	95,86
PSH-98-41.1	metapelite	7517980	3457930	bt	III	core	34,37	1,64	18,99	0,18	23,57	0,08	6,56	0,00	0,26	9,41	0,00	0,09	0,12	0,00	0,24	0,16	95,68
PSH-98-41.1	metapelite	7517980	3457930	bt	III	rim	34,68	1,24	19,39	0,00	24,01	0,04	6,44	0,01	0,19	9,14	0,00	0,11	0,08	0,00	0,34	0,12	95,81
PSH-98-41.2.2	metapelite	7517980	3457930	bt	III	matrix	34,31	1,46	19,17	0,08	24,41	0,00	6,60	0,06	0,29	8,97	0,06	0,20	0,04	0,03	0,32	0,18	96,16
PSH-98-41.2.2	metapelite	7517980	3457930	bt	III	alt. from grt	34,45	1,68	18,89	0,14	24,18	0,00	6,63	0,06	0,25	8,93	0,09	0,07	0,09	0,10	0,47	0,16	96,20
92.3-MJV-99	metapelite	7482200	3529044	bt	VI	alt. from grt	33,95	1,62	18,15	n.d.	23,25	0,02	8,09	0,01	0,05	8,76	0,15	n.d.	n.d.	n.d.	n.d.	n.d.	94,05
92.3-MJV-99 B	metapelite	7482200	3529044	bt	VI	core	34,23	1,56	18,30	n.d.	21,92	0,08	8,79	0,00	0,34	8,65	0,29	n.d.	n.d.	n.d.	n.d.	n.d.	94,16
PSH-01-17.2 B	metapelite	7521105	3535306	bt	VI	core	34,71	1,70	19,40	n.d.	21,63	0,07	8,93	0,00	0,44	8,81	0,30	n.d.	n.d.	n.d.	n.d.	n.d.	95,98
PSH-01-8.2	metapelite	7504537	3513451	bt	VI	at grt	36,30	1,59	18,69	n.d.	19,21	0,18	10,33	0,00	0,21	9,35	0,10	n.d.	n.d.	n.d.	n.d.	n.d.	95,97
PSH-01-8.2	metapelite	7504537	3513451	bt	VI	matrix, core	36,23	1,55	18,44	n.d.	18,93	0,16	10,63	0,00	0,26	9,06	0,01	n.d.	n.d.	n.d.	n.d.	n.d.	95,27
PSH-98-11B	metapelite	7466644	3466995	bt	VI.2	core	38,62	1,88	18,78	0,08	9,47	0,00	17,17	0,00	0,18	9,15	0,00	0,08	n.d.	0,00	0,29	0,04	95,73
PSH-98-15.2	metapelite	7481728	3449834	bt	VI.2	matrix, core	34,88	1,93	18,35	0,11	22,32	0,11	7,77	0,09	0,04	9,69	0,08	0,04	0,08	0,00	0,34	0,19	96,02
PSH-98-15.2	metapelite	7481728	3449834	bt	VI.2	at grt	34,90	1,57	18,34	0,04	21,66	0,04	8,39	0,00	0,11	9,42	0,13	0,03	0,00	0,00	0,34	0,12	95,08
PSH-98-69.1	metapelite	7469020	3472710	bt	VI.2	matrix, core	37,24	1,38	18,93	0,04	15,38	0,26	13,01	0,00	0,24	9,32	0,12	0,16	n.d.	0,03	0,38	0,00	96,50
PSH-98-97.1B	metapelite	7495065	3416255	bt	VI.2	at grt	37,43	1,63	18,91	0,05	15,29	0,27	13,41	0,11	0,22	9,23	0,00	0,00	n.d.	0,00	0,26	0,01	96,82
PSH-98-97.1B	metapelite	7495065	3416255	bt	VI.2	matrix, core	37,17	1,50	18,80	0,09	16,06	0,28	13,00	0,09	0,20	9,07	0,00	0,02	n.d.	0,03	0,33	0,02	96,64
JTV-98-38.1A	metapelite	7498984	3391353	bt	VI.3	core at st	36,31	1,84	18,64	0,00	15,70	0,17	12,39	0,08	0,22	8,99	0,32	0,04	0,05	0,00	0,28	0,17	95,20
JTV-98-38.1B	metapelite	7498984	3391353	bt	VI.3	core	37,13	1,81	18,96	0,08	16,58	0,18	12,22	0,04	0,24	9,35	0,29	0,12	0,05	0,00	0,33	0,22	97,61
PSH-00-10.3	metapelite	7557588	3409925	bt	VI.3	at grt	26,62	0,80	21,49	n.d.	28,42	0,06	11,13	0,09	0,00	1,13	0,05	0,06	0,06	n.d.	0,00	0,13	90,04
PSH-00-10.3	metapelite	7557588	3409925	bt	VI.3	core	34,23	1,86	18,45	n.d.	23,22	0,02	7,78	0,09	0,04	8,40	0,21	0,01	0,04	n.d.	0,00	0,21	94,61
PSH-98-85.3	metapelite	7505446	3378078	bt	VI.3	core	36,55	2,25	16,66	0,00	16,79	0,65	12,20	0,00	0,00	10,14	0,00	0,15	0,03	0,05	0,33	0,25	96,06
PSH-98-98.3	metapelite	7494615	3418736	bt	VI.3	at grt	36,60	1,49	18,49	0,01	16,76	0,17	12,43	0,09	0,20	9,15	0,18	0,01	n.d.	0,08	0,39	0,13	96,20
PSH-98-98.3	metapelite	7494615	3418736	bt	VI.3	matrix, core	36,83	1,28	18,92	0,07	16,10	0,34	12,56	0,02	0,15	9,58	0,12	0,11	n.d.	0,06	0,35	0,20	96,67
Chlorites																							
PSH-00-54	meta-andesite	7555569	3431031	chl	II	core	26,70	0,17	22,40	0,08	15,39	0,00	21,39	0,06	0,00	0,06	0,00	0,04	n.d.	0,00	0,14	0,02	86,45
PSH-01-14.3 B	metapelite	7521952	3519947	chl	III	core	24,62	0,08	23,71	n.d.	23,04	0,23	15,92	0,00	0,00	0,00	0,00	n.d.	n.d.	n.d.	n.d.	n.d.	87,60
PSH-98-60.4	metapelite	7518130	3481410	chl	III	alt. from grt	23,94	0,07	22,53	0,09	29,35	0,03	12,33	0,00	0,00	0,00	0,05	0,07	0,00	0,13	0,14	0,07	88,79
PSH-98-61.2	metapelite	7517370	3478400	chl	III	core	24,46	0,13	22,67	0,12	27,18	0,15	13,60	0,00	0,00	0,00	0,00	0,02	n.d.	0,00	0,34	0,02	88,68
PSH-99-47	metabasalt	7510050	3451480	chl	IV.1	core	25,36	0,07	20,80	0,02	24,03	0,37	15,19	0,06	0,00	0,00	0,00	0,06	n.d.	0,00	0,23	0,00	86,21
PSH-00-101.2	metabasalt	7511014	3490940	chl	IV.1	core	26,94	0,05	20,73	0	20,15	0,1	17,91	0,13	0	0,03	0,08	0,12	n.d.	0,03	0,18	0,05	86,51
PSH-00-32	metabasalt	7531488	3444800	chl	IV.1	core	24,62	0,07	20,66	0,03	25,38	0,44	13,89	0,06	0,00	0,03	0,00	0,00	n.d.	0,00	0,16	0,00	85,34

Appendix 1. Continued

Sample	Rock type	Northing	Easting	Mineral	Zone	Site	SiO2	TiO2	Al2O3	Cr2O3	FeO	MnO	MgO	CaO	Na2O	K2O	BaO	NiO	ZnO	SrO	F	Cl	Total
PSH-00-46.2	metabasalt	7542782	3440573	chl	IV.1	core	25,22	0,09	20,96	0	24,72	0,44	14,68	0,04	0	0,02	0	0,07	n.d.	0	0,08	0,02	86,34
PSH-00-67	metabasalt	7524944	3452524	chl	IV.1	core	25,81	0,14	21,7	0,17	20,35	0,25	16,2	0,04	0	0,01	0	0,03	n.d.	0,09	0,11	0,01	84,9
PSH-00-82	metabasalt	7538649	3409705	chl	IV.1	core	25,61	0,06	19,82	0,04	24,9	0,35	14,1	0,08	0	0	0,04	0	n.d.	0	0,18	0,01	85,17
PSH-00-84	metabasalt	7529460	3404642	chl	IV.1	core	24,76	0,01	19,82	0	29,45	0,41	11,33	0,05	0	0	0,07	0,06	n.d.	0	0,15	0,01	86,13
PSH-00-86	metabasalt	7509896	3456787	chl	IV.1	core	25,48	0,06	20,94	0,03	23,36	0,48	15,37	0,03	0	0,03	0,05	0	n.d.	0,11	0,22	0	86,16
PSH-00-88	metabasalt	7509862	3458002	chl	IV.1	core	25,17	0	20,53	0,13	25,82	0,4	13,55	0,04	0	0,05	0	0	n.d.	0,04	0,15	0,02	85,89
PSH-98-101	metabasalt	7533821	3399791	chl	IV.1	core	25,72	0,03	21,08	0,06	21,9	0,29	16,86	0,04	0	0,02	0	0	n.d.	0,16	0,16	0,02	86,34
PSH-99-107	metabasalt	7550487	3433491	chl	IV.1	core	24,98	0,15	19,49	0,00	26,75	0,25	13,49	0,02	0,00	0,00	0,00	0,00	n.d.	0,09	0,19	0,02	85,41
PSH-99-88.1	metabasalt	7562138	3421613	chl	IV.1	core	25,38	0,13	20,66	0,07	25,07	0,28	13,8	0,05	0	0	0	0	n.d.	0,03	0,14	0,07	85,68
83.2-MJV-99	Fe-formation	7478895	3474068	chl	IV.2	core	22,95	0,02	22,62	0,02	32,38	0,14	7,96	0,02	0	0,03	0,01	0	n.d.	0	0,09	0,05	86,29
PSH-98-15.2	metapelite	7481728	3449834	chl	VI.2	alt. from grt	24,71	0,12	21,95	0,00	27,30	0,12	13,06	0,06	0,00	0,07	0,03	0,00	0,01	0,00	0,23	0,02	87,68
PSH-98-18.2B	metapelite	7485693	3447609	chl	VI.2	alt. from grt	24,27	0,17	22,70	0,03	24,07	0,50	15,40	0,05	0,00	0,01	0,00	0,12	0,11	0,00	0,32	0,02	87,77
PSH-98-69.1	metapelite	7469020	3472710	chl	VI.2	matrix, core	25,62	0,00	23,08	0,01	18,54	0,46	19,08	0,00	0,00	0,02	0,00	0,03	n.d.	0,05	0,29	0,06	87,25
PSH-98-69.1	metapelite	7469020	3472710	chl	VI.2	matrix, core	25,62	0,00	23,08	0,01	18,54	0,46	19,08	0,00	0,00	0,02	0,00	0,03	n.d.	0,05	0,29	0,06	87,25
PSH-00-10.3	metapelite	7557588	3409925	chl	VI.3	at grt	24,82	0,14	21,45	n.d.	27,73	0,23	13,31	0,00	0,00	0,00	0,05	0,10	0,05	n.d.	0,00	0,07	87,96
PSH-98-97.1B	metapelite	7495065	3416255	chl	VI.3	at grt	26,26	0,20	22,47	0,03	17,99	0,48	19,80	0,00	0,00	0,00	0,07	0,01	n.d.	0,05	0,18	0,00	87,54
Clinopyroxene																							
PSH-97-19.1L	amphibolite	7574600	3494935	cpx	I	core	49,50	0,19	2,71	n.d.	12,91	0,14	10,98	21,06	0,66	0,00	0,00	n.d.	n.d.	n.d.	n.d.	n.d.	98,15
Cordierites																							
PSH-97-28.4 B	crd-oam rock	7543200	3495550	crd	3	matrix, core	47,69	0,00	32,96	n.d.	8,79	0,06	8,24	0,03	0,42	0,01	0,00	n.d.	n.d.	n.d.	n.d.	n.d.	98,20
PSH-98-11B	metapelite	7466644	3466995	crd	VI.2	core	49,05	0,03	33,13	0,00	3,00	0,09	11,63	0,03	0,13	0,01	0,00	0,00	n.d.	0,06	0,12	0,03	97,31
PSH-98-69.1	metapelite	7469020	3472710	crd	VI.2	at grt	49,27	0,00	32,80	0,00	5,33	0,62	9,93	0,00	0,18	0,02	0,00	0,00	n.d.	0,05	0,00	0,01	98,22
PSH-98-69.1	metapelite	7469020	3472710	crd	VI.2	matrix, core	48,94	0,02	33,02	0,00	5,42	0,80	9,78	0,02	0,14	0,01	0,00	0,00	n.d.	0,11	0,01	0,00	98,25
Epidotes																							
PSH-99-88.1	metabasalt	7562138	3421613	ep	II	core	37,63	0	25,41	0	8,84	0,08	0,04	23,73	0	0,02	0	0	n.d.	0	0,06	0,02	95,83
PSH-99-47	metabasalt	7510050	3451480	ep	IV.1	core	38,57	0,14	28,44	0,03	5,40	0,07	0,03	23,41	0,00	0,01	0,02	0,00	n.d.	0,04	0,04	0,00	96,20
PSH-00-101.2	metabasalt	7511014	3490940	ep	IV.1	core	37,43	0,03	24,5	0,11	10,34	0,14	0,02	23,23	0,02	0	0,04	0,06	n.d.	0,12	0,08	0,03	96,14
PSH-00-32	metabasalt	7531488	3444800	ep	IV.1	core	38,08	0,00	27,81	0,02	6,43	0,03	0,04	23,67	0,00	0,02	0,05	0,00	n.d.	0,05	0,09	0,00	96,27
PSH-00-46.2	metabasalt	7542782	3440573	ep	IV.1	core	38,02	0,07	28,03	0	6,24	0,1	0,04	23,47	0	0,01	0,03	0,01	n.d.	0,03	0,12	0	96,16
PSH-00-67	metabasalt	7524944	3452524	ep	IV.1	core	38,39	0,08	28,44	0,06	5,8	0,15	0	23,39	0	0	0	0	n.d.	0	0,11	0,03	96,45
PSH-00-82	metabasalt	7538649	3409705	ep	IV.1	core	37,72	0	24,41	0,03	9,6	0,06	0	23,41	0	0,02	0	0,01	n.d.	0,13	0,14	0	95,54
PSH-00-86	metabasalt	7509896	3456787	ep	IV.1	core	38,22	0,25	28,64	0	5,5	0,01	0,03	23,86	0	0,03	0,01	0	n.d.	0	0,11	0,03	96,68
PSH-00-88	metabasalt	7509862	3458002	ep	IV.1	core	38,05	0,04	27,93	0	6,32	0,25	0,03	23,2	0	0,03	0	0	n.d.	0,21	0,07	0	96,11
PSH-98-101	metabasalt	7533821	3399791	ep	IV.1	core	38,14	0,04	29,11	0,02	4,63	0	0,02	24	0	0	0	0	n.d.	0,08	0,1	0,01	96,14
PSH-99-107	metabasalt	7550487	3433491	ep	IV.1	core	37,36	0,06	22,51	0,06	12,55	0,17	0,00	22,47	0,00	0,00	0,00	0,00	n.d.	0,32	0,07	0,00	95,58

Appendix 1. Continued

Sample	Rock type	Northing	Easting	Mineral	Zone	Site	SiO2	TiO2	Al2O3	Cr2O3	FeO	MnO	MgO	CaO	Na2O	K2O	BaO	NiO	ZnO	SrO	F	Cl	Total
Garnets																							
PSH-00-40	amphibolite	7596329	3455725	grt	I	core	37,87	0,16	20,91	n.d.	25,24	0,96	3,60	11,07	0,00	0,00	0,00	n.d.	n.d.	n.d.	n.d.	n.d.	99,80
PSH-00-40	amphibolite	7596329	3455725	grt	I	corona	37,28	0,06	20,92	n.d.	26,06	2,32	1,86	10,96	0,00	0,00	0,00	n.d.	n.d.	n.d.	n.d.	n.d.	99,45
PSH-00-42.1	amphibolite	7590218	3440182	grt	I	core	36,88	0,19	21,23	n.d.	27,37	0,69	5,46	7,50	0,00	0,00	0,00	n.d.	n.d.	n.d.	n.d.	n.d.	99,32
PSH-00-42.1	amphibolite	7590218	3440182	grt	I	rim	36,95	0,11	21,30	n.d.	28,12	1,37	4,35	7,52	0,00	0,00	0,00	n.d.	n.d.	n.d.	n.d.	n.d.	99,73
PSH-97-19.1L	amphibolite	7574600	3494935	grt	I	core	37,38	0,08	21,26	n.d.	29,12	1,11	4,94	6,99	0,00	0,00	0,00	n.d.	n.d.	n.d.	n.d.	n.d.	100,88
PSH-97-20.2 A	amphibolite	7572940	3494520	grt	I	core	37,56	0,07	21,19	n.d.	27,77	0,98	4,54	8,01	0,00	0,00	0,00	n.d.	n.d.	n.d.	n.d.	n.d.	100,12
PSH-97-20.2 A	amphibolite	7572940	3494520	grt	I	rim	37,59	0,04	21,03	n.d.	28,79	1,39	3,89	7,54	0,05	0,00	0,00	n.d.	n.d.	n.d.	n.d.	n.d.	100,33
PSH-97-20.2 B	amphibolite	7572940	3494520	grt	I	corona	37,04	0,05	20,92	n.d.	27,92	1,40	4,68	7,64	0,00	0,00	0,00	n.d.	n.d.	n.d.	n.d.	n.d.	99,65
PSH-97-22.8	amphibolite	7563820	3493470	grt	I	core	35,88	0,02	21,00	n.d.	31,10	1,29	1,59	8,45	0,00	0,00	0,00	n.d.	n.d.	n.d.	n.d.	n.d.	99,33
PSH-97-22.8	amphibolite	7563820	3493470	grt	I	rim	37,47	0,03	21,58	n.d.	28,53	0,65	1,35	11,27	0,05	0,00	0,01	n.d.	n.d.	n.d.	n.d.	n.d.	100,93
JTV-98-47.2	metapelite	7563830	3450920	grt	II	core	36,61	0,10	20,58	0,00	32,86	2,41	3,70	1,83	0,00	0,01	0,00	0,00	n.d.	0,15	0,33	0,00	98,59
JTV-98-47.2	metapelite	7563830	3450920	grt	II	rim	37,19	0,00	20,70	0,06	34,36	1,29	3,90	2,62	0,00	0,03	0,00	0,09	n.d.	0,12	0,20	0,00	100,55
JTV-98-49.1	metapelite	7576663	3445005	grt	II	core	37,33	0,04	20,65	0,00	34,63	1,62	4,31	1,34	0,00	0,00	0,00	0,04	0,11	0,12	0,20	0,01	100,39
JTV-98-49.1	metapelite	7576663	3445005	grt	II	rim	36,78	0,04	20,49	0,00	35,56	1,71	3,44	1,42	0,00	0,00	0,03	0,03	0,00	0,05	0,24	0,00	99,79
JTV-98-28.2	metapelite	7552687	3458503	grt	III	core	36,87	0,00	20,35	0,02	30,80	4,69	2,25	4,32	0,00	0,03	0,00	0,00	0,00	0,00	0,24	0,03	99,61
JTV-98-28.2	metapelite	7552687	3458503	grt	III	rim	37,36	0,00	20,72	0,02	32,56	0,14	3,40	5,00	0,00	0,00	0,08	0,00	0,00	0,03	0,29	0,00	99,61
PSH-00-38.2	amphibolite	7528956	3454965	grt	III	core	36,67	0,02	20,51	n.d.	33,60	3,84	0,76	3,90	0,07	0,15	0,04	0,00	0,05	n.d.	0,00	0,07	99,68
PSH-00-38.2	amphibolite	7528956	3454965	grt	III	rim	36,84	0,18	20,15	n.d.	32,40	3,92	0,88	5,21	0,00	0,04	0,03	0,00	0,04	n.d.	0,00	0,02	99,70
PSH-01-14.3 B	metapelite	7521952	3519947	grt	III	core	36,10	0,00	20,87	n.d.	31,74	3,14	3,09	4,56	0,00	0,00	0,00	n.d.	n.d.	n.d.	n.d.	n.d.	99,50
PSH-01-14.3 B	metapelite	7521952	3519947	grt	III	rim	36,69	0,10	20,67	n.d.	31,15	3,00	2,63	5,35	0,00	0,00	0,00	n.d.	n.d.	n.d.	n.d.	n.d.	99,59
PSH-97-1.1	amphibolite	7544752	3493952	grt	III	core	36,27	0,16	20,94	n.d.	31,52	3,68	2,83	4,49	0,00	0,00	0,00	n.d.	n.d.	n.d.	n.d.	n.d.	99,88
PSH-97-1.1	amphibolite	7544752	3493952	grt	III	rim	37,06	0,05	20,82	n.d.	33,17	1,43	3,33	4,71	0,09	0,01	0,00	n.d.	n.d.	n.d.	n.d.	n.d.	100,66
PSH-97-28.3	crd-oam rock	7543200	3495550	grt	III	rim	35,63	0,07	20,74	n.d.	36,45	1,44	3,37	1,76	0,00	0,00	0,00	n.d.	n.d.	n.d.	n.d.	n.d.	99,46
PSH-97-28.4 B	crd-oam rock	7543200	3495550	grt	III	rim	35,82	0,05	21,18	n.d.	37,36	0,99	3,50	0,71	0,08	0,00	0,00	n.d.	n.d.	n.d.	n.d.	n.d.	99,69
PSH-98-41.1	metapelite	7517980	3457930	grt	III	core	37,23	0,00	20,45	0,00	33,22	1,15	2,56	4,90	0,00	0,00	0,00	0,00	0,00	0,08	0,19	0,01	99,78
PSH-98-41.1	metapelite	7517980	3457930	grt	III	near-rim	36,72	0,08	20,24	0,13	39,46	0,42	1,67	1,66	0,00	0,00	0,00	0,08	0,02	0,10	0,19	0,00	100,78
PSH-98-41.1	metapelite	7517980	3457930	grt	III	rim	36,59	0,00	20,15	0,04	39,12	0,20	1,77	1,43	0,00	0,03	0,03	0,06	0,02	0,00	0,31	0,00	99,75
PSH-98-41.2.2	metapelite	7517980	3457930	grt	III	core	37,17	0,00	20,30	0,02	32,35	1,92	4,23	3,85	0,00	0,00	0,06	0,00	0,00	0,00	0,24	0,02	100,16
PSH-98-41.2.2	metapelite	7517980	3457930	grt	III	rim	36,59	0,00	20,09	0,02	38,59	1,01	1,45	1,95	0,00	0,02	0,00	0,04	0,01	0,05	0,33	0,00	100,17
PSH-98-60.4	metapelite	7518130	3481410	grt	III	rim	36,67	0,00	20,02	0,00	33,37	1,16	2,59	4,87	0,00	0,02	0,00	0,02	0,00	0,07	0,19	0,04	99,01
PSH-98-61.2	metapelite	7517370	3478400	grt	III	rim	37,02	0,04	20,30	0,00	34,18	0,99	2,78	4,01	0,00	0,00	0,00	0,00	n.d.	0,02	0,21	0,00	99,56
83.2-MJV-99	Fe-formation	7478895	3474068	grt	IV.2	rim	37,12	0,35	20,82	0,01	31,33	5,95	0,87	3,01	0	0,05	0	0	n.d.	0	0,2	0	99,72
83.2-MJV-99	Fe-formation	7478895	3474068	grt	IV.2	core	37,02	0,11	20,97	0	31,15	6,26	0,91	3,3	0	0,02	0	0,05	n.d.	0	0,15	0	99,93
PSH-00-1.7	skarn	7525947	3385536	grt	IV.2	core	36,63	0,11	20,76	n.d.	29,78	7,08	0,63	5,46	0,00	0,00	0,00	0,00	0,00	n.d.	0,00	0,01	100,45
PSH-00-1.7	skarn	7525947	3385536	grt	IV.2	rim	37,20	0,13	20,71	n.d.	28,19	7,65	0,58	6,46	0,00	0,00	0,06	0,01	0,00	n.d.	0,00	0,00	100,97
92.3-MJV-99	metapelite	7482200	3529044	grt	V.5	core	35,94	0,03	20,39	n.d.	34,78	2,07	3,99	1,71	0,00	0,00	0,00	n.d.	n.d.	n.d.	n.d.	n.d.	98,91
92.3-MJV-99	metapelite	7482200	3529044	grt	V.5	rim	36,18	0,01	20,60	n.d.	35,35	2,89	2,69	1,50	0,08	0,00	0,00	n.d.	n.d.	n.d.	n.d.	n.d.	99,28
98.3-MJV-99	metapelite	7486916	3449031	grt	V.5	rim	36,24	0,01	19,95	n.d.	35,45	3,40	2,65	1,64	0,10	0,00	0,00	n.d.	n.d.	n.d.	n.d.	n.d.	99,44

Appendix 1. Continued

Sample	Rock type	Northing	Easting	Mineral	Zone	Site	SiO2	TiO2	Al2O3	Cr2O3	FeO	MnO	MgO	CaO	Na2O	K2O	BaO	NiO	ZnO	SrO	F	Cl	Total
PSH-01-17.2 A	metapelite	7521105	3535306	grt	V.5	core	36,17	0,00	20,66	n.d.	34,43	3,34	3,24	1,44	0,04	0,00	0,00	n.d.	n.d.	n.d.	n.d.	n.d.	99,31
PSH-01-17.2 A	metapelite	7521105	3535306	grt	V.5	rim	35,90	0,02	20,53	n.d.	34,73	4,16	2,61	1,33	0,00	0,00	0,05	n.d.	n.d.	n.d.	n.d.	n.d.	99,33
PSH-01-8.2	metapelite	7504537	3513451	grt	V.5	core	37,31	0,03	20,56	n.d.	29,09	8,49	3,14	2,07	0,00	0,00	0,00	n.d.	n.d.	n.d.	n.d.	n.d.	100,68
PSH-01-8.2	metapelite	7504537	3513451	grt	V.5	rim	37,24	0,00	20,65	n.d.	27,97	10,35	2,54	1,68	0,00	0,01	0,00	n.d.	n.d.	n.d.	n.d.	n.d.	100,44
PSH-98-15.2	metapelite	7481728	3449834	grt	VI.2	core	37,44	0,05	20,61	0,00	35,07	0,09	3,29	3,21	0,00	0,00	0,07	0,00	0,06	0,01	0,18	0,00	100,08
PSH-98-15.2	metapelite	7481728	3449834	grt	VI.2	rim	37,12	0,11	20,19	0,02	35,29	0,67	2,88	3,13	0,00	0,02	0,00	0,00	0,03	0,06	0,20	0,01	99,73
PSH-98-16.1	amphibolite	7481654	3450010	grt	VI.2	core	37,12	0,18	20,11	0,00	28,16	3,91	1,73	8,11	0,00	0,00	0,00	0,00	0,00	0,10	0,19	0,00	99,60
PSH-98-16.1	amphibolite	7481654	3450010	grt	VI.2	rim	37,16	0,09	20,08	0,01	28,25	3,05	1,94	8,07	0,00	0,02	0,05	0,00	0,01	0,08	0,17	0,02	99,01
PSH-98-18.2B	metapelite	7485693	3447609	grt	VI.2	near rim	36,78	0,22	20,02	0,00	25,60	10,16	1,68	4,80	0,00	0,00	0,00	0,04	0,00	0,17	0,17	0,01	99,63
PSH-98-69.1	metapelite	7469020	3472710	grt	VI.2	core	36,91	0,00	20,45	0,05	24,56	12,80	3,22	1,80	0,00	0,00	0,00	0,02	n.d.	0,13	0,12	0,00	100,08
PSH-98-69.1	metapelite	7469020	3472710	grt	VI.2	rim	36,96	0,01	20,27	0,00	23,44	13,56	2,87	1,89	0,01	0,03	0,00	0,00	n.d.	0,15	0,13	0,03	99,35
PSH-98-97.1B	metapelite	7495065	3416255	grt	VI.2	core	37,02	0,26	20,40	0,03	24,88	10,87	3,24	2,76	0,00	0,02	0,02	0,01	n.d.	0,11	0,11	0,00	99,72
PSH-98-97.1B	metapelite	7495065	3416255	grt	VI.2	rim	37,07	0,00	20,52	0,00	25,01	11,44	3,22	2,12	0,00	0,00	0,00	0,00	n.d.	0,06	0,19	0,03	99,66
JTV-98-38.1B	metapelite	7498984	3391353	grt	VI.3	core	37,02	0,20	20,47	0,04	24,41	10,63	3,59	2,93	0,05	0,00	0,00	0,00	0,06	0,08	0,07	0,00	99,54
JTV-98-38.1B	metapelite	7498984	3391353	grt	VI.3	rim	37,11	0,00	20,36	0,06	25,49	11,42	3,53	1,24	0,00	0,00	0,04	0,03	0,00	0,03	0,14	0,01	99,44
PSH-00-10.3	metapelite	7557588	3409925	grt	VI.3	core	37,87	0,01	21,08	n.d.	33,62	1,17	4,26	2,36	0,00	0,01	0,05	0,00	0,00	n.d.	0,00	0,00	100,44
PSH-00-10.3	metapelite	7557588	3409925	grt	VI.3	rim	37,37	0,00	20,74	n.d.	33,74	4,46	2,58	1,74	0,00	0,02	0,03	0,00	0,01	n.d.	0,00	0,01	100,70
PSH-98-85.3	metapelite	7505446	3378078	grt	VI.3	core	36,99	0,13	18,79	0,00	14,07	19,13	2,08	7,87	0,00	0,00	0,07	0,00	0,03	0,07	0,07	0,00	99,30
PSH-98-98.3	metapelite	7494615	3418736	grt	VI.3	core	37,29	0,10	20,16	0,00	23,72	12,23	2,99	3,16	0,04	0,03	0,09	0,07	n.d.	0,08	0,06	0,05	100,08
PSH-98-98.3	metapelite	7494615	3418736	grt	VI.3	rim	37,19	0,02	20,54	0,01	25,45	11,65	3,53	1,33	0,00	0,02	0,03	0,00	n.d.	0,08	0,25	0,02	100,12
Amphiboles																							
PSH-00-40	amphibolite	7596329	3455725	amph	I	core	39,04	1,62	14,48	n.d.	21,44	0,23	6,23	11,36	1,53	1,76	0,00	n.d.	n.d.	n.d.	n.d.	n.d.	97,70
PSH-00-42.1	amphibolite	7590218	3440182	amph	I	core	43,63	1,00	11,83	n.d.	16,01	0,13	10,66	11,65	1,37	1,02	0,02	n.d.	n.d.	n.d.	n.d.	n.d.	97,30
PSH-00-42.1	amphibolite	7590218	3440182	amph	I	rim	44,14	0,88	11,55	n.d.	15,86	0,09	11,22	11,36	1,31	0,92	0,01	n.d.	n.d.	n.d.	n.d.	n.d.	97,34
PSH-97-19.1L	amphibolite	7574600	3494935	amph	I	core	41,39	1,51	11,25	n.d.	18,67	0,10	9,47	11,20	1,62	0,79	0,00	n.d.	n.d.	n.d.	n.d.	n.d.	96,00
PSH-97-20.2 A	amphibolite	7572940	3494520	amph	I	core	39,00	1,62	13,45	n.d.	20,08	0,20	7,67	11,14	1,44	1,41	0,11	n.d.	n.d.	n.d.	n.d.	n.d.	96,13
PSH-97-20.2 A	amphibolite	7572940	3494520	amph	I	rim	39,49	1,63	13,33	n.d.	20,09	0,22	7,46	11,09	1,65	1,31	0,00	n.d.	n.d.	n.d.	n.d.	n.d.	96,27
PSH-97-20.2 B	amphibolite	7572940	3494520	amph	I	rim	40,04	1,05	13,93	n.d.	19,07	0,17	8,18	11,20	1,54	0,88	0,00	n.d.	n.d.	n.d.	n.d.	n.d.	96,06
PSH-97-22.8	amphibolite	7563820	3493470	amph	I	core	37,58	0,90	14,64	n.d.	25,55	0,14	3,82	11,12	1,59	1,53	0,00	n.d.	n.d.	n.d.	n.d.	n.d.	96,88
PSH-97-22.8	amphibolite	7563820	3493470	amph	I	rim	37,13	0,52	16,02	n.d.	25,21	0,13	3,63	11,11	1,25	1,56	0,00	n.d.	n.d.	n.d.	n.d.	n.d.	96,56
PSH-00-54	meta-andesite	7555569	3431031	amph	II	core	49,56	0,29	7,75	0,15	10,92	0,04	14,72	11,01	0,62	0,08	0,05	0,00	n.d.	0,01	0,16	0,05	95,41
PSH-00-38.2	amphibolite	7528956	3454965	amph	III	core	39,55	0,24	16,75	n.d.	23,52	0,18	3,45	10,66	1,22	0,55	0,00	0,02	0,04	n.d.	0,00	0,06	96,23
PSH-00-38.2	amphibolite	7528956	3454965	amph	III	rim	40,18	0,40	16,69	n.d.	23,43	0,30	3,24	10,25	1,16	0,55	0,00	0,03	0,00	n.d.	0,00	0,00	96,23
PSH-97-1.1	amphibolite	7544752	3493952	amph	III	core	42,29	0,60	14,22	n.d.	19,49	0,07	8,72	10,28	1,85	0,29	0,00	n.d.	n.d.	n.d.	n.d.	n.d.	97,80
PSH-97-1.1	amphibolite	7544752	3493952	amph	III	rim	42,00	0,46	13,59	n.d.	20,00	0,19	8,17	10,59	1,65	0,27	0,00	n.d.	n.d.	n.d.	n.d.	n.d.	96,91
PSH-97-28.3	crd-oam rock	7543200	3495550	ged	III	rim	40,23	0,15	16,30	n.d.	29,59	0,38	8,03	0,21	1,77	0,01	0,00	n.d.	n.d.	n.d.	n.d.	n.d.	96,67
PSH-97-28.3	crd-oam rock	7543200	3495550	ged	III	core	42,09	0,17	14,03	n.d.	30,26	0,31	9,34	0,20	1,55	0,00	0,00	n.d.	n.d.	n.d.	n.d.	n.d.	97,95
PSH-99-47	metabasalt	7510050	3451480	amph	IV.1	core	53,00	0,00	2,01	0,07	13,56	0,34	14,23	12,12	0,02	0,05	0,00	0,00	n.d.	0,00	0,19	0,02	95,59

Appendix 1. Continued

Sample	Rock type	Northing	Easting	Mineral	Zone	Site	SiO2	TiO2	Al2O3	Cr2O3	FeO	MnO	MgO	CaO	Na2O	K2O	BaO	NiO	ZnO	SrO	F	Cl	Total
PSH-00-101.2	metabasalt	7511014	3490940	amph	IV.1	core	51,54	0,35	4,31	0,15	11,65	0,14	15,02	12,06	0,49	0,13	0	0,03	n.d.	0,18	0,11	0,09	96,25
PSH-00-32	metabasalt	7531488	3444800	amph	IV.1	core	53,18	0,07	1,95	0,00	13,09	0,23	14,43	12,49	0,08	0,03	0,00	0,00	n.d.	0,05	0,17	0,01	95,78
PSH-00-46.2	metabasalt	7542782	3440573	amph	IV.1	core	52,87	0,05	2,15	0,03	14,67	0,29	13,58	12,42	0,12	0,08	0	0	n.d.	0,1	0,12	0,02	96,49
PSH-00-67	metabasalt	7524944	3452524	amph	IV.1	core	51,9	0,2	4,44	0,12	11,84	0,28	14,47	11,87	0,29	0,09	0	0,03	n.d.	0	0,21	0,01	95,76
PSH-00-82	metabasalt	7538649	3409705	amph	IV.1	core	52,32	0,12	2,99	0,07	14,31	0,33	13,28	12,38	0,25	0,05	0	0	n.d.	0	0,19	0,01	96,31
PSH-00-84	metabasalt	7529460	3404642	amph	IV.1	core	51,96	0	1,48	0,07	19,04	0,56	10,61	11,91	0,08	0,11	0	0,05	n.d.	0,15	0,17	0,01	96,19
PSH-00-86	metabasalt	7509896	3456787	amph	IV.1	core	51,22	0,19	4,8	0	12,77	0,2	13,99	12,64	0,32	0,18	0	0,05	n.d.	0	0,12	0	96,46
PSH-00-88	metabasalt	7509862	3458002	amph	IV.1	core	48,67	0	7,04	0,06	16,72	0,34	10,5	12,05	0,46	0,32	0	0,02	n.d.	0	0,2	0,04	96,42
PSH-98-101	metabasalt	7533821	3399791	amph	IV.1	core	53,64	0,03	2,16	0,26	11,1	0,25	15,64	12,7	0,07	0,08	0	0,05	n.d.	0,05	0,13	0,01	96,17
PSH-99-107	metabasalt	7550487	3433491	amph	IV.1	core	49,03	0,15	5,55	0,15	17,08	0,24	11,36	11,75	0,73	0,14	0,00	0,00	n.d.	0,00	0,18	0,03	96,39
PSH-99-88.1	metabasalt	7562138	3421613	amph	IV.1	core	42,57	0,37	12,72	0	19,19	0,3	7,4	11,09	1,29	0,1	0	0,05	n.d.	0,09	0,22	0	95,38
83.2-MJV-99	Fe-formation	7478895	3474068	amph	IV.2	core	39,49	0,19	19,21	0	21,94	0,38	2,47	10,65	0,83	0,39	0	0,14	n.d.	0,01	0,25	0,12	96,07
83.2-MJV-99	Fe-formation	7478895	3474068	amph	IV.2	rim	39	0,5	19,41	0,03	21,67	0,32	2,59	11,26	0,87	0,53	0	0	n.d.	0,12	0,29	0,17	96,75
PSH-00-1.7	skarn	7525947	3385536	amph	IV.2	core	37,83	0,35	15,90	n.d.	25,79	0,48	2,60	10,49	1,48	0,71	0,14	0,07	0,10	n.d.	0,00	1,16	97,10
PSH-00-1.7	skarn	7525947	3385536	amph	IV.2	rim	38,05	0,46	14,04	n.d.	27,13	0,53	2,51	10,51	1,53	1,00	0,00	0,00	0,09	n.d.	0,00	1,56	97,40
PSH-98-16.1	amphibolite	7481654	3450010	amph	VI.2	core	41,87	0,59	12,87	0,02	20,92	0,19	7,05	10,94	1,34	0,34	0,00	0,06	0,00	0,11	0,25	0,03	96,58
PSH-98-16.1	amphibolite	7481654	3450010	amph	VI.2	rim	42,06	0,40	12,95	0,00	20,66	0,22	7,11	11,07	1,38	0,31	0,00	0,00	0,00	0,01	0,24	0,03	96,45
Muscovites																							
JTV-98-47.2	metapelite	7563830	3450920	ms	II	core	46,07	0,50	35,43	0,00	0,99	0,02	0,69	0,01	1,78	8,43	0,28	0,07	n.d.	0,07	0,10	0,01	94,46
JTV-98-28.2	metapelite	7552687	3458503	ms	III	core	46,52	0,34	35,43	0,10	1,09	0,05	0,68	0,04	1,05	8,66	0,33	0,04	0,00	0,07	0,09	0,02	94,49
PSH-01-14.3 A	metapelite	7521952	3519947	ms	III	matrix c.	45,51	0,35	33,83	n.d.	2,55	0,00	0,92	0,00	1,15	9,49	0,28	n.d.	n.d.	n.d.	n.d.	n.d.	94,06
PSH-01-14.3 B	metapelite	7521952	3519947	ms	III	core	45,43	0,18	36,02	n.d.	2,40	0,01	0,55	0,00	0,78	9,42	0,67	n.d.	n.d.	n.d.	n.d.	n.d.	95,46
PSH-98-41.1	metapelite	7517980	3457930	ms	III	core	46,73	0,49	33,80	0,06	2,09	0,02	0,79	0,04	1,39	9,13	0,33	0,08	0,02	0,10	0,07	0,01	95,17
PSH-98-41.2.2	metapelite	7517980	3457930	ms	III	matrix	46,19	0,44	34,45	0,09	1,38	0,00	0,62	0,01	1,57	8,94	0,34	0,00	0,00	0,08	0,08	0,00	94,20
PSH-98-41.2.2	metapelite	7517980	3457930	ms	III	alt.	46,58	0,16	35,99	0,09	1,20	0,06	0,38	0,00	1,77	8,95	0,07	0,06	0,00	0,02	0,08	0,02	95,41
PSH-98-60.4	metapelite	7518130	3481410	ms	III	core	45,69	0,30	34,32	0,00	2,12	0,03	0,50	0,02	1,49	9,13	0,29	0,00	0,06	0,11	0,12	0,00	94,20
PSH-98-61.2	metapelite	7517370	3478400	ms	III	core	46,44	0,30	35,16	0,03	2,02	0,02	0,30	0,00	1,73	8,54	0,15	0,07	n.d.	0,02	0,13	0,00	94,92
92.3-MJV-99	metapelite	7482200	3529044	ms	V.5	alt.from g	45,98	0,70	35,18	n.d.	2,51	0,00	0,54	0,00	1,14	9,15	0,31	n.d.	n.d.	n.d.	n.d.	n.d.	95,50
92.3-MJV-99	metapelite	7482200	3529044	ms	V.5	core	46,22	0,42	35,12	n.d.	2,36	0,00	0,45	0,00	1,04	9,03	0,48	n.d.	n.d.	n.d.	n.d.	n.d.	95,12
PSH-01-8.2	metapelite	7504537	3513451	ms	V.5	at grt	46,12	0,58	34,01	n.d.	2,85	0,00	0,62	0,01	1,25	9,31	0,48	n.d.	n.d.	n.d.	n.d.	n.d.	95,24
PSH-01-8.2	metapelite	7504537	3513451	ms	V.5	matrix, core	45,60	0,42	34,17	n.d.	2,97	0,00	0,82	0,00	0,95	9,24	0,21	n.d.	n.d.	n.d.	n.d.	n.d.	94,38
PSH-98-11B	metapelite	7466644	3466995	ms	VI.2	core	45,66	0,70	34,35	0,06	1,57	0,02	0,64	0,03	1,02	10,01	0,30	0,09	n.d.	0,00	0,12	0,03	94,60
PSH-98-15.2	metapelite	7481728	3449834	ms	VI.2	matrix, core	46,32	0,54	34,80	0,00	2,06	0,03	0,54	0,00	1,56	8,94	0,28	0,06	0,06	0,01	0,10	0,02	95,32
PSH-98-15.2	metapelite	7481728	3449834	ms	VI.2	alt. from g.	46,21	0,11	37,09	0,01	1,18	0,00	0,17	0,08	0,61	10,20	0,44	0,01	0,00	0,00	0,07	0,00	96,18
PSH-98-18.2B	metapelite	7485693	3447609	ms	VI.2	alt. from grt	46,46	0,24	35,37	0,04	2,71	0,07	0,42	0,05	1,03	9,70	0,29	0,08	0,00	0,09	0,08	0,00	96,63
PSH-98-69.1	metapelite	7469020	3472710	ms	VI.2	at grt	45,95	0,35	34,64	0,00	2,85	0,09	0,54	0,05	1,48	9,31	0,30	0,02	n.d.	0,02	0,10	0,02	95,73
PSH-98-69.1	metapelite	7469020	3472710	ms	VI.2	matrix, core	46,81	0,18	34,70	0,01	2,75	0,01	0,55	0,03	1,37	9,39	0,28	0,11	n.d.	0,00	0,00	0,00	96,18
PSH-98-97.1B	metapelite	7495065	3416255	ms	VI.2	at grt	46,20	0,40	34,55	0,02	2,32	0,00	0,54	0,09	1,46	9,20	0,58	0,00	n.d.	0,04	0,06	0,01	95,47

Appendix 1. Continued

Sample	Rock type	Northing	Easting	Mineral	Zone	Site	SiO2	TiO2	Al2O3	Cr2O3	FeO	MnO	MgO	CaO	Na2O	K2O	BaO	NiO	ZnO	SrO	F	Cl	Total
PSH-98-97.1B	metapelite	7495065	3416255	ms	VI.2	matrix, core	46,26	0,48	34,19	0,06	2,70	0,00	0,67	0,01	1,43	9,16	0,53	0,02	n.d.	0,03	0,14	0,00	95,66
JTV-98-38.1A	metapelite	7498984	3391353	ms	VI.3	core	45,93	0,76	34,23	0,04	2,70	0,07	0,64	0,03	1,20	9,29	0,96	0,08	0,01	0,00	0,02	0,04	95,99
JTV-98-38.1A	metapelite	7498984	3391353	ms	VI.3	rim	45,80	0,51	33,96	0,00	2,56	0,00	0,62	0,00	1,19	9,44	1,19	0,02	0,01	0,00	0,12	0,00	95,43
PSH-00-10.3	metapelite	7557588	3409925	ms	VI.3	at grt	45,64	0,34	35,09	n.d.	2,71	0,00	0,58	0,06	1,08	9,03	0,60	0,00	0,07	n.d.	0,00	0,00	95,19
PSH-00-10.3	metapelite	7557588	3409925	ms	VI.3	core	47,31	0,39	36,14	n.d.	2,30	0,01	0,40	0,04	1,13	8,88	0,61	0,00	0,02	n.d.	0,00	0,00	97,22
PSH-98-85.3	metapelite	7505446	3378078	ms	VI.3	core	45,51	0,00	36,29	0,04	1,62	0,04	0,13	0,32	0,03	11,62	0,00	0,00	0,00	0,05	0,09	0,00	95,75
PSH-98-98.3	metapelite	7494615	3418736	ms	VI.3	at grt	45,74	0,94	34,48	0,09	2,60	0,03	0,55	0,06	1,17	9,44	0,95	0,00	n.d.	0,00	0,15	0,01	96,22
PSH-98-98.3	metapelite	7494615	3418736	ms	VI.3	matrix, core	44,74	0,49	37,19	0,08	2,23	0,01	0,43	0,02	0,83	9,03	0,66	0,03	n.d.	0,03	0,11	0,00	95,89
Plagioclases																							
PSH-00-40	amphibolite	7596329	3455725	pl	I	core	56,64	0,01	26,59	n.d.	0,05	0,03	0,04	9,26	6,00	0,25	0,00	n.d.	n.d.	n.d.	n.d.	n.d.	98,86
PSH-00-40	amphibolite	7596329	3455725	pl	I	rim	57,61	0,00	25,99	n.d.	0,08	0,03	0,03	8,48	6,82	0,25	0,02	n.d.	n.d.	n.d.	n.d.	n.d.	99,31
PSH-00-42.1	amphibolite	7590218	3440182	pl	I	core	59,88	0,00	25,39	n.d.	0,07	0,00	0,00	6,66	7,85	0,06	0,02	n.d.	n.d.	n.d.	n.d.	n.d.	99,93
PSH-97-19.1L	amphibolite	7574600	3494935	pl	I	core	56,55	0,00	26,87	n.d.	0,11	0,00	0,00	9,12	6,23	0,17	0,03	n.d.	n.d.	n.d.	n.d.	n.d.	99,07
PSH-97-20.2 A	amphibolite	7572940	3494520	pl	I	core	54,37	0,00	28,08	n.d.	0,09	0,00	0,00	10,60	5,99	0,14	0,03	n.d.	n.d.	n.d.	n.d.	n.d.	99,30
PSH-97-20.2 A	amphibolite	7572940	3494520	pl	I	rim	53,75	0,00	28,60	n.d.	0,14	0,00	0,00	10,80	5,71	0,11	0,00	n.d.	n.d.	n.d.	n.d.	n.d.	99,11
PSH-97-20.2 B	amphibolite	7572940	3494520	pl	I	rim	54,28	0,00	27,96	n.d.	0,20	0,00	0,00	10,77	5,50	0,11	0,00	n.d.	n.d.	n.d.	n.d.	n.d.	98,83
PSH-97-22.8	amphibolite	7563820	3493470	pl	I	core	60,89	0,00	23,96	n.d.	0,01	0,01	0,01	5,49	8,55	0,14	0,00	n.d.	n.d.	n.d.	n.d.	n.d.	99,07
PSH-97-22.8	amphibolite	7563820	3493470	pl	I	rim	59,98	0,00	24,75	n.d.	0,19	0,00	0,00	6,55	8,13	0,22	0,00	n.d.	n.d.	n.d.	n.d.	n.d.	99,81
JTV-98-47.2	metapelite	7563830	3450920	pl	II	core	63,62	0,00	22,26	0,00	0,00	0,00	0,00	3,60	9,31	0,14	0,00	0,00	n.d.	0,15	0,05	0,00	99,13
JTV-98-49.1	metapelite	7576663	3445005	pl	II	core	63,76	0,02	22,56	0,02	0,04	0,00	0,00	4,15	9,16	0,04	0,01	0,01	0,02	0,18	0,08	0,00	100,04
PSH-00-54	meta-andesite	7555569	3431031	pl	II	core	53,61	0,00	28,89	0,00	0,18	0,00	0,07	11,10	5,18	0,10	0,07	0,00	n.d.	0,08	0,01	0,02	99,30
PSH-99-88.1	amphibolite	7562138	3421613	pl	II	core	67,11	0,09	20,35	0	0,04	0	0,01	1,09	11,19	0,04	0	0	n.d.	0	0,06	0	99,97
JTV-98-28.2	metapelite	7552687	3458503	pl	III	core	60,64	0,00	24,28	0,02	0,04	0,00	0,01	6,00	8,03	0,06	0,00	0,03	0,13	0,19	0,00	0,00	99,42
PSH-00-38.2	amphibolite	7528956	3454965	pl	III	core	64,38	0,03	22,40	n.d.	0,49	0,01	0,00	3,46	9,56	0,17	0,06	0,00	0,00	n.d.	0,01	0,03	100,59
PSH-01-14.3 A	metapelite	7521952	3519947	pl	III	matrix c.	56,67	0,00	26,85	n.d.	0,07	0,00	0,02	8,93	6,97	0,04	0,00	n.d.	n.d.	n.d.	n.d.	n.d.	99,56
PSH-01-14.3 B	metapelite	7521952	3519947	pl	III	core	57,61	0,00	26,05	n.d.	0,06	0,00	0,03	7,97	7,64	0,06	0,03	n.d.	n.d.	n.d.	n.d.	n.d.	99,45
PSH-97-1.1	amphibolite	7544752	3493952	pl	III	core	61,42	0,00	23,25	n.d.	0,00	0,01	0,00	4,64	9,29	0,04	0,00	n.d.	n.d.	n.d.	n.d.	n.d.	98,66
PSH-97-1.1	amphibolite	7544752	3493952	pl	III	rim	62,29	0,00	22,77	n.d.	0,02	0,04	0,03	4,17	9,71	0,06	0,00	n.d.	n.d.	n.d.	n.d.	n.d.	99,09
PSH-97-28.3	crd-oam rock	7543200	3495550	pl	III	matrix, core	64,83	0,02	21,50	n.d.	0,00	0,00	0,00	2,19	10,49	0,05	0,00	n.d.	n.d.	n.d.	n.d.	n.d.	99,09
PSH-97-28.4 A	crd-oam rock	7543200	3495550	pl	III	at grt	67,00	0,00	20,24	n.d.	0,02	0,00	0,02	0,53	11,57	0,03	0,06	n.d.	n.d.	n.d.	n.d.	n.d.	99,48
PSH-98-41.1	metapelite	7517980	3457930	pl	III	core	61,46	0,00	23,86	0,02	0,07	0,01	0,00	5,61	8,41	0,13	0,00	0,00	0,00	0,14	0,03	0,02	99,75
PSH-98-41.2.2	metapelite	7517980	3457930	pl	III	alt. from grt?	61,85	0,08	23,60	0,02	0,10	0,00	0,00	5,40	8,52	0,11	0,00	0,00	0,00	0,17	0,02	0,00	99,88
PSH-98-41.2.2	metapelite	7517980	3457930	pl	III	alt. from grt?	61,85	0,08	23,60	0,02	0,10	0,00	0,00	5,40	8,52	0,11	0,00	0,00	0,00	0,17	0,02	0,00	99,88
PSH-98-60.4	metapelite	7518130	3481410	pl	III	core	60,00	0,00	24,69	0,03	0,04	0,00	0,00	6,70	7,70	0,02	0,05	0,00	0,00	0,21	0,00	0,01	99,48
PSH-98-61.2	metapelite	7517370	3478400	pl	III	core	60,59	0,06	24,31	0,05	0,19	0,07	0,00	6,17	7,95	0,08	0,00	0,01	n.d.	0,22	0,00	0,00	99,69
PSH-99-47	metabasalt	7510050	3451480	pl	IV.1	core	67,42	0,00	19,82	0,02	0,16	0,00	0,00	0,31	11,73	0,09	0,00	0,00	n.d.	0,00	0,05	0,01	99,60
PSH-00-101.2	metabasalt	7511014	3490940	pl	IV.1	core	67,41	0	19,94	0,04	0,14	0	0	0,82	11,43	0,04	0	0	n.d.	0,04	0	0,02	99,89
PSH-00-32	metabasalt	7531488	3444800	pl	IV.1	core	70,12	0,12	18,27	0,00	0,12	0,00	0,01	0,67	10,31	0,05	0,00	0,00	n.d.	0,00	0,07	0,04	99,80

Appendix 1. Continued

Sample	Rock type	Northing	Easting	Mineral	Zone	Site	SiO2	TiO2	Al2O3	Cr2O3	FeO	MnO	MgO	CaO	Na2O	K2O	BaO	NiO	ZnO	SrO	F	Cl	Total
PSH-00-46.2	metabasalt	7542782	3440573	pl	IV.1	core	67,4	0,09	20,08	0	0,06	0	0,11	1,02	11,06	0,04	0	0	n.d.	0,11	0,01	0	99,98
PSH-00-67	metabasalt	7524944	3452524	pl	IV.1	core	66,8	0,03	20,59	0,03	0,09	0,02	0	1,51	10,32	0,09	0	0	n.d.	0	0,17	0,01	99,67
PSH-00-82	metabasalt	7538649	3409705	pl	IV.1	core	67,63	0	19,56	0	0,19	0,01	0,01	0,41	11,54	0,06	0	0	n.d.	0,01	0,04	0,05	99,51
PSH-00-84	metabasalt	7529460	3404642	pl	IV.1	core	67,66	0	19,85	0	0,22	0	0,04	0,47	11,09	0,05	0	0,04	n.d.	0,13	0,09	0,02	99,66
PSH-00-86	metabasalt	7509896	3456787	pl	IV.1	core	67,39	0	19,96	0,01	0,1	0	0,01	0,4	11,88	0,06	0	0,04	n.d.	0	0	0	99,86
PSH-00-88	metabasalt	7509862	3458002	pl	IV.1	core	66,11	0,1	20,78	0	0,17	0	0	1,7	10,72	0,08	0	0	n.d.	0,12	0,07	0,01	99,86
PSH-98-101	metabasalt	7533821	3399791	pl	IV.1	core	67,82	0,02	19,67	0,01	0,11	0,03	0	0,42	11,39	0,03	0,05	0	n.d.	0	0,05	0,02	99,6
PSH-99-107	metabasalt	7550487	3433491	pl	IV.1	core	67,60	0,01	19,77	0,03	0,07	0,00	0,00	0,35	11,73	0,07	0,00	0,06	n.d.	0,07	0,00	0,00	99,74
83.2-MJV-99	Fe-formation	7478895	3474068	pl	IV.2	core	48,83	0,01	32,62	0,01	0,3	0	0	15,5	2,58	0,02	0	0	n.d.	0,07	0,05	0	99,99
PSH-00-1.7	skarn	7525947	3385536	pl	IV.2	core near grt	60,15	0,00	25,40	n.d.	0,23	0,00	0,00	6,91	7,90	0,06	0,00	0,06	0,00	n.d.	0,00	0,03	100,74
PSH-00-1.7	skarn	7525947	3385536	pl	IV.2	core, matrix	57,94	0,08	26,83	n.d.	0,33	0,00	0,00	8,29	6,85	0,02	0,00	0,01	0,00	n.d.	0,00	0,00	100,34
92.3-MJV-99	metapelite	7482200	3529044	pl	V.5	incl. in grt	63,42	0,00	23,16	n.d.	0,01	0,00	0,00	4,80	9,04	0,07	0,00	n.d.	n.d.	n.d.	n.d.	n.d.	100,52
92.3-MJV-99	metapelite	7482200	3529044	pl	V.5	core	61,36	0,00	23,05	n.d.	0,04	0,00	0,00	4,85	9,37	0,05	0,00	n.d.	n.d.	n.d.	n.d.	n.d.	98,73
PSH-01-17.2 B	metapelite	7521105	3535306	pl	V.5	core	59,64	0,00	25,48	n.d.	0,04	0,00	0,04	7,17	7,62	0,04	0,00	n.d.	n.d.	n.d.	n.d.	n.d.	100,03
PSH-01-8.2	metapelite	7504537	3513451	pl	V.5	matrix, core	59,14	0,00	25,25	n.d.	0,02	0,03	0,00	6,81	7,75	0,05	0,00	n.d.	n.d.	n.d.	n.d.	n.d.	99,05
PSH-98-15.2	metapelite	7481728	3449834	pl	VI.2	matrix, core	62,56	0,06	23,15	0,00	0,06	0,04	0,00	4,53	8,81	0,07	0,13	0,00	0,00	0,14	0,11	0,02	99,68
PSH-98-15.2	metapelite	7481728	3449834	pl	VI.2	alt. from g.	62,74	0,00	23,21	0,00	0,02	0,00	0,01	4,60	8,72	0,14	0,02	0,01	0,00	0,13	0,01	0,01	99,62
PSH-98-16.1	amphibolite	7481654	3450010	pl	VI.2	core, matrix	61,88	0,02	23,45	0,00	0,14	0,04	0,02	5,27	8,58	0,08	0,01	0,01	0,00	0,15	0,08	0,00	99,74
PSH-98-16.1	amphibolite	7481654	3450010	pl	VI.2	core, next to grt	61,28	0,04	23,64	0,06	0,11	0,07	0,00	5,30	8,46	0,04	0,00	0,00	0,06	0,29	0,03	0,02	99,40
PSH-98-18.2B	metapelite	7485693	3447609	pl	VI.2	alt. from grt	62,55	0,00	23,43	0,00	0,03	0,00	0,00	5,05	8,72	0,03	0,00	0,07	0,03	0,07	0,03	0,01	100,02
PSH-98-97.1B	metapelite	7495065	3416255	pl	VI.2	at grt	61,87	0,04	23,74	0,00	0,13	0,03	0,00	5,53	8,29	0,02	0,00	0,04	n.d.	0,24	0,03	0,01	99,98
PSH-98-97.1B	metapelite	7495065	3416255	pl	VI.2	at grt	61,87	0,04	23,74	0,00	0,13	0,03	0,00	5,53	8,29	0,02	0,00	0,04	n.d.	0,24	0,03	0,01	99,98
JTV-98-38.1A	metapelite	7498984	3391353	pl	VI.3	core at st	61,08	0,01	23,61	0,01	0,06	0,00	0,00	5,54	8,37	0,07	0,06	0,06	0,00	0,20	0,10	0,00	99,18
JTV-98-38.1B	metapelite	7498984	3391353	pl	VI.3	core	61,59	0,00	23,82	0,08	0,09	0,03	0,00	5,67	8,22	0,03	0,08	0,00	0,00	0,12	0,08	0,01	99,82
PSH-00-10.3	metapelite	7557588	3409925	pl	VI.3	core	62,07	0,00	24,34	n.d.	0,00	0,00	0,01	5,35	8,67	0,09	0,09	0,02	0,00	n.d.	0,00	0,00	100,64
PSH-00-10.3	metapelite	7557588	3409925	pl	VI.3	rim	63,19	0,06	25,25	n.d.	0,06	0,00	0,00	5,55	8,39	0,05	0,02	0,03	0,00	n.d.	0,00	0,00	102,61
PSH-98-85.3	metapelite	7505446	3378078	pl	VI.3	core	44,07	0,00	35,25	0,00	0,28	0,00	0,00	19,21	0,34	0,02	0,00	0,07	0,03	0,10	0,02	0,02	99,43
PSH-98-98.3	metapelite	7494615	3418736	pl	VI.3	matrix, core	61,69	0,03	23,89	0,00	0,05	0,01	0,00	5,89	8,21	0,04	0,00	0,09	n.d.	0,07	0,07	0,00	100,03
PSH-98-98.3	metapelite	7494615	3418736	pl	VI.3	rim	61,46	0,00	24,09	0,02	0,00	0,04	0,00	5,80	8,26	0,11	0,00	0,00	n.d.	0,20	0,00	0,00	99,99
Staurolites																							
PSH-01-14.3 A	metapelite	7521952	3519947	st	III	core	27,53	0,54	53,72	0,07	13,16	0,29	1,78	0,01	0,05	0,00	0,01	n.d.	0,04	n.d.	n.d.	n.d.	97,19
PSH-01-17.2 B	metapelite	7521105	3535306	st	III	core	27,95	0,57	52,50	0,10	15,28	0,25	1,65	0,00	0,00	0,00	0,00	n.d.	0,10	n.d.	n.d.	n.d.	98,40
PSH-98-69.1	metapelite	7469020	3472710	st	VI.2	matrix, core	27,77	0,47	51,87	0,05	12,01	0,87	1,97	0,00	0,42	0,03	0,00	0,10	2,44	0,03	0,10	0,00	98,12
PSH-98-97.1B	metapelite	7495065	3416255	st	VI.2	core, at grt	27,46	0,64	52,33	0,01	13,12	1,03	2,33	0,03	0,01	0,00	0,00	0,05	0,34	0,10	0,06	0,00	97,53
PSH-98-97.1B	metapelite	7495065	3416255	st	VI.2	rim	27,12	0,48	52,71	0,08	13,07	0,93	2,23	0,00	0,06	0,00	0,00	0,07	0,38	0,07	0,08	0,00	97,28
JTV-98-38.1A	metapelite	7498984	3391353	st	VI.3	core	27,21	0,52	52,11	0,00	12,84	1,01	2,28	0,01	0,10	0,02	0,00	0,00	0,78	0,10	0,17	0,01	97,16
JTV-98-38.1A	metapelite	7498984	3391353	st	VI.3	core	26,74	0,62	52,52	0,13	12,81	0,76	2,26	0,00	0,11	0,03	0,01	0,02	0,81	0,11	0,11	0,00	97,05
PSH-98-98.3	metapelite	7494615	3418736	st	VI.3	core	27,19	0,44	52,89	0,08	12,18	0,93	2,08	0,00	0,15	0,04	0,01	0,00	1,00	0,00	0,12	0,01	97,12
PSH-98-98.3	metapelite	7494615	3418736	st	VI.3	rim	27,01	0,46	52,59	0,00	12,65	0,83	2,32	0,03	0,17	0,04	0,00	0,09	0,73	0,05	0,15	0,02	97,13

Appendix 2

Appendix 2. THERMOCALC average P-T results for mafic rocks.

Sample	**PSH-00-42**		**PSH-00-42**		**PSH-97-19.1L**		**PSH-97-20.2A**		**PSH-97-20.2A**		**PSH-97-20.2B**		**PSH-97-22.8**		**PSH-97-22.8**		**PSH-00-40**	
P-T stage	Peak		Cooling		Peak		Peak		Cooling		Cooling		Peak		Cooling		Peak	
Zone	I		I		I		I		I		I		I		I		I	
Activities	at 850°C		at 800°C		at 850°C		at 850°C		at 800°C		at 800°C		at 850°C		at 800°C		at 850°C	
Garnet	core		rim		core		core		rim		grt corona		core		rim		core	
prp	0.0205		0.0115		0.0141		0.0126		0.00790		0.0121		0.000750		0.000560		0.00770	
grs	0.0149		0.0143		0.0105		0.0160		0.0122		0.0119		0.0170		0.0360		0.0350	
alm	0.130		0.150		0.160		0.150		0.180		0.150		0.230		0.200		0.120	
Amphibole	core		rim		core		core		rim		rim		core		rim		mean	
tr	0.0250		0.0362		0.0161		0.00809		0.00640		0.0152		0.000533		0.000833		0.00268	
fact	0.000520		0.000420		0.000960		0.000720		0.000900		0.00100		0.00360		0.00399		0.00100	
ts	0.00230		0.00170		0.000300		0.000200		0.000300		0.000800		0.00007		0.000130		0.000300	
parg	0.0490		0.0610		0.0224		0.0202		0.0166		0.0417		0.00271		0.00512		0.0113	
gl	-		0.000813		-		-		-		0.0007595		-		-		-	
Plagioclase	mean		mean		core		core		rim		rim		core		rim		core	
an	0.410		0.410		0.560		0.630		0.650		0.660		0.340		0.400		0.570	
ab	0.690		0.690		0.560		0.520		0.500		0.490		0.740		0.690		0.540	
Clinoprproxene					core													
di	-		-		0.510		-		-		-		-		-		-	
hed	-		-		0.300		-		-		-		-		-		-	
cats	-		-		0.0400		-		-		-		-		-		-	
Other	qtz H2O		qtz H2O		qtz H2O		qtz H2O		qtz H2O		qtz H2O		qtz H2O		qtz H2O		qtz H2O	
Results																		
*a*H2O	1.0	0.4	1.0	0.4	1.0	0.4	1.0	0.4	1.0	0.4	1.0	0.4	1.0	0.4	1.0	0.4	1.0	0.4
T°C	**894**	**853**	**807**	**772**	**943**	**887**	**911**	**879**	**858**	**828**	**848**	**812**	**794**	**772**	**743**	**722**	**1011**	**966**
s.d.(T)	99	89	112	80	79	70	118	109	110	102	99	90	117	110	105	99	146	133
P kbar	**12.7**	**11.8**	**11.1**	**10.4**	**10.5**	**9.7**	**11.6**	**10.7**	**10.3**	**9.5**	**9.7**	**9.0**	**11.8**	**11.1**	**11.6**	**10.9**	**14.4**	**13.2**
s.d.(P)	1.8	1.7	2.0	1.5	1.4	1.3	1.9	1.8	1.8	1.7	1.6	1.5	2.0	1.9	1.8	1.7	2.2	2.0
correl.	0.527	0.487	0.607	0.574	0.372	0.328	0.552	0.495	0.532	0.478	0.538	0.490	0.738	0.699	0.753	0.715	0.698	0.639
fit	0.83	0.58	1.27	0.93	0.90	0.61	0.83	0.62	0.97	0.74	0.84	0.69	0.37	0.21	0.40	0.27	0.63	0.43
NR	4	4	4	4	7	7	4	4	4	4	4	4	4	4	4	4	4	4
end members eliminated	-	-	-	gl	-	-	-	-	-	-	gl	gl	-	-	-	-	-	-

Appendix 2. Continued

Appendix 2. THERMOCALC Average P-T results for mafic rocks.																		
Sample	**PSH-00-40**		**PSH-97-1.1**		**PSH-97-1.1**		**PSH-00-38.2**		**PSH-00-38.2**		**PSH-98-16.1**		**PSH-98-16.1**		**PSH-00-1.7**		**PSH-00-1.7**	
P-T stage	Cooling		pre-peak		Peak		pre-peak		Peak		pre-peak		Peak		pre-peak		Peak	
Zone	I		II		II		III.1		III.1		VI.2		VI.2		IV.2		IV.2	
Activities	at 800°C		at 650°C		at 700°C		at 550°C		at 550°C		at 650°C		at 650°C		at 550°C		at 550°C	
Garnet	corona		core		rim		core		rim		core		rim		core		rim	
prp	0.00134		0.00310		0.00450		0.000068		0.000107		0.000910		0.00130		0.000044		0.000035	
grs	0.0330		0.00300		0.00300		0.00150		0.00330		0.0120		0.0130		0.00400		0.00600	
alm	0.160		0.250		0.280		0.410		0.360		0.210		0.220		0.260		0.230	
Amphibole	mean		core		rim		core		rim		core		rim		core		rim	
tr	0.00315		0.0456		0.0338		0.00280		0.00169		0.0205		0.0213		0.00125		0.000899	
fact	0.00100		0.00196		0.00297		0.0123		0.0107		0.00620		0.00590		0.0223		0.0245	
ts	0.000300		0.00150		0.00130		0.00110		0.00110		0.00110		0.00130		0.000120		0.00002	
parg	0.0119		0.106		0.0784		0.00898		0.00669		0.0359		0.0371		0.00494		0.00216	
gl	-		0.00952		0.00418		0.00141		0.00143		0.00125		0.00130		0.00166		0.000632	
Plagioclase	rim		core		rim		core		core		matrix		next to grt		matrix		next to grt	
an	0.520		0.320		0.350		0.280		0.280		0.380		0.380		0.640		0.530	
ab	0.590		0.790		0.760		0.830		0.830		0.750		0.750		0.610		0.680	
Other	qtz H2O		qtz H2O		qtz H2O		qtz H2O		qtz H2O		qtz H2O		qtz H20		qtz H2O		qtz H2O	
Results																		
*a*H2O	1.0	0.4	1.0	0.4	1.0	0.4	1.0	0.4	1.0	0.4	1.0	0.4	1.0	0.4	1.0	0.4	1.0	0.4
T°C	**733**	**709**	**645**	**615**	**692**	**666**	**514**	**493**	**560**	**533**	**710**	**673**	**732**	**693**	**474**	**456**	**527**	**507**
s.d.(T)	96	90	55	50	62	57	62	56	66	64	72	61	70	62	46	43	57	54
P kbar	**11.1**	**10.4**	**7.2**	**6.8**	**7.4**	**7.0**	**4.5**	**4.1**	**5.9**	**5.4**	**8.1**	**7.4**	**8.6**	**7.9**	**3.2**	**2.8**	**4.1**	**3.7**
s.d.(P)	1.7	1.5	1.4	1.4	1.5	1.5	1.5	1.5	1.8	1.8	1.7	1.4	1.6	1.5	1.0	1.0	1.1	1.1
correl.	0.669	0.624	0.672	0.666	0.647	0.638	0.590	579	0.656	0.651	0.706	0.688	0.711	0.692	0.544	0.536	0.594	569
fit	0.95	0.73	0.79	0.60	0.69	0.51	1.22	1.19	1.28	1.33	1.09	0.88	1.04	0.84	0.70	0.78	0.45	41
NR	4	4	5	5	5	5	5	5	5	5	5	5	5	5	5	5	5	5
end members eliminated	gl	-	-	-	-	-	-	-	-	-	-	-	-	-	-	-	-	-

Appendix 2. Continued

Appendix 2 (cont.). THERMOCALC Average P-T results for pelitic rocks.																		
Sample	**JTV-98-47**		**JTV-98-47**		**JTV-98-49**		**JTV-98-49**		**JTV-98-28**		**JTV-98-28**		**PSH-98-41.1**		**PSH-98-41.1**		**PSH-98-41.2**	
P-T stage	pre-peak		Peak		Peak		Cooling		Pre-peak		Peak		peak, M1		cooling, M2		Peak	
Zone	II		II		II		II		II		II		III.1		III.1		III.1	
Activities	at 650°C		at 650°C		at 650°C		at 650°C		at 650°C		at 650°C		at 650°C		at 650°C		at 650°C	
Garnet	core		rim		core		rim		core		rim		core		rim		core	
prp	0.00500		0.00570		0.00650		0.00360		0.00138		0.00490		0.00210		0.000530		0.00750	
grs	0.00026		0.00059		0.000088		0.000098		0.00210		0.00410		0.00330		0.000079		0.00160	
alm	0.390		0.360		0.400		0.440		0.280		0.340		0.360		0.650		0.270	
Biotite	core		core		core		core		core		core		core		core		core	
phl	0.0700		0.0700		0.0520		0.0520		0.0800		0.0800		0.0210		0.0210		0.0198	
ann	0.0390		0.0390		0.0510		0.0510		0.0330		0.0330		0.110		0.110		0.120	
east	0.0570		0.0570		0.0450		0.0450		0.0560		0.0560		0.0220		0.0220		0.0220	
Muscovite	core		core						core		core		core		core		core	
mu	0.690		0.690		-		-		0.680		0.680		0.640		0.640		0.690	
pa	-		-		-		-		0.680		0.680		0.700		0.700		0.800	
cel	0.0160		0.0160		-		-		0.0160		0.0160		0.0210		0.0210		0.0160	
Plagioclase	core		core		core		core		core		core		core		core		core	
an	0.260		0.260		0.300		0.300		0.430		0.430		0.400		0.400		0.380	
ab	-		-		-		-		0.710		0.710		0.730		0.730		0.740	
Other	ky qtz H2O		ky qtz H2O		ky qtz H2O		ky qtz H2O		ky qtz H2O		ky qtz H2O		qtz H2O		qtz H2O		qtz H2O	
Results																		
*a*H2O	1.0	0.4	1.0	0.4	1.0	0.4	1.0	0.4	1.0	1.0	1.0	1.0	1.0	0.4	1.00	0.4	1.00	0.4
T°C	**602**	**602**	**598**	**598**	**694**	**694**	**602**	**602**	**650**	**602**	**670**	**643**	**601**	**551**	**590**	**536**	**598**	**549**
s.d.(T)	78	78	76	76	120	120	102	102	29	30	22	30	32	35	47	44	65	64
P kbar	**7.9**	**7.9**	**8.5**	**8.5**	**7.4**	**7.4**	**6.2**	**6.2**	**8.6**	**7.6**	**9.9**	**9.3**	**8.3**	**7.6**	**5.5**	**5.0**	**7.8**	**7.2**
s.d.(P)	1.4	1.4	1.4	1.4	2.1	2.1	1.8	1.8	1.4	1.1	1.0	1.1	1.1	1.4	1.8	1.8	2.4	2.6
correl.	0.737	0.736	0.760	0.76	0.831	0.831	0.821	0.821	0.785	0.785	0.764	0.794	0.752	0.760	0.734	0.759	0.726	0.740
fit	0.33	0.33	0.34	0.34	0.19	0.19	0.19	0.19	1.33	0.93	0.76	0.53	1.1	1.42	1.75	1.87	2.34	2.68
NR	5	5	5	5	3	3	3	3	6	5	6	5	5	5	5	5	5	5
end members eliminated	-	-	-	-	-	-	-	-	-	ky	-	ky	-	-	-	-	-	-

Appendix 2. Continued

Appendix 2 (cont.). THERMOCALC Average P-T results for pelitic rocks.																		
Sample	**PSH-98-41.2**		**PSH-98-60.4**		**PSH-98-61.2**		**PSH-98-61.2**		**PSH-98-61.2**		**PSH-01-14.3**		**PSH-01-14.3**		**PSH-01-14.3**		**PSH-01-17.2**	
P-T stage	cooling, M2		M2		M2		M2		M2		Peak		Peak		cooling, M2		Peak	
Zone	III.1		III		III		III		III		III		III		III		V.5	
Activities	at 650°C		at 550°C		at 550°C		at 550°C		at 550°C		at 650°C		at 650°C		at 550°C		at 650°C	
Garnet	rim		rim		rim		rim		rim		core		core		rim		core	
prp	0.000300		0.00240		0.00260		0.00260		0.00260		0.00450		0.00450		0.00280		0.00340	
grs	0.000170		0.00300		0.00180		0.00180		0.00180		0.00330		0.00330		0.00460		0.000107	
alm	0.600		0.350		0.390		0.390		0.390		0.240		0.240		0.260		0.370	
Biotite	core										matrix, core		matrix, core				core	
phl	0.0194		-		-		-		-		0.0580		0.0580		-		0.0350	
ann	0.110		-		-		-		-		0.0410		0.0410		-		0.0650	
east	0.0210		-		-		-		-		0.0600		0.0600		-		0.0380	
Muscovite	core		alt. from g		alt. from g		alt. from g		alt. from g		matrix, core		matrix, core		alt. from g			
mu	0.730		0.690		0.690		0.690		0.690		0.650		0.650		0.690		-	
pa	0.890		0.950		0.970		0.970		0.970		0.780		0.780		0.591		-	
cel	0.00930		0.0130		0.00740		0.00740		0.00740		0.0230		0.0230		0.00850		-	
Chlorite			alt. from g		alt. from g		alt. from g		alt. from g						alt. from g			
clin	-		0.0114		0.0180		0.0180		0.0180		-		-		0.040		-	
daph	-		0.0450		0.0330		0.0330		0.0330		-		-		0.0150		-	
ames	-		0.0197		0.0270		0.0270		0.0270		-		-		0.0480		-	
Plagioclase	core		core		core		core		core		core		core		core		core	
an	0.380		0.530		0.490		0.490		0.490		0.660		0.660		0.590		0.500	
ab	0.740		0.680		0.710		0.710		0.710		0.600		0.600		0.640		-	
Other	qtz H2O		and ky qtz H2O		and ky qtz H2O		and ky qtz H2O		and ky qtz H2O		mst 0.0019 fst 0.39 ky and qtz H2O		mst 0.0019 fst 0.39 ky and qtz H2O		mst 0.0011 fst 0.45 ky and qtz H2O		mst 0.00089 fst 0.470 sill qtz H2O	
Results																		
*a*H2O	1.0	0.4	1.0	1.0	1.0	0.4	1.0	0.4	1.0	0.4	1.0	1.0	1.0	0.4	1.0	0.4	1.0	0.4
T°C	**559**	**509**	**576**	**563**	**564**	**507**	**582**	**528**	**584**	**530**	**616**	**586**	**588**	**543**	**594**	**537**	**596**	**553**
s.d.(T)	27	24	23	23	17	15	13	13	20	18	27	20	27	30	25	21	32	29
P kbar	**5.0**	**4.5**	**6.3**	**4.5**	**4.6**	**3.9**	**6.8**	**6.1**	**6.1**	**5.5**	**7.9**	**4.8**	**7.3**	**6.9**	**6.3**	**5.6**	**4.4**	**4.1**
s.d.(P)	1.1	1.0	1.4	0.3	0.2	0.2	0.8	0.9	1.0	1.0	1.2	0.3	1.1	1.3	1.3	1.2	1.5	1.4
correl.	0.744	0.769	0.579	0.657	0.901	0.853	0.622	0.690	0.780	0.816	0.776	0.904	0.740	0.758	0.666	0.720	0.940	0.946
fit	0.52	0.43	1.75	1.81	1.88	1.74	1.07	1.17	1.42	1.46	1.11	1.70	1.00	1.27	1.69	1.64	0.55	0.83
NR	5	5	6	7	7	7	6	6	6	6	7	9	5	5	7	7	5	5
end members eliminated	-	-	ky	-	-	-	and	and	ky	ky	ky and	-	mst ky fst and	mst ky fst and	-	-	-	-

Appendix 2. Continued

Appendix 2 (cont.). THERMOCALC Average P-T results for pelitic rocks.																		
Sample	**PSH-01-17.2**		**PSH-01-8.2**		**PSH-01-8.2**		**MJV-99-98**		**MJV-99-98**		**PSH-98-15.2**		**PSH-98-15.2**		**PSH-98-69.1**		**PSH-98-69.1**	
P-T stage	Cooling		Peak		Cooling		Peak		Cooling		Peak		Cooling		Peak		Peak	
Zone	V.5		V.5		V.5		VI.2		VI.2		VI.2		VI.2		VI.2		VI.2	
Activities	at 650°C		at 600°C		at 600°C		at 650°C		at 600°C		at 600°C		at 600°C		at 600°C		at 600°C	
Garnet	rim		core		rim		core		rim		core		rim		core		core	
prp	0.00180		0.00270		0.00140		0.00610		0.00180		0.00380		0.00250		0.00290		0.00290	
grs	0.000079		0.000260		0.000140		0.000180		0.000110		0.00115		0.000910		0.00018		0.00018	
alm	0.390		0.230		0.220		0.340		0.380		0.440		0.440		0.130		0.130	
Biotite	core		matrix, core		core, at grt		core		alt. from g		matrix, core		at grt		matrix, core		matrix, core	
phl	0.0350		0.0570		0.0540		0.0320		0.0241		0.0276		0.0350		0.0950		0.0950	
ann	0.0650		0.0500		0.0530		0.0640		0.0690		0.0920		0.0840		0.0250		0.0250	
east	0.0380		0.0470		0.0450		0.0350		0.0310		0.0280		0.0330		0.0710		0.0710	
Muscovite			matrix core		core, at grt		core		alt. from g		matrix, core		alt. from g		matrix, core		matrix, core	
mu	-		0.630		0.640		0.670		0.650		0.670		0.800		0.660		0.660	
pa	-		0.566		0.710		0.570		0.660		0.830		0.518		0.77		0.77	
cel	-		0.0180		0.0150		0.0105		0.0120		0.0130		0.00410		0.014		0.014	
Chlorite													alt. from g.		matrix, core		matrix, core	
clin	-		-		-				-		-		0.0164		0.0850		0.0850	
daph	-		-		-				-		-		0.0360		0.00460		0.00460	
ames	-		-		-				-		-		0.0205		0.0770		0.0770	
Plagioclase	core		core		core		core		incl. in g		matrix, core		alt.from g		-		-	
an	0.500		0.500		0.500		0.330		0.360		0.350		0.350		qtz crd 0.61		qtz crd 0.61	
ab	-		0.680		0.680		0.780		0.780		0.780		0.770		fcrd 0.048		fcrd 0.048	
Other	mst 0.00089		sill qtz		sill qtz		sill qtz		sill qtz		qtz H2O		qtz H2O		mncrd 0.0016		mncrd 0.0016	
	fst 0.470		H2O		H2O		H2O		H2O						mst 0.0051		mst 0.0051	
	sill qtz H2O														fst 0.29 H2O		fst 0.29 H2O	
															spss 0.023 and		spss 0.023 and	
Results																		
*a*H2O	1.0	0.4	1.0	0.4	1.0	0.4	1.0	0.4	1.0	0.4	1.0	0.4	1.0	0.4	1.0	0.4	1.0	0.4
T°C	**581**	**539**	**619**	**562**	**568**	**518**	**672**	**609**	**623**	**565**	**611**	**560**	**588**	**532**	**597**	**542**	**591**	**531**
s.d.(T)	32	30	27	25	25	23	29	26	28	26	27	29	22	22	15	19	33	43
P kbar	**3.7**	**3.4**	**5.3**	**4.9**	**4.0**	**3.6**	**7.2**	**6.6**	**5.6**	**5.1**	**8.1**	**7.5**	**6.0**	**5.3**	**5.1**	**4.2**	**5.1**	**4.1**
s.d.(P)	1.4	1.4	1.1	1.1	1.0	1.0	1.2	1.1	1.1	1.1	1.1	1.2	1.3	1.4	0.5	0.7	0.8	1.1
correl.	0.943	0.951	0.908	0.918	0.916	0.929	0.907	0.917	0.913	0.932	0.732	0.748	0.529	0.641	0.831	0.851	0.917	0.920
fit	0.23	0.45	0.93	1.08	0.85	0.98	0.70	0.98	0.51	0.72	0.89	1.23	1.59	1.70	1.19	1.70	1.18	1.77
NR	5	5	6	6	6	6	6	6	6	6	5	5	8	8	12	12	9	9
end members eliminated	-	-	-	-	-	-	-	-	-	-	-	-	-	-	grs pa	grs pa	grs pa chl	grs pa chl

Appendix 2. Continued

Appendix 2 (cont.). THERMOCALC Average P-T results for pelitic rocks.																		
Sample	**PSH-98-69.1**		**PSH-98-18.2**		**PSH-98-11B**		**PSH-98-97.1**				**PSH-98-97.1**				**PSH-98-98.3**			
P-T stage	Cooling		Cooling		Cooling		Peak				Cooling				Peak			
Zone	VI.2		VI.2		VI.2		VI.2				VI.2				VI.3			
Activities	at 600°C		at 600°C				at 650°C				at 650°C				at 650°C			
Garnet	rim		rim				core				rim				core			
prp	0.00210		0.000600		-		0.00310				0.00290				0.00250			
grs	0.00021		0.00260		-		0.000670				0.000310				0.000850			
alm	0.130		0.170		-		0.150				0.160				0.120			
Biotite					core		core				at grt							
phl	-		-		0.200 0.00450		0.0900				0.0990				0.0910			
ann	-		-		0.113		0.0260				0.0230				0.0300			
east	-		-		core		0.0660				0.0700				0.0660			
Muscovite	at grt		alt. from g		0.720		core				at grt							
mu	0.650		0.680		0.72		0.640				0.670				0.670			
pa	0.82		0.660		0.0170		0.700				0.750				0.479			
cel	0.0130		0.00990				0.0160				0.0130				-			
Chlorite	matrix, core		alt. from g		-						at grt							
clin	0.0850		0.030		-		-				0.0920				-			
daph	0.00460		0.0157		-		-				0.00360				-			
ames	0.0770		0.0410				-				0.0750				-			
Plagioclase	-		alt. from g		-		core				at grt							
an			0.380		-		0.400				0.400				0.420			
ab	and qtz H2O		0.760				0.740				0.740				0.720			
Other	crd 0.620				crd 0.800													
	fcrd 0.0480				fcrd 0.0150		mst 0.0065				mst 0.0056				mst 0.0058			
	mncrd 0.00098				ky and sill		fst 0.26				fst 0.28				fst 0.27			
	spss 0.028				qtz H2O		and sill qtz H2O				and sill qtz H2O				sill qtz H2O			
Results																		
*a*H2O	1.0	0.4	1.0	0.4	1.0	1.0	1.0	1.0	1.0	0.4	1.0	1.0	1.0	0.4	1.0	1.0	1.0	0.4
T°C	**570**	**511**	**548**	**501**	**505**	**492**	**549**	**637**	**595**	**549**	**552**	**591**	**608**	**562**	**646**	**666**	**617**	**566**
s.d.(T)	21	21	27	24	8	36	12	35	29	26	7	14	24	22	53	47	31	28
P kbar	**3.7**	**2.6**	**6.0**	**5.4**	**3.8**	**3.5**	**3.3**	**6.3**	**6.6**	**6.2**	**3.3**	**5.4**	**6.1**	**5.8**	**6.9**	**6.7**	**6.6**	**6.1**
s.d.(P)	0.7	0.7	1.5	1.4	0.1	0.7	0.3	1.2	1.1	1.0	0.2	0.7	1.1	1.0	2.3	1.9	1.1	1.1
correl.	0.931	0.955	0.499	0.579	0.754	0.990	0.129	0.948	0.766	0.783	0.186	0.877	0.941	0.948	0.941	0.911	0.773	0.790
fit	0.99	1.08	1.83	1.82	0.75	0.84	1.73	1.23	0.31	0.35	1.25	0.83	0.79	0.71	2.00	1.59	0.38	0.19
NR	7	7	5	5	6	5	9	8	5	5	12	11	8	8	7	5	4	4
end members eliminated	grs pa	grs pa	-	-	pa	and	-	sill	mst fst sill and	mst fst sill and	-	and	and ames clin daph	and ames clin daph	-	fst mst	fst mst sill	fst mst sill

Appendix 2. Continued

Appendix 2 (cont.). THERMOCALC Average P-T results for pelitic rocks.																		
Sample	**PSH-98-98.3**		**JTV-98-38.1**				**JTV-98-38.1**		**PSH-00-10**		**PSH-00-10**							
P-T stage	Cooling		Peak				Cooling		Peak		Cooling							
Zone	VI.3		VI.3				VI.3		VI.3		VI.3							
Activities	at 650°C		at 650°C				at 650°C		at 650°C		at 650°C							
Garnet	rim		core				rim		core		rim							
prp	0.00290		0.00440				0.00350		0.00710		0.00150							
grs	0.000310		0.000830				0.000067		0.000530		0.000160							
alm	0.160		0.130				0.170		0.390		0.400							
Biotite	at grt		matrix, core				alt. from st		matrix core		at grt							
phl	0.0990		0.0780				0.0840		0.0234		0.0223							
ann	0.0230		0.0310				0.0270		0.0740		0.0450							
east	0.0700		0.0600				0.0650		0.0280		0.0380							
Muscovite	at grt		core				rim		matrix core		at grt							
mu	0.670		0.630				0.660		0.660		0.650							
pa	0.750		0.620				0.650		0.590		0.580							
cel	0.0130		0.0150				0.0160		0.00880		0.0120							
Chlorite											at grt							
clin	-		-				-		-		0.0160							
daph	-		-				-		-		0.0360							
ames	-		-				-		-		0.0201							
Plagioclase	rim		matrix, core				at st		core		rim							
an	0.400		0.410				0.400		0.380		0.400							
ab	0.740		0.730				0.740		0.750		0.740							
Other	mst 0.0056		mst 0.0065				mst 0.0055		sill qtz		sill qtz							
	fst 0.28		fst 0.26				fst 0.280		H2O		H2O							
	sill qtz H2O		sill qtz H2O				sill qtz H2O											
Results																		
*a*H2O	1.0	0.4	1.0	0.4	1.0	0.4	1.0	0.4	1.0	1.0	1.0	1.0						
T°C	**608**	**562**	**643**	**591**	**611**	**526**	**598**	**552**	**616**	**667**	**577**	**574**						
s.d.(T)	24	22	32	27	30	26	24	22	32	34	18	18						
P kbar	**6.1**	**5.8**	**7.3**	**6.9**	**6.9**	**6.5**	**5.1**	**4.9**	**7.3**	**8.1**	**3.9**	**4.3**						
s.d.(P)	1.1	1.0	1.4	1.3	1.1	1.0	1.1	1.0	1.4	1.3	0.9	1.0						
correl.	0.941	0.948	0.936	0.941	0.765	0.781	0.945	0.950	0.911	0.737	0.847	0.611						
fit	0.79	0.71	1.29	1.20	0.36	0.64	0.94	0.92	1.29	1.08	1.19	1.22						
NR	8	8	8	8	5	5	8	8	6	5	9	8						
end members eliminated	-	-	-	-	mst fst sill	mst fst sill	-	-	-	sill	-	sill						